MICROCOPY RESOLUTION TEST CHART

NATIONAL BUREAU OF STANDARDS-1963-A

TECHNICAL REPORT RR-84-9

REAL TIME LARGE MEMORY OPTICAL PATTERN RECOGNITION

Don A. Gregory
Research Directorate
US Army Missile Laboratory

JUNE 1984

U.S. ARMY MISSILE COMMAND
Redstone Arsenal, Alabama   35898-5000

DTIC
ELECTE
AUG 20 1985
S D
B

85 - 8 20 079

REPORT DOCUMENTATION PAGE		READ INSTRUCTIONS BEFORE COMPLETING FORM
1. REPORT NUMBER RR-84-9	2. GOVT ACCESSION NO. *HB A15Bo23*	3. RECIPIENT'S CATALOG NUMBER
4. TITLE *(and Subtitle)* Real Time Large Memory Optical Pattern Recognition		5. TYPE OF REPORT & PERIOD COVERED Technical Report
		6. PERFORMING ORG. REPORT NUMBER
7. AUTHOR(s) Don A. Gregory		8. CONTRACT OR GRANT NUMBER(s)
9. PERFORMING ORGANIZATION NAME AND ADDRESS Commander, US Army Missile Command ATTN: AMSMI-RR Redstone Arsenal, AL 35898-5248		10. PROGRAM ELEMENT, PROJECT, TASK AREA & WORK UNIT NUMBERS
11. CONTROLLING OFFICE NAME AND ADDRESS Commander, US Army Missile Command ATTN: AMSMI-RR Redstone Arsenal, AL 35898-5248		12. REPORT DATE June 1984
		13. NUMBER OF PAGES 116
14. MONITORING AGENCY NAME & ADDRESS*(if different from Controlling Office)*		15. SECURITY CLASS. *(of this report)* Unclassified
		15a. DECLASSIFICATION/DOWNGRADING SCHEDULE

16. DISTRIBUTION STATEMENT *(of this Report)*

Approved for public release; distribution unlimited.

17. DISTRIBUTION STATEMENT *(of the abstract entered in Block 20, if different from Report)*

18. SUPPLEMENTARY NOTES

19. KEY WORDS *(Continue on reverse side if necessary and identify by block number)*
Pattern Recognition
Optical Correlation
Liquid Crystal
Optical Memory
Matched Filter

20. ABSTRACT *(Continue on reverse side if necessary and identify by block number)*
A large memory optical recognition system has been developed and tested. The memory consists of an array of stored holographic Fourier transform matched filters in a VanderLugt type correlator. The filters are stored (on high resolution Kodak plates) and addressed using a novel holographic multi-focus lens. This element acts as a diffraction grating, splitting the input beam into 25 elements and as a lens, producing the Fourier transform of each of the 25 elements. The filters are created and addressed using a HeNe laser and a Hughes

DD FORM 1473 EDITION OF 1 NOV 65 IS OBSOLETE
DD , JAN 73 1473

liquid crystal light valve (LCLV) to produce a coherent image from a television monitor. The LCLV also allows the filters to be addressed in "real time" thereby making the use of a transparency as an input scene unnecessary. This provides for real time recognition. Thus far, more than 70 matched filters have been stored on a single holographic plate and addressed in parallel and in real time with good correlations resulting. This research and the results obtained should contribute to allowing serious consideration to be given to the use of optical recognition systems for a wide variety of civilian and military applications.

Accession For	
NTIS GRA&I	☑
DTIC TAB	☐
Unannounced	☐
Justification	

By_____
Distribution/_____
Availability Codes

Dist	Avail and/or Special
A-1	

CONTENTS

iii

CONTENTS (Concluded)

ILLUSTRATIONS

ILLUSTRATIONS (Continued)

ILLUSTRATIONS (Concluded)

vii

I. INTRODUCTION

A. Historical Background

The history of Fourier transform techniques in optic dates back to the experiments of Abbe (1873) [1], [2] and later, Porter (1903) [3]. These experiments dealt with manipulating the spatial frequency content of a scene. As an example of the results obtained in these early investigations, consider an input scene consisting of a regular array of squares as shown in Figure 1. If this is illuminated with reasonably monochromatic, collimated light and focused, the spatial frequency spectrum of Figure 1 results in the focal plane. Abbe and Porter were the first to discover that an obstacle placed in this plane could dramatically alter the reimaged scene. A small slit placed in the focal plane in the horizontal direction was shown to cause the omission of the horizontal components of the resulting reimaged scene. The same slit, allowing only the vertical spectra to pass, produced a horizontal bar pattern, filtering out the vertical pattern. This is illustrated in Figures 2 and 3. Abbe and Porter also observed that when a small stop is placed in the focal plane blocking the lowest order (central) spatial frequency component, a contrast reversal took place in the resulting image. These very basic experiments had far-reaching effects in the development of phase contrast microscopy as proposed by Fritz Zernike in 1935 [4]. The desire was to construct a microscope so that the intensity reaching the viewer is linearly related to the phase change undergone by the light in passing through the subject under study. This was to prove very useful in the study of nearly transparent subjects. Zernike achieved this result by placing a "phase changing plate" in the focal plane of the microscope. This plate can be a small dot on a transparent medium with the dot centered on the focal point. The thickness of the dot and its index of refraction can be chosen so that it retards the phase of the focused illumination by $\pi/2$ (or $3\pi/2$) relative to the phase retardation of the light diffracted from the subject. Thus, the image intensity becomes related linearly to the phase shift caused by the subject. It is by this method that we are able to view a phase shift as a change in intensity.

In 1948, Dennis Gabor published a paper setting down the basic formulation of what he called holography [5]. He reasoned that both amplitude and phase information could be recorded if the illuminating coherent light could be interfered with the illumination carrying the image information. The basic arrangement for making a Gabor hologram is shown in Figure 4. In making a Gabor hologram, the object must consist of a semitransparent scene on a transparent background, a limitation that was not removed for 14 years. The transmitted light then consisted of a scattered portion produced by the image and an unscattered part transmitted by the transparent part of the transparency. The two then interfered at the film. This mechanism is discussed in Section II. To view the reconstructed image one had only to reilluminate the developed hologram transparency as shown in Figure 5. The Gabor hologram did possess two real weaknesses. As mentioned before the object had to be quite transparent. This severely limited the types of objects that could be used. A second problem which is shown in Figure 5 is the generation of a so-called twin image. The illuminated hologram not only transmitted the incident light but also reflected a sizeable portion which produced an image on the other side of the hologram and the two could not be

1

IMAGE PLANE

FREQUENCY PLANE

LENS

INPUT SCENE

f
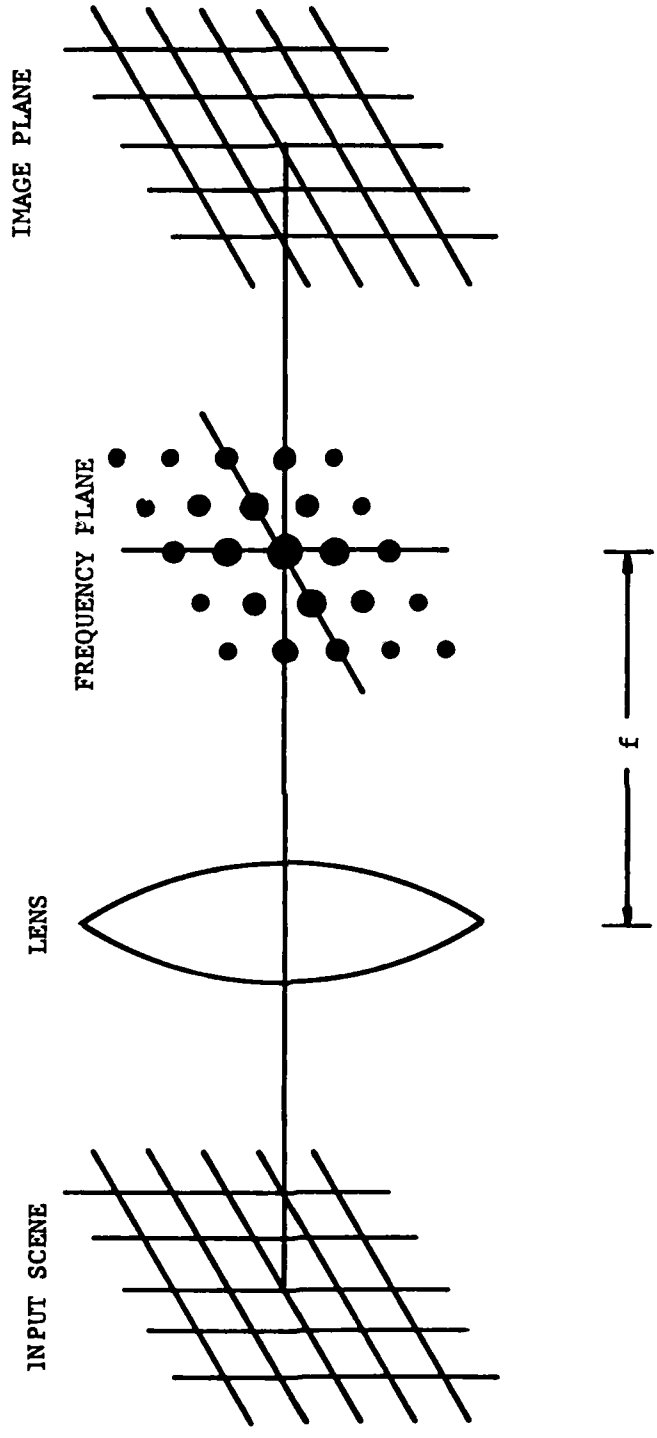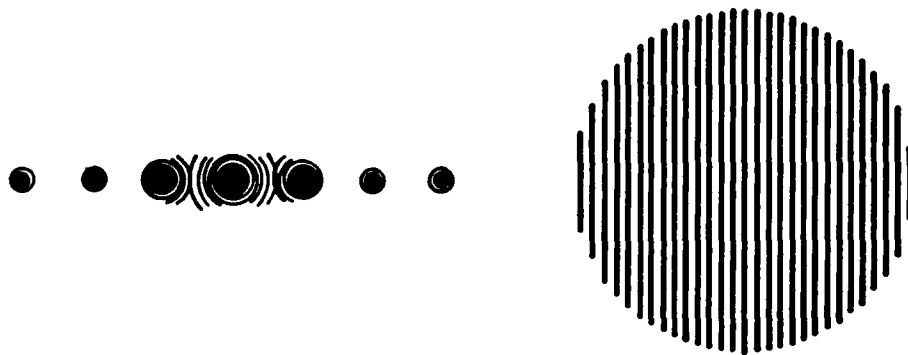
Figure 2.   Spatial filtering (after Goodman [38], p. 144),
            mesh filtered with horizontal slit.

Figure 3.   Spatial filtering (after Goodman [38], p. 144),
            mesh filtered with vertical slit.
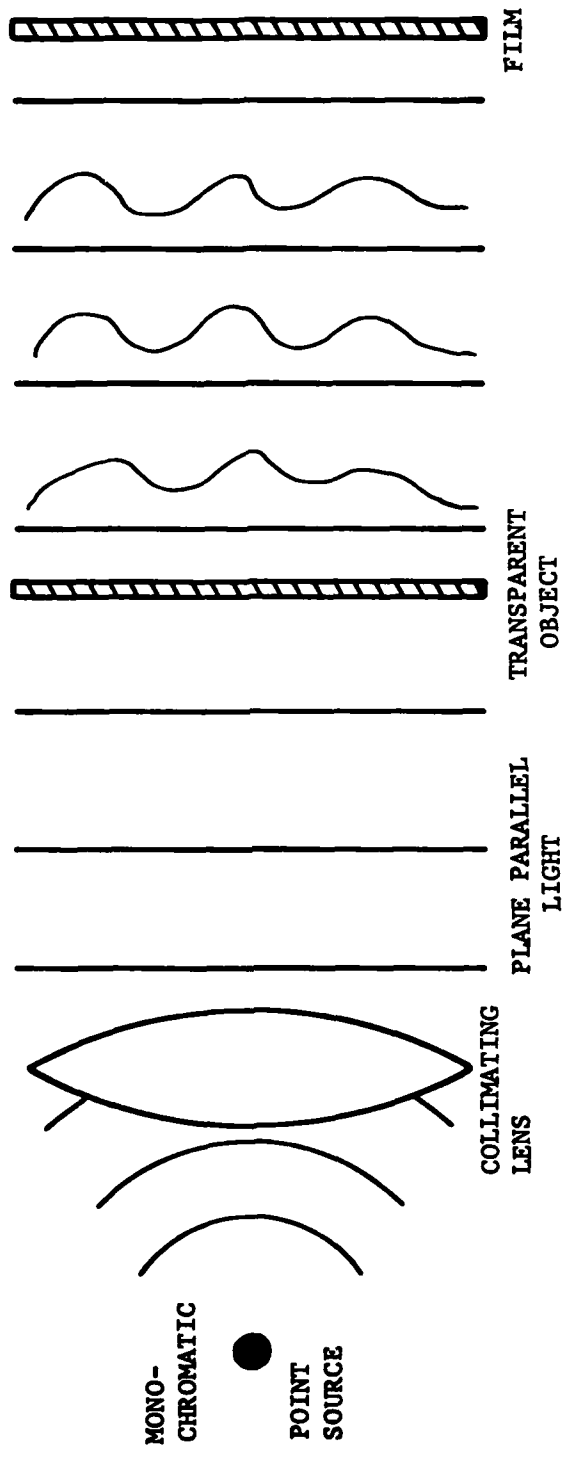
Figure 4. Making a Gabor hologram (after Goodman [38], p. 206).

MONO-
CHROMATIC

POINT
SOURCE

COLLIMATING
LENS

PLANE PARALLEL
LIGHT

TRANSPARENT
OBJECT

FILM

4

16

SOURCE

TWIN IMAGE

DEVELOPED FILM
TRANSPARENCY

IMAGE

d

d
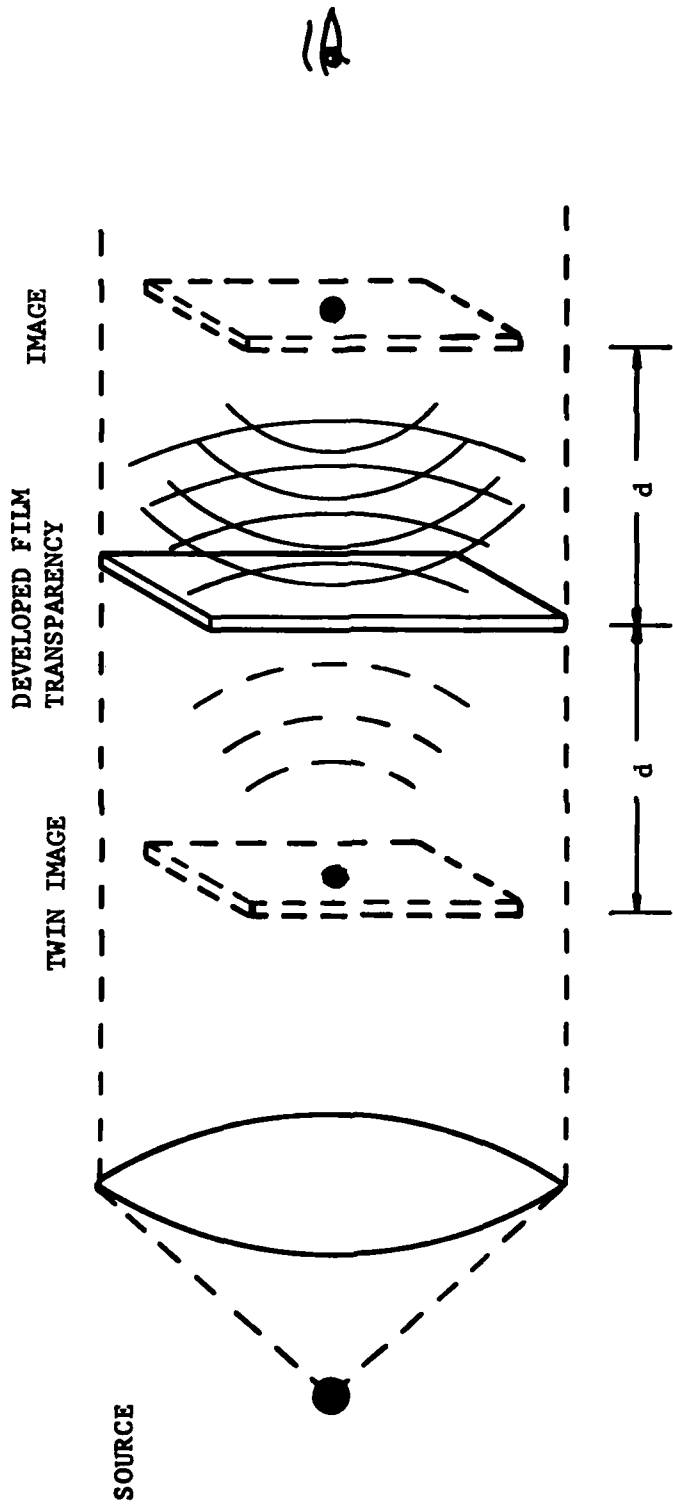
Figure 5. Viewing a Garbor hologram -- the twin images (after Goodman [38], p. 207).

5

separated. If one focused on the real image, the out-of-focus virtual image was present and vice versa. For all of its limitations the Gabor hologram did set the foundation for the development of modern holography.

It was also at about this time that the concept of a matched filter was introduced by North in 1943 [6], and applied to signal detection by Peterson, Birdsall, and Fox in 1954 [7]. A matched filter is described by these authors to be the optimum linear filter for signal detection in white noise. Of course, these early matched filters were used for the detection of electrical signals embedded in noise but the concepts carried over into optical processing.

Perhaps the most dramatic successes in optical spatial filtering came in the area of photograph improvements. Maréchal at the Institut d'Optique, Universite de Paris in the early 1950's is probably the most noteworthy [8]. He believed that defects in photographs arose from problems in the ability of the photographic system to faithfully transfer the spatial frequency content of the original scene. He attempted to insert appropriate attenuating and phase shifting plates in the focal plane in order to develop filters which would remove some of the defects. Probably Maréchal's most important discovery was that small details in the image could be enchanced if the low spatial frequency components could be blocked out or attenuated. The reverse of this was also observed in the filtering of the periodic structure associated with the halftone printing process. This produced a continuous image rather than an image obviously made up of black dots on a white background. Maréchal also made a considerable contribution to the removal of image blur by using an absorbing plate and a dephasing plate in the focal plane of the filtering system.

In the decade of the 1950's the similarities between the fields of optics and electrical engineering (particularly in communications) became obvious and a great deal of exchange began to take place. The problems associated with filtering and detection shared common approaches to solution. A paper published in the Journal of the Optical Society of America by a communications theorist, Peter Elias and others in 1953 [9] prompted the initial exchange of ideas. The combining of the fields was perhaps best provided by a physicist, E. L. O'Neill in 1956 [10] and by a symposium in 1960 entitled "Communication and Information Theory Aspects of Modern Optics" [11]. At present the fields are quite closely intertwined and one will find articles in electrical and communication engineering journals written by opticists and articles in optical journals written by engineers. It all comes down to the methods by which information is transferred from one point to another – whether it be by electrical or optical means.

In 1960, the advances in optics and communication engineering began to accelerate rapidly. The laser was developed [12] which gave the fields a new source of high intensity coherent light to use. Radar signal processing using coherent filtering got underway at the University of Michigan Radar Laboratory. The publication of a paper entitled, "Optical Data Processing and Filtering Systems" in 1960 by this group [13] under the direction of L. J. Cutrona, was to be the first of many to draw the attention of both engineers

6

and physicists. The military's interest in the area of optical data processing began at about this point in time. The Michigan group was funded to investigate the processing of data collected by "synthetic array" antennas aboard reconnaissance planes [14]. In order to use microwave radar and get reasonable resolution, the size of the antenna would be much too large to be flown aboard a surveillance plane. The resolution at a range R goes approximately like $\lambda R/D$, where λ is the wavelenght and D is the linear size of the antenna. For a resolution of one meter, a plane flying at an altitude of 3 km would need an antenna 450 m long if the radiation used had a wavelength of 15 cm. In order to solve this problem, a system was developed which used pulses of radiation so that the information obtained is a periodic sampling of the terrain. The task of the Michigan group was to turn this sampled information into a real image which they did using the data obtained to form a moving film transparecny, then demodulating it using an optical system of their own device.

This brief survey is by no means complete. Optical processing has been used successfully in many other fields such as Fourier spectroscopy and seismic wave analysis, both of which have benefited greatly from the basic analysis methods discussed here.

B. Recent Investigations

This section must surely be in with the application of Gabor's theories and experiments in holography by Leith and Upatnieks of the University of Michigan's Radar Laboratory in 1962 [15]. Although this is after the development of the laser in 1960, the first investigations were done without a laser. The Leith-Upatnieks hologram was a vast improvement on Gabor's in that it removed two of the most serious limitations of the Gabor hologram: the requirement of a transparent object and the production of an inseparable image twin. The basic experimental arrangement for making a Leith-Upatnieks hologram is given in Figure 6. The noticeable difference between the Gabor hologram and the Leith-Uptanieks hologram is the separate reference beam. In Figure 6 a semitransparent object is used, but even that is not necessary. An opaque object or even a real solid model may be used and the light collected by reflection instead of transmission. Light from the object intefers with the reference beam at the location of the film plate. After developing the film the recreated image may be viewed by reillumination with the source. The image occurs in focus off axis along the path of the original reference beam. The mathematical details of the analysis of this type system are left to Section II. It is also interesting to note that the first hologram using a laser as the source was produced by this group [16].

One year later, in 1963, A. B. VanderLugt of the University of Michigan's Radar Laboratory proposed and demonstrated a new technique for synthesizing frequency plane masks for coherent processors [17]. The filters constructed using this technique, like holograms, have the unique property of being able to control both the amplitude and phase of a transfer function. The technique used in making these filters is almost identical to that used in making an ordinary hologram except that the input scene is Fourier-transformed by a lens before it is allowed to interfere with a reference beam at a holographic film plate. Properly stated, filters made using this technique
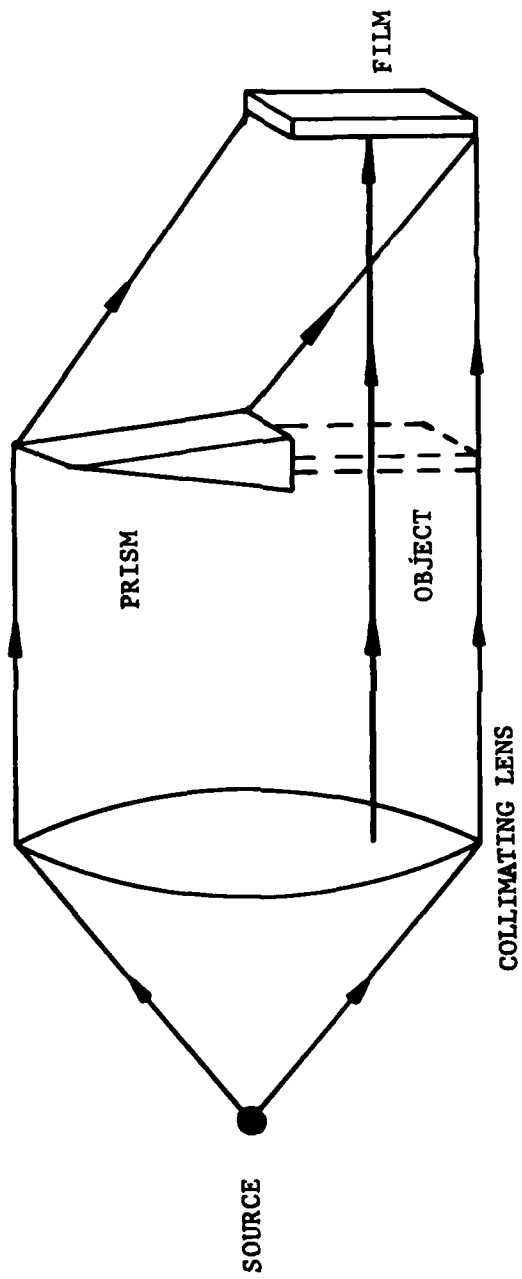
Figure 6. The Leith-Upatnieks hologram (after Goodman [38], p. 209).

SOURCE

COLLIMATING LENS

PRISM

OBJECT

FILM

8

should be called holographic Fourier transform matched filters. A sketch of the experimental arrangement used in making this type of matched filter is given in Figure 7.

After the exposed film is developed, it is placed in an optical system as sketched in Figure 8. If the input scene is the same one used to record the matched filter, a correlation intensity will be recorded by the detector along the axis of the original reference beam. The mathematical details of this phenomena are given in Section II. The important point to be made here is that using the previously described experimental arrangement, an optical identification device was first demonstrated. The VanderLugt technique for making matched filters is the basis for virtually all the work done in this area today.

In the time from 1965 to 1970, many authors investigated a variety of topics dealing with optical matched filtering. One of the most pressing problems was that of multiple recognition. The VanderLugt arrangement just described was limited to the recognition of one input scene per filter. LaMachia and White proposed a method of multiplexing using angularly separated reference beams [18]. VanderLugt suggested a similar method of superimposing a number of filters with each filter on a different carrier [19]. Leith devised a technique of coding the superimposed filters by rotating the holographic plate for each exposure [20]. Groh used point holograms to produce spatially separated filters with different carriers [21]. Later, Shi proposed color multiplexing using a multiple wavelength source [22]. In 1972, Grumet developed an NxN array of holographic lenses which were used to Fourier transform a scene in a VanderLugt type optical correlator [23].

From 1972 to 1977, considerable effort was placed on determining the usefulness of optical matched filers in object recognition and detection. In 1972, the Harris Electro-Optics Center of Radiation produced, under contract to the US Army Missile Command, a report discussing the possible use of optical matched filters for terminal missile guidance [24]. The technical aspect of this research was under the direction of A. B. VanderLugt. The investigation concerned incoherent (mask matching) correlation and coherent (holographic Fourier transform) correlation. Conclusions drawn from the research include: incoherent system suffers two major drawbacks; (1) diffraction effects and the presence of a large, often nonuniform bias in the output, and (2) the coeherent system was shown to have little of either problem. Experiments were performed which showed that the correlation intensity increases with the resolution, spatial frequency, of the input scene for a coherent or incoherent system. Rotation and scale change experiments were also done which showed that the coherent correlation intensity fell by 13 dB when the input scene was rotated by about one degree and the intensity fell by 20 dB with a 1 percent change in scale. The input scene used was an urban scene containing moderately high spatial frequencies. Results of several coherent and incoherent matched filter experiments were given which show the definitive advantage of the coherent system, especially for high spatial frequency input scenes. This report was also one of the first to mention the need for a real time correlator without specially prepared transparencies for input scenes. A photo-plastic device developed by Harris Electro-Optics was tested and found to be moderately useful but slow in reacting (about 5 seconds).
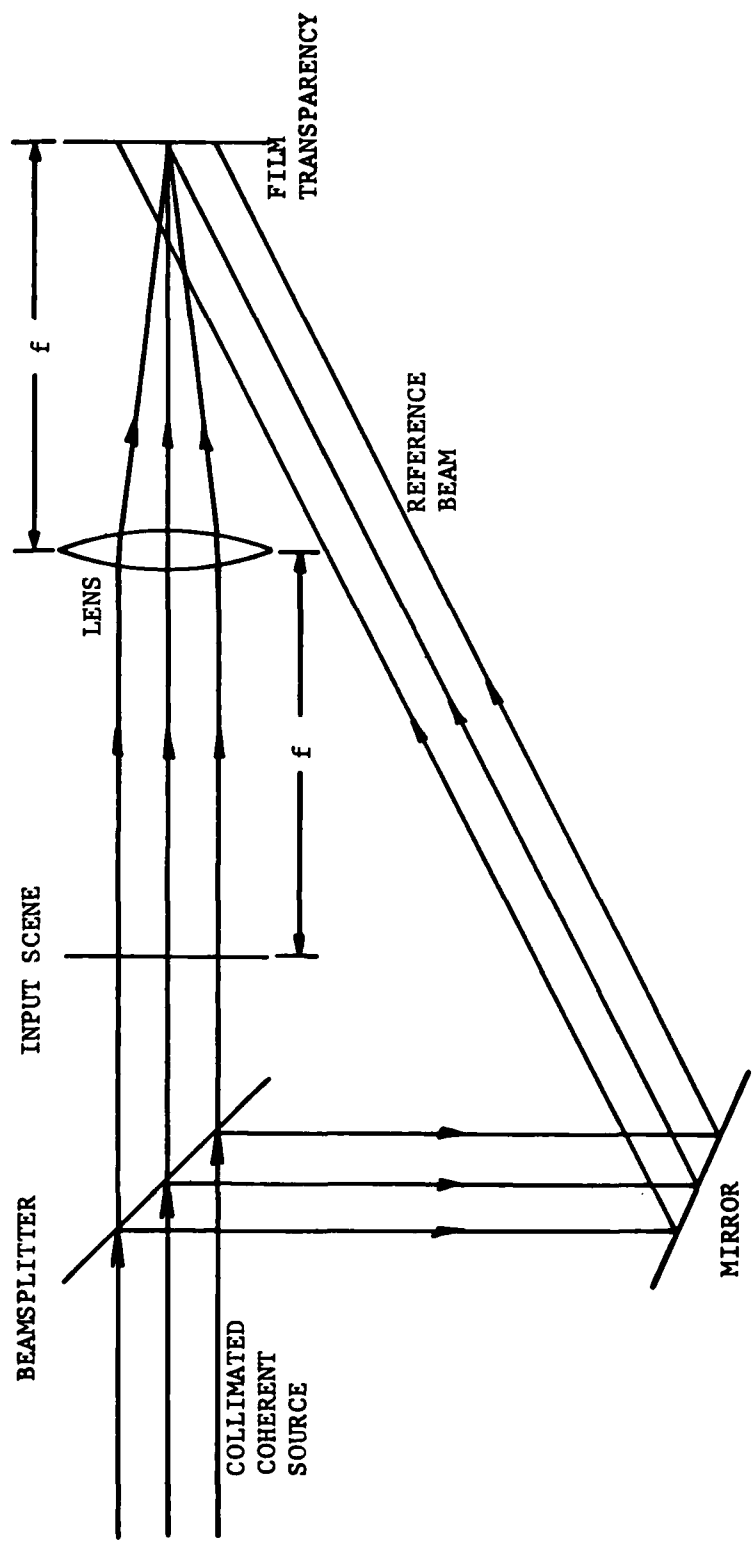
Figure 7. The VanderLugt matched filter.

10
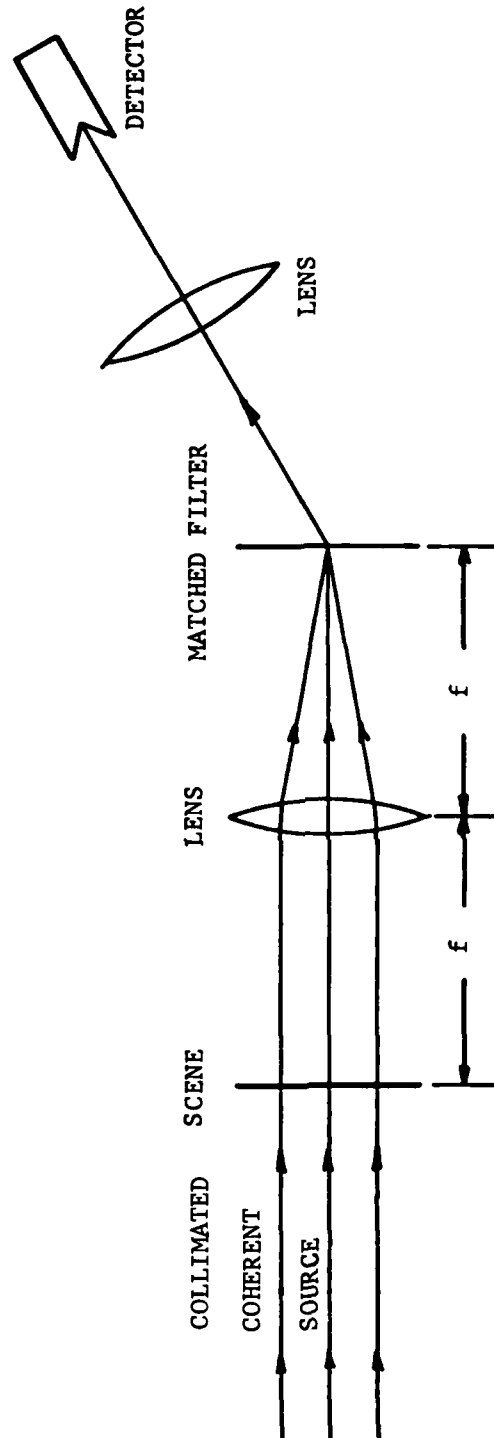
Figure 8. _Detecting the correlation in the VanderLugt arrangement._

11

In 1977, Casasent and Furman published one of their many papers dealing with optical correlation [25]. This particular paper is of interest because they investigated the effects of rotation, scale and filter shifts on the correlation and obtained results similar to those of Vander Lugt's group, just discussed. The low resolution scene used was an aerial map of Huntsville, AL having a resolution of details on the map of ~ 30 μm. The magnification of the map itself was not given.

This map contained both urban (high spatial frequency) and rural (low spatial frequency) scenery. The input scenes were 35 mm slides (Kodak high speed holographic 50-153 film). The dimensions of the photographs were not given so an estimate of the spatial frequency content of the slide itself is not possible, although it appears to be near that of the Harris investigation.

In 1978, Grumman Aerospace concluded an investigation into using optical Fourier transform matched filters for aerial reconnaissance film screening. Kenneth Leib was the principal investigator. This team developed the first application of a multifocus holographic element to matched filtering. In the 1978 article discussing this work, the investigators reported on a holographic element capable of producing a 2X2 array of Fourier transforms addressable with 35 mm slides (Kodak SO-173 film) [26]. The primary input scene of interest was a scale model of a US Army M-60 tank, but later some terrain imagery was used. The noteworthy facet of this investigation was the attempt at multiple exposures of the input scene while using the 2X2 array (Fourier transform image overlaps). They found that no more than four Fourier transforms could be stored at the same spot without significant loss, 84 percent, in correlation when compared to the correlation from a single stored scene. This study was done using the terrain scene of moderate spatial frequency content. A study of the rotational dependence of the correlation was done which showed that for the low spatial frequency input (M-60 tank), the scene could be rotated by more than 7 degrees before the correlation dropped by 50 percent. This is in contrast to the work by Harris and Casasent where only tenths of degrees were needed for the same decrease. The wide difference in spatial frequencies of the input scenes may explain the difference in results.

In 1978, another important modification to the optical correlator was made by the addition of an incoherent-to-coherent image converter, liquid crystal light valve (LCLV), first described by Hughes in 1975. This device allowed the use of real input scenes such as those viewed by the eye. The making of a transparency was no longer necessary. The device was reasonably fast-reacting, allowing 25 ms "real time" correlations for the first time [28]. This device is described in Section III.

This experiment also demonstrated for the first time, millisecond tracking of a target. An interesting facet of optical correlation is its translational invariance, that is, the input scene can be moved without losing the correlation; in fact the correlation spot will move along with the input scene. This was demonstrated quite vividly in a paper by Guenther [29] and in a video tape produced by Farr [30]. The real time correlator could distinguish between two similar vehicles and track a vehicle as it moved through the field of view.

Christensen, in 1979, showed that up to eight matched filters could be stored at a single focal point using multiple exposure techniques [31]. This was done with the aid of an LCLV making it real time recognition. Leib, of Grumman Aerospace, was able to store 4 filters using a holographic lens array [32]. This was not done using an LCLV, but did demonstrate the parallel – addressing ability of such a system – more than one matched filter could be addressed at a time.

More recently, Liu and Duthie have proposed a multiplexing method incorporating a special contact screen in a real time matched filter correlator [33]. The screen used in that investigation is described in Section II. Essentially the screen split an input scene into an NxN array of identical scenes, which were Fourier-transformed using a conventional lens in a Vander Lugt type correlator. Further developments in this approach finally led to a single holographic element which could both split the scene into an array and Fourier-transform it. Results and a complete description are given in a paper by Gregory and Liu [34].

One of the newest fields is that of white light optical processing. A promising techique by Yu employs a high diffraction efficiency grating in contact with the input image transparency along with an achromatic transform lens [35]. The diffraction grating separates the white light into its color components and the lens transforms each component.

The problem of recognition has been addressed by computer experts in some detail. At present digital processes of recognition are being used for such diverse applications as lung tumor detection and chromosome karyotyping [36]. This technique requires some highly sophisticated computer hardware and software and must be tailored for the specific recognition problem. In addition to being quite slow, these systems have a fairly high error associated with them. It is hoped that many of the recognition problems now handled digitally can be done optically if enough matched filter memory can be stored and accessed.

The military has contributed greatly in funding for optical recognition research. The desire is to be able to distinguish between friend or foe without having to place personnel in particularly dangerous environments. A device which could recognize a military vehicle, ship, or plane and recognize it immediately would have particular application in unmanned reconnaissance missions. In terminal missile guidance, a system such as this would allow the programming of particular highly localized targets into the memory of the guidance system, thereby making pinpoint attacks possible. The tracking capability of such a system would allow real time identification to be made on moving targets as well.

The goal of the present investigation is to bring together many of the topics just discussed, in combination with a new holographic element produced by Liu [33], in an attempt to investigate a large memory optical recognition system operating in real time. The memory consists of an array of holographic Fourier transform matched filters, addressable in series or parallel.

The basic holographic equations are given in Section II along with simple models of the correlation of scenes that have been tilted, rotated, or magnified. An outline of the basic principles of the Liu holographic element is also given.

The experimental procedures followed in producing the matched filter arrays are given in Section III. The liquid crystal light valve (LCLV) used in this investigation is described and its operating parameters given along with a list of the other basic equipment used.

The experimental results given in Section IV range from basic tests of the holographic element and the LCLV, to the storing and accessing of more than seventy different matched filters. The present state of the system allows the parallel-addressing of 25 different filters or the series-addressing of up to a demonstrated 73 filters, in real time, with good correlations resulting.

II. THEORY

A. The Fourier Transform

It is well known that any function $f(\digamma)$ that represents a real physical phenomena can be expanded in terms of orthonormal functions $U_n(\digamma)$ [37]:

$$f(\digamma) = \sum_{n=1}^{\infty} a_n U_n(\digamma) , \tag{1}$$

where the coefficients a_n are given by:

$$a_n = \int_a^b U_n^*(\digamma) f(\digamma) d\digamma . \tag{2}$$

The integration limits span the interval of the function $f(\digamma)$.

As an example, consider the orthogonal functions sine and cosine. The expansion of a function in terms of these functions is called a Fourier series. The series equivalent of Equation (1) is:

$$f(\digamma) = \frac{1}{2} A_0 + \sum_{m=1}^{\infty} \left[A_m \cos\left(\frac{2\pi m \xi}{a}\right) + B_m \sin\left(\frac{2\pi m \xi}{a}\right) \right] , \tag{3}$$

where the interval in $\digamma$ is $(-a/2, a/2)$ and,

$$A_m = \frac{2}{a} \int_{-a/2}^{a/2} f(\digamma) \cos\left(\frac{2\pi m \xi}{a}\right) d\digamma \tag{4}$$

$$B_m = \frac{2}{a} \int_{-a/2}^{a/2} f(\digamma) \sin\left(\frac{2\pi m \xi}{a}\right) d\digamma . \tag{5}$$

We could have started with an orthonormal set of complex functions:

$$U_m(r) = \frac{1}{\sqrt{a}} \, e^{i(2\pi m r/a)} \tag{6}$$

$m = 0, \pm 1, \pm 2 \ldots,$ on the interval $(-a/2, a/2)$ as before. An expansion would then be written:

$$f(r) = \frac{1}{\sqrt{a}} \sum_{m=-\infty}^{\infty} A_m \, e^{i(2\pi m r/a)} \tag{7}$$

where

$$A_m = \frac{1}{\sqrt{a}} \int_{-a/2}^{a/2} e^{-i(2\pi m r'/a)} \, f(r') \, dr' \, . \tag{8}$$

If the function is well-behaved and at least piecewise continuous, let the interval become infinite $(a \to \infty)$ and transform:

$$\frac{2\pi m}{a} \longrightarrow k \tag{9}$$

$$\sum \longrightarrow \int_{-\infty}^{\infty} dm = \frac{a}{2\pi} \int_{-\infty}^{\infty} dk \tag{10}$$

$$A_m \longrightarrow \sqrt{\frac{2\pi}{a}} \, A(k) \, . \tag{11}$$

The result is the well-known Fourier integral:

$$f(r) = \frac{1}{\sqrt{2\pi}} \int_{-\infty}^{\infty} A(k) \, e^{ikr} dk \tag{12}$$

where

$$A(k) = \frac{1}{\sqrt{2\pi}} \int_{-\infty}^{\infty} f(r) \, e^{-ikr} dr \, . \tag{13}$$

16

Equations (12) and (13) are the mathematical basis for a wide variety of theories related to signal propagation, electrical or optical.

B. Fourier Transforming Properties of Lenses

The analysis of how a simple focusing lens performs the Fourier transform of a scene is the foundation of the description of Fourier transform matched filtering. Consider the sketch of a spherical lens in Figure 9. The phase delay ϕ, experienced by an incoming spatially and temporally coherent wave, at any (x,y) coordinate, after passing through the lens, is calculated by beginning with the expression for the velocity of light V_s in a medium having an index of refraction, n: [38] (p. 77)

$$V = \frac{\lambda \nu}{n} \quad , \quad \frac{\omega}{2\pi} = \nu \quad . \tag{14}$$

Substituting:

$$V = \frac{\lambda \omega}{2\pi n} \quad ; \tag{15}$$

multiplying both sides by time, t :

$$Vt = \frac{\lambda \omega t}{2\pi n} \quad , \qquad \omega t = \phi \tag{16}$$

thus:

$$\Delta = \frac{\lambda \phi}{2\pi n} \quad , \qquad k = \frac{2\pi}{\lambda} \quad . \tag{17}$$

Solving for ϕ :

$$\phi = \frac{2\pi n \Delta}{\lambda} = n\Delta k \quad . \tag{18}$$

The wave also travels the distance $\Delta_0 - \Delta$ in open air (n = 1). Thus the total phase delay is: [38] (p. 77)

$$\phi_T = n\Delta k + k(\Delta_0 - \Delta)$$

$$= k\Delta(n-1) + k\Delta_0 \quad . \tag{19}$$

Now, define a transform of the form:

$$t_\ell(x,y) = e^{i\phi_T} .$$

Substituting ϕ_T from Equation (19) gives:

$$t_\ell(x,y) = e^{ik\Delta_0} e^{ik\Delta(n-1)} \quad . \tag{20}$$

17
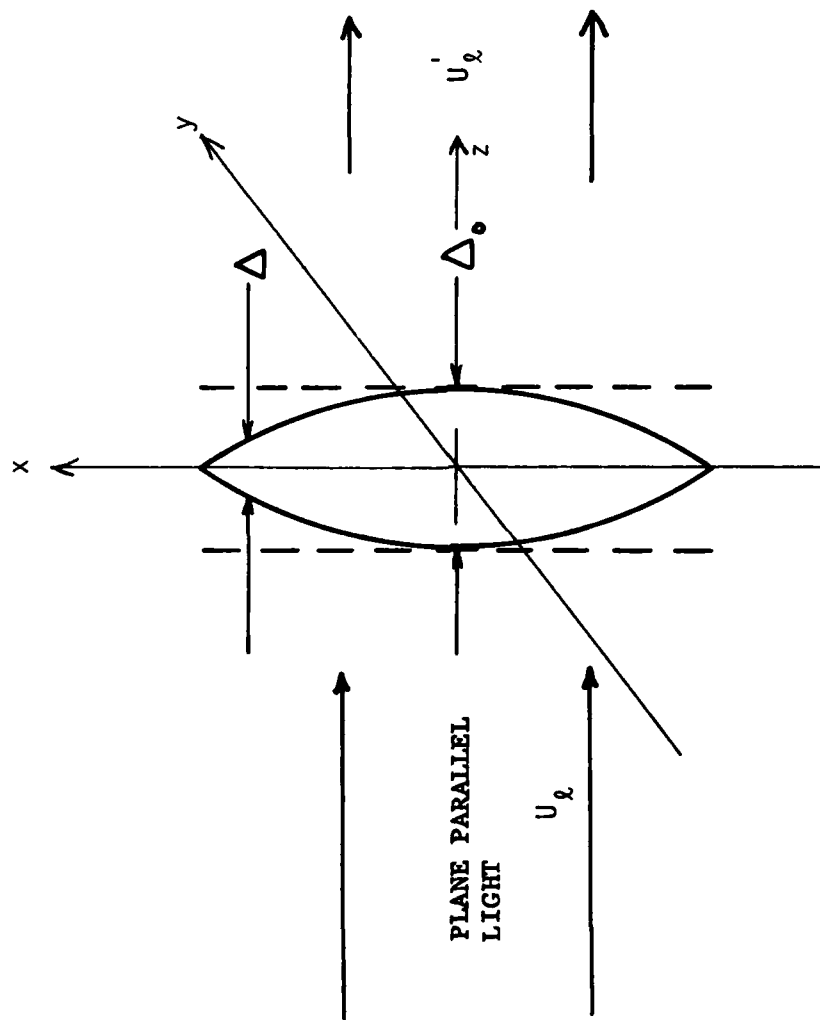
Figure 9. Geometry for calculating phase delay through a lens.

18

Thus the field U_ℓ' is related to the field U_ℓ by:

$$U_\ell'(x,y) = t_\ell(x,y) \; U_\ell(x,y) \quad .$$ (21)

The problem now is to find an expression for the thickness function $\Delta(x,y)$. Using a little geometry one can arrive at the following expression for $\Delta(x,y)$ [38] (p. 77):

$$\Delta(x,y) = \Delta_0 - R_1 \left[1 - \sqrt{1 - \frac{x^2 + y^2}{R_1^2}} \right] + R_2 \left[1 - \sqrt{1 - \frac{x^2 + y^2}{R_2^2}} \right] ,$$ (22)

where R_1 and R_2 are the radii of curvature of the lens. A binomial expansion (paraxial approximation) of the square root terms gives:

$$\sqrt{1 - \frac{x^2 + y^2}{R_1^2}} \approx 1 - \frac{x^2 + y^2}{2 R_1^2}$$ (23)

and similarly for the term involving R_2. Substituting this into Equation (22) yields:

$$\Delta(x,y) \quad \Delta_0 - \frac{x^2 + y^2}{2} \left(\frac{1}{R_1} - \frac{1}{R_2} \right) .$$ (24)

If $R_2 = - R_1 = R$ (bi-convex lens), then:

$$\Delta(x,y) \approx \Delta_0 - \frac{x^2 + y^2}{R^2} \quad .$$ (25)

Note that for any thin symmetric lens:

$$\frac{1}{f} = 2(n-1) \frac{1}{R}$$ (26)

where f is the focal length of the lens. Therefore, the final form of the lens transform function t may be written as:

$$t_\ell(x,y) = e^{ikn\Delta_0} \; e^{-\frac{ik}{2f}(x^2 + y^2)} \quad .$$ (27)

To apply this lens transformation, consider the typical optical system of Figure 10. The input plane (ξ,n) contains a pattern (scene) stored on a transparency. This transparency is back-illuminated with coherent, collimated light. We desire to know what the image looks like a distance f away from the thin spherical lens.
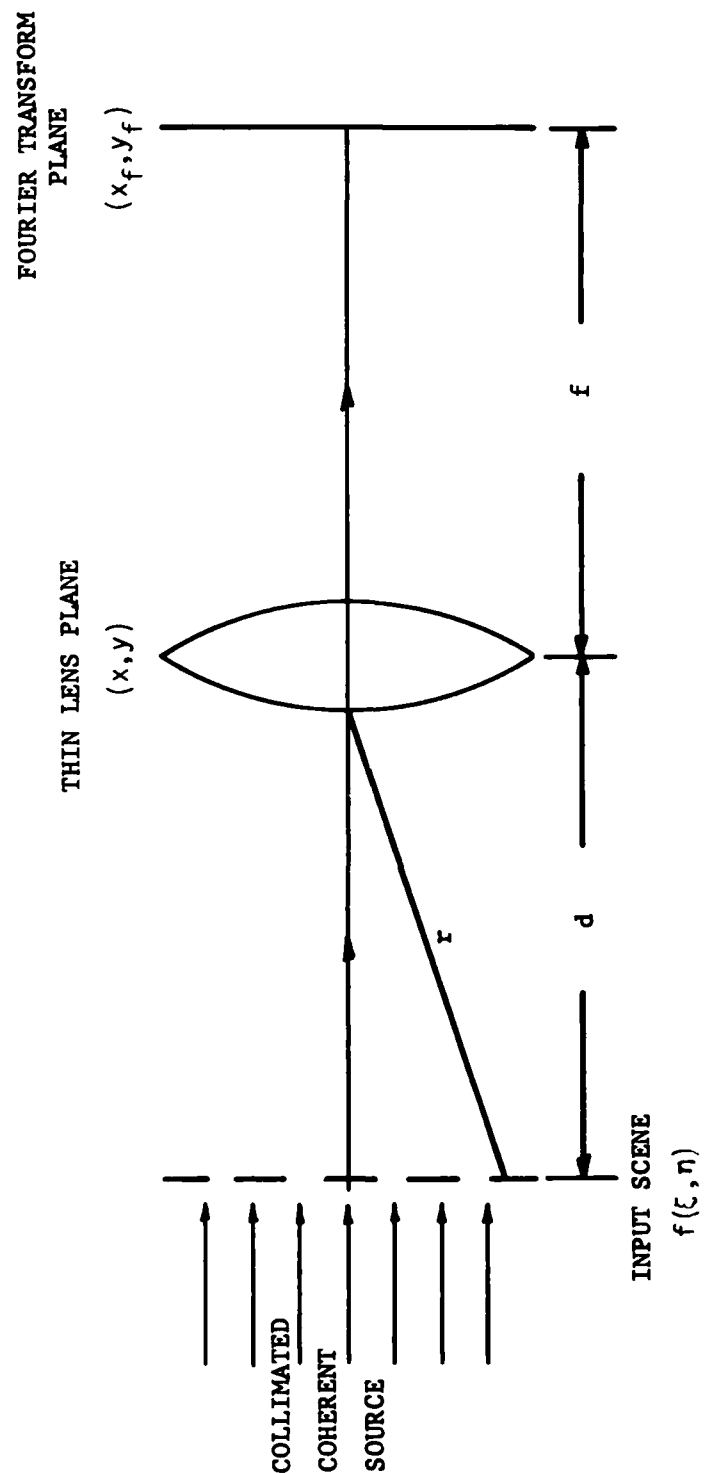
Figure 10. The Fourier transform produced by a spherical lens.

Between the (ξ, η) plane and the (x,y) plane, apply Huygens principle [39] (p. 153):

$$g(x,y) = C \iint\limits_{s} f(\xi, \eta) \; e^{ikr} d\xi d\eta \qquad (28)$$

where $g(x,y)$ represents the field at the entrance to the lens, s denotes the surface integral, and C is an arbitrary complex constant related to the amplitude of the incident field. The distance r may be written as:

$$r = \left[d^2 + (x-\xi)^2 + (y-\eta)^2 \right]^{1/2} \quad . \qquad (29)$$

Using the binomial expansion (paraxial approximation) gives:

$$r \approx d + \frac{1}{2d} \left[(x-\xi)^2 + (y-\eta)^2 \right] \quad . \qquad (30)$$

Equation (28) may be rewritten as:

$$g(x,y) = C' f(\xi, \eta) \; * \; h_1(\xi, \eta) \qquad (31)$$

where C' is again a complex constant and

$$h_1(\xi, \eta) = \exp \left[\frac{i\pi}{\lambda d} (\xi^2 + \eta^2) \right] \qquad (32)$$

and the * denotes convolution. In general, convolution is defined as:

$$f(z) \; * \; g(z) = \int\limits_{-\infty}^{\infty} f(z') \; g(z-z')dz' \qquad (33)$$

Upon going through the lens, the transform t_ℓ derived earlier may be applied to give the field as the wave exits the lens:

$$U'_\ell = g(x,y) \; t_\ell(x,y) \quad . \qquad (34)$$

Traveling from the lens a distance f to the screen at (x_f, y_f), we may again apply Huygens principle. Thus, the field at the screen can be written as:

$$U(x_f, y_f) = C'' \left\{ \left[f(\xi, \eta) * h_1(\xi, \eta) \right] t_\rho(x,y) \right\} * h_2(x,y) \qquad (35)$$

where

$$h_2 = \exp \left[\frac{i\pi}{\lambda f} (x^2 + y^2) \right] \qquad (36)$$

and C'' is a complex constant. Equation (35) may be rewritten as:

$$U(x_f, y_f) = C'' \iint_{s_1} \left[\iint_{s_2} e^{\frac{ik\gamma}{2}} \, dxdy \right] f(\xi, \eta) \, d\xi d\eta \qquad (37)$$

s_1 and s_2 denote integration over the (ξ, η) plane and the (x,y) plane, respectively. The term γ is given by [39] (p. 155):

$$\gamma = \frac{1}{d} \left[(x-\xi)^2 + (y-\eta)^2 \right] + \frac{1}{f} \left[(x_f - x)^2 + (y_f - y)^2 - (x^2 + y^2) \right] \quad . \qquad (38)$$

Using the binomial expansion again produces:

$$\gamma \approx \frac{1}{f} \left[v\xi^2 + vx^2 + x_f^2 - 2v\xi x - 2xx_f + v\eta^2 + vy^2 + y_f^2 \right.$$

$$\left. - 2v\eta y - 2yy_f \right] \qquad (39)$$

where

$$v = \frac{f}{d} \quad . \qquad (40)$$

After a great deal more manipulation [39] (p. 156) (not involving any more approximations) the following expression for the field at the screen results:

$$U(x_f, y_f) = A \exp \left[\frac{-ik}{2f} \left(\frac{1-v}{v} \right) \left(x_f^2 + y_f^2 \right) \right]$$

$$\cdot \iint_{s_1} f(\xi, \eta) \exp \left[\frac{-ik}{f} (x_f \xi + y_f \eta) \right] \, d\xi d\eta \quad . \qquad (41)$$

Now letting the distance d equal f, that is, placing the transparency a focal length in front of the lens ($d = f \Rightarrow v = 1$):

$$U(x_f, y_f) = A \iint\limits_{s_1} f(\xi, \eta) \exp\left[\frac{-ik}{f}(x_f\xi + y_f\eta)\right] d\xi d\eta \quad . \qquad (42)$$

Comparing Equation (42) with Equation (12), we see that the true Fourier transform does result. Very often this equation will be written in the form:

$$U(x_f, y_f) = A \iint\limits_{s_1} f(\xi, \eta) \exp\left[-2\pi i (\Omega_x\xi + \Omega_y\xi)\right] d\xi d\eta \qquad (43)$$

where Ω_x and Ω_y are the spatial frequencies of the input scene defined by: [38] (p. 61)

$$\Omega_x = \frac{x_f}{\lambda f} \quad , \quad \Omega_y = \frac{y_f}{\lambda f} \quad , \qquad (44)$$

and $A = 1/i\lambda f$ for unit amplitude plane wave illumination of the input $f(\xi, \eta)$. It can be noticed that there is a direct correspondence between the spatial measurements and frequencies given here and the time and frequencies used in the Fourier analysis of time-varying signals. The Fourier transform of a scene is produced by a lens when the transparency is placed a focal length in front of the lens and the viewing screen a focal length behind the screen. This remarkable result forms the basis for all Fourier transform matched filter work done today.

C. Holography and Optical Correlation

Suppose that, in the previous discussion, the viewing screen is replaced by a photographic film plate (such as Kodak 649F) and a collimated reference beam (derived from the original source) is allowed to interfere with the Fourier transformed image, thereby, exposing the plate. Figure 11 is a schematic representation of this. The reference beam may be represented as a plane wave having amplitude B of the form: [38] (p. 172)

$$U_r = B\, e^{-i2\pi\alpha y_f} \qquad (45)$$

where $\alpha = (\sin\theta)/\lambda$, the spatial frequency of the reference beam. The total field at the film plate is then:

$$U_T = U(x_f, y_f) + U_r(y_f) \quad . \qquad (46)$$

Substituting $U(x_f, y_f)$ from Equation (43) and $U_r(y_f)$ from Equation (45) yields:

$$U_T(x_f, y_f) = \frac{1}{\lambda f}\, F\{f(\xi, \eta)\} + B\, e^{-i2\pi\alpha y_f} \qquad (47)$$

where $F\{\ \}$ denotes the Fourier transform. The intensity of these combined beams hitting the film is:

$$I \propto |U_T|^2 = U_T^* U_T \qquad (48)$$

23
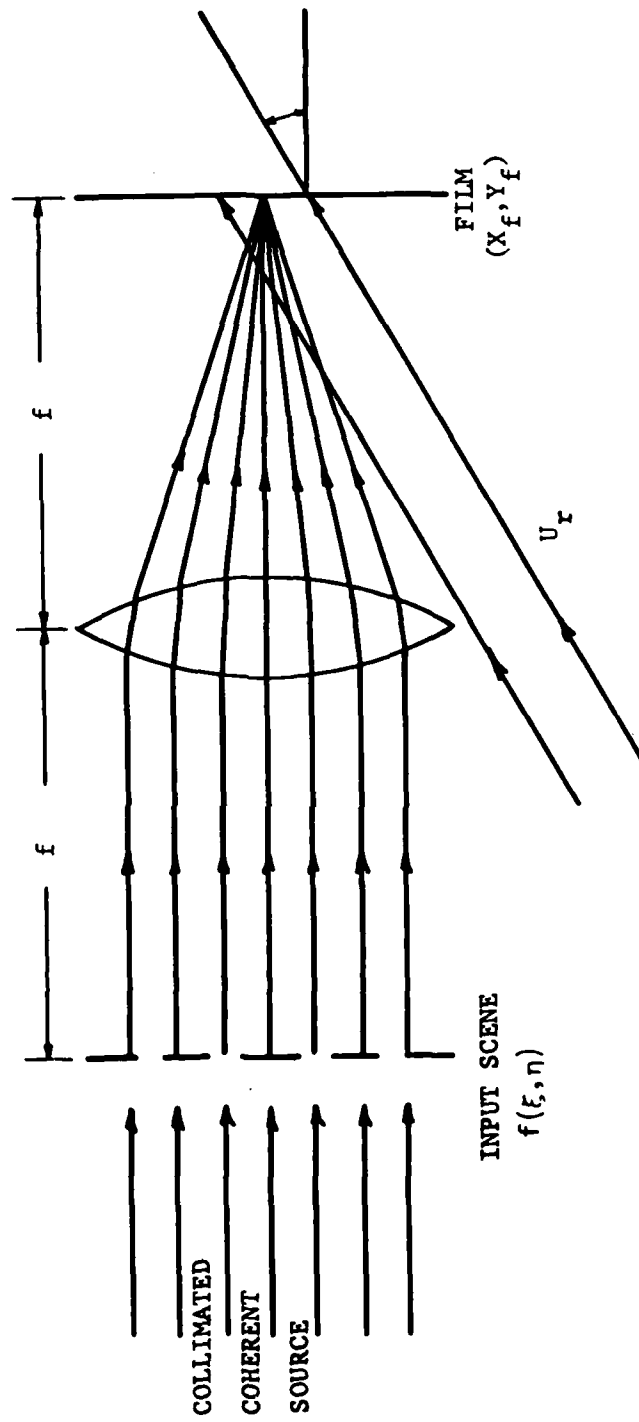
Figure 11. Fourier transform holography.

where the * (super star) denotes the complex conjugate. Performing this operation we arrive at: [38] (p. 172)

$$I = \text{const.} \left[\frac{1}{\lambda^2 f^2} \left| F \left\{ f(\xi, \eta) \right\} \right|^2 + B^2 + \frac{B}{\lambda f} e^{i2\pi\alpha y_f} F \left\{ f(\xi, \eta) \right\} \right.$$
$$\left. + \frac{B}{\lambda f} e^{-i2\pi\alpha y_f} F^* \left\{ f(\xi, \eta) \right\} \right] . \quad (49)$$

Suppose for a moment that the Fourier transform $F \{f(\xi, \eta)\}$ can be written as an amplitude and phase product such as: [38] (p. 209)

$$F \left\{ f(\xi, \eta) \right\} = A(\xi, \eta) e^{-i\psi(\xi, \eta)} \quad , \quad (50)$$

much the same way as the Fourier transform of a time-varying signal is often written as an amplitude and phase product. After substitution and a little manipulation, the intensity can be rewritten as:

$$I = \text{const.} \left[\frac{1}{\lambda^2 f^2} A^2 + B^2 + \frac{2AB}{\lambda f} \cos (\psi - 2\pi\alpha y_f) \right] . \quad (51)$$

Notice that the intensity is a function of the amplitude and phase. If the photographic plate is exposed, and assuming a linear response by the film, then the developed film will have an amplitude transmission proportional to the intensity of the interfering beams

$$t(x_f, y_f) = D \ I(x_f, y_f) \quad , \quad (52)$$

where t is the transmission and D is the film response constant. This is the mechanism by which both amplitude and phase information may be stored on an intensity-sensitive photographic plate [38] (p. 210). The developed film is called a VanderLugt or holographic Fourier transform matched filter, matched to the input scene $\{f(\xi, \eta)\}$. If this developed holographic film is placed in the arrangement sketched in Figure 12, an interesting result occurs. The function $g(\xi, \eta)$ now represents a test input scene, maybe different from $f(\xi, \eta)$. The field $F \{ g(\xi, \eta) \}$ falls on the film (again assuming coherent plane wave, unit amplitude illumination of $g(\xi, \eta)$ and is partially transmitted. The transmission is given by the product of the field and the transmission of the plate given by Equations (52) and (49):

$$U(\text{trans}) = F\{g(x, y)\} \bullet \left| F\{f(\xi, \eta)\} \right|^2 \quad (53)$$

where the constants have been omitted. This can be rewritten as (using Equation (49)):
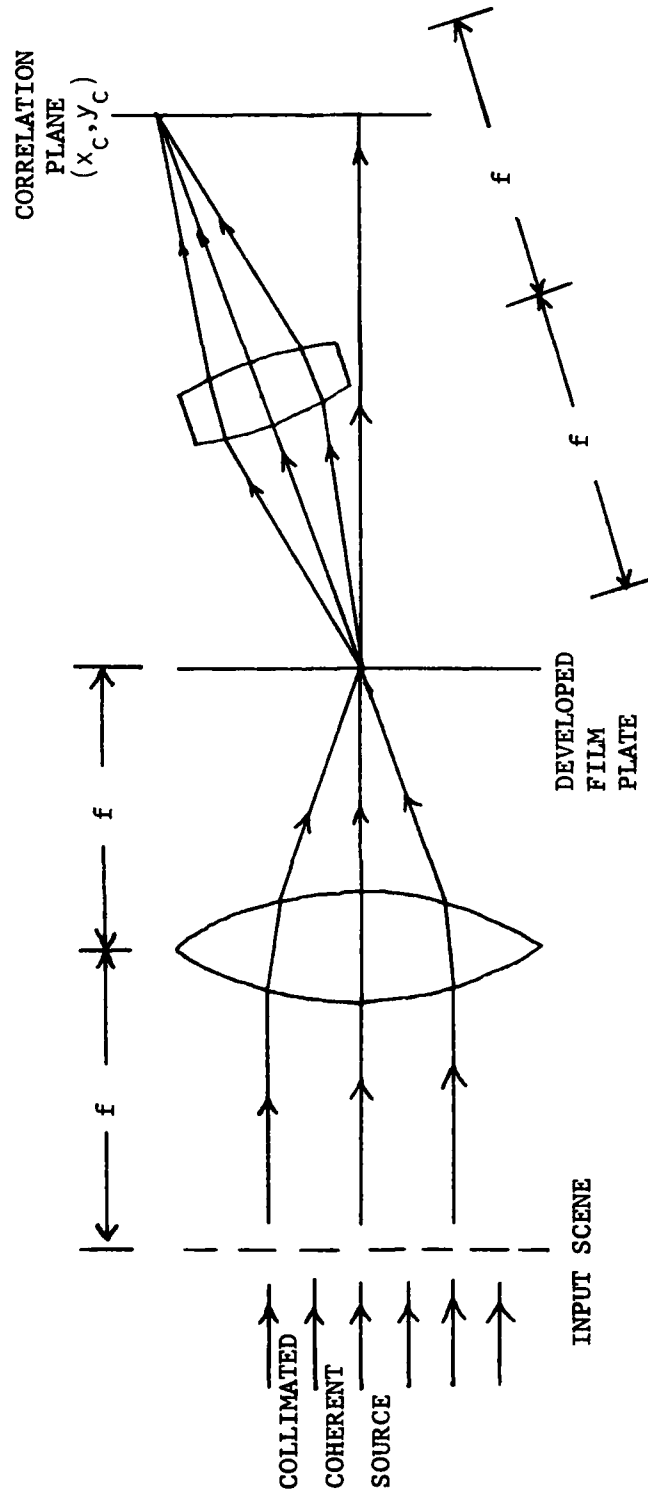
Figure 12. Holographic Fourier transform matched filtering.

$$U(\text{trans}) = \frac{B^2 \bar{G}}{\lambda f} + \frac{1}{\lambda^3 f^3} \left| \bar{F} \right|^2 \bar{G} + \frac{B}{\lambda^2 f^2} \bar{F} \bar{G} e^{i2\pi\alpha y_f}$$
$$+ \frac{B}{\lambda^2 f^2} \bar{F}^* \bar{G} e^{-i2\pi\alpha y_f} \quad , \qquad (54)$$

where

$$\bar{G} = F\{g(\xi,\eta)\} \ , \qquad (55)$$

$$\bar{F} = F\{f(\xi,\eta)\} \ . \qquad (56)$$

The final lens L_2 Fourier transforms U(trans) so that the field in the plane (x_c,y_c) is given by: [38] (p. 175)

$$U_c = B^2 g(x_c,y_c) + \frac{1}{\lambda^2 f^2}\left[f(x_c,y_c) * f^*(-x_c,-y_c) * g(x_c,y_c) \right]$$
$$+ \frac{B}{\lambda f} f(x_c,y_c) * g(x_c,y_c) * \delta(x_c,y_c + \alpha\lambda f)$$
$$+ \frac{B}{\lambda f}\left[f^*(-x_c,-y_c) * g(x_c,y_c) * \delta(x_c,y_c - \alpha\lambda f) \right] \quad , \qquad (57)$$

where we have used the relation [40]

$$F\{\bar{F}\bar{G}\} = F\{\bar{F}\} * F\{\bar{G}\} \qquad (58)$$

and * denotes the convolution. The δ function comes from the integration of $\exp(-i2\pi\alpha y_f)$. Autocorrelation is defined mathematically to be: [39] (p. 10)

$$\int_{-\infty}^{\infty} h(x)\, h^*(x-a)\, dx \quad . \qquad (59$$

The final term of Equation (57) may be written as:

$$\iint g(\xi,\eta)\, f^*(\xi-x_c, \eta-y_c + \alpha\lambda f)\, d\xi d\eta \qquad (60)$$

which is the mathematical definition of cross-correlation. Note that the value of the integral is zero unless $y_c = \alpha\lambda f$. Physically this means that the cross-correlation of $g(\xi,\eta)$ and $f(\xi,\eta)$ may be found in the (x_c,y_c) plane but only at the location when $y_c = \alpha\lambda f$; that is, when:

$$y_c = \frac{\sin\theta}{\lambda}(\lambda f) \ , \qquad (61)$$

$$y_c = f \sin\theta \quad . \qquad (62)$$

The cross-correlation is found along the trajectory of the original reference beam in the (x_c,y_c) plane. If $g(\xi,\eta) = f(\xi,\eta)$ then the result from Equation (60) is called the auto-correlation.

In application, the correlation (auto- or cross-) is a measure of the similarity of two scenes. If we have two transparencies of a scene, and lay one over the other, the amount of overlap of the two scenes is proportional to the correlation. When the two are exactly aligned, the overlap (correlation) is a maximum and when they are completely separated, the overlap (correlation) is a minimum. If light is shone through these transparencies, the transmitted intensity is a maximum when the scenes exactly align. This reasoning carries over into the Fourier transform plane in much the same way.

D. Sensitivity to Rotation

As a simple example, consider a Ronchi ruling as the input scene to the optical correlator. A Ronchi ruling in its usual capacity is a series of opaque straight parallel lines on a transparent substrate; the width of the opaque lines being equal to the separation between them. The resulting matched filter consists of a series of exposed spots - roughly circular - on either side of a strong zeroth order, very similar to what would be expected in the far field of a diffraction grating illuminated by a coherent light. A more exact description is given in Appendix A. If the exposed plate looks similar to Figure 13, the distance from the center of the zeroth order to the center of either of the closest dark circles is given by

$$x_f = \Omega \lambda f , \tag{63}$$

where Ω is the fundamental spatial frequency of the Ronchi ruling, equal to $1/(2a)$, where a is the spacing, λ is the wavelength of the illumination and f is the focal length of the Fourier-transforming lens. If the matched filter just made is addressed with the same Ronchi ruling input, it is desired to determine how the correlation will change when the input is rotated. Figure 14 illustates this phenomena. The correlation should be dependent on the area of overlap of the two circles in the Fourier transform plane. This area is given by: [41]

$$A_0 = 2 \left[R^2 \cos^{-1} \left(\frac{d}{2R} \right) - \frac{d}{2} \sqrt{R^2 - \frac{d^2}{4}} \right] . \tag{64}$$

Thus, writing $d \approx X_f \theta$, the correlation should be proportional to: [42]

$$C = \frac{2}{\pi R^2} \left[R^2 \cos^{-1} \left(\frac{X_f \theta}{2R} \right) - \frac{X_f \theta}{2} \sqrt{R^2 - \frac{X_f^2 \theta^2}{4}} \right] , \tag{65}$$

where πR^2 is a normalization factor. A plot of this equation is given in Figure 15. This may seem like a trivial example but it contains information about how the correlation intensity changes with the rotation angle and gives an indication of the role played by the spatial frequency content of the scene. The variable X_f in Equation (65) is related to the spatial frequency:

$$\Omega = \frac{X_f}{\lambda f} . \tag{66}$$

Thus, Equation (65) may be rewritten as:

28
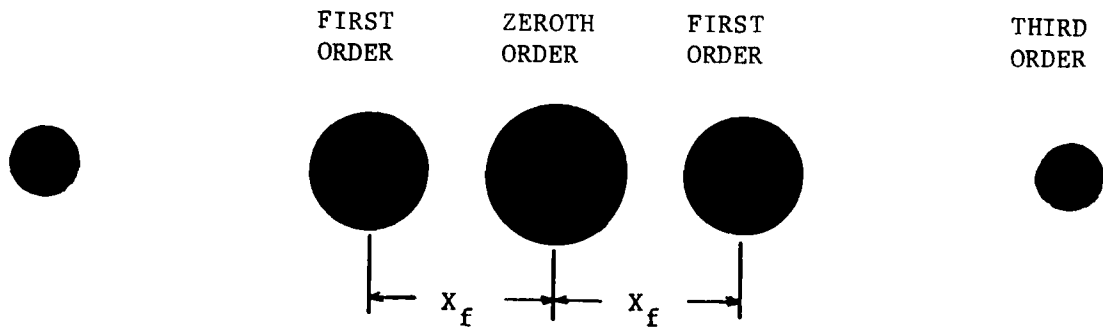
Figure 13. Schematic representation of the Fourier transform of a Ronchi ruling.
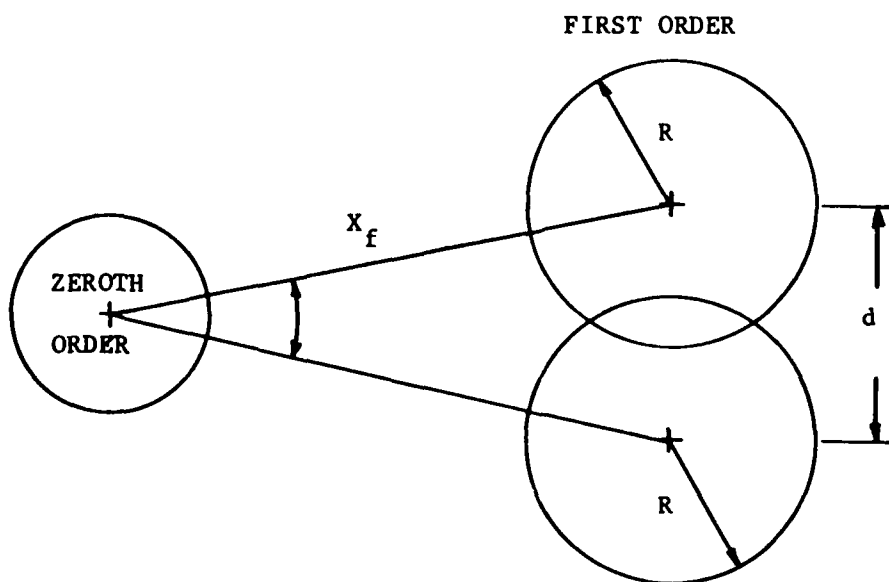
Figure 14. Geometry used in correlation versus rotation model.
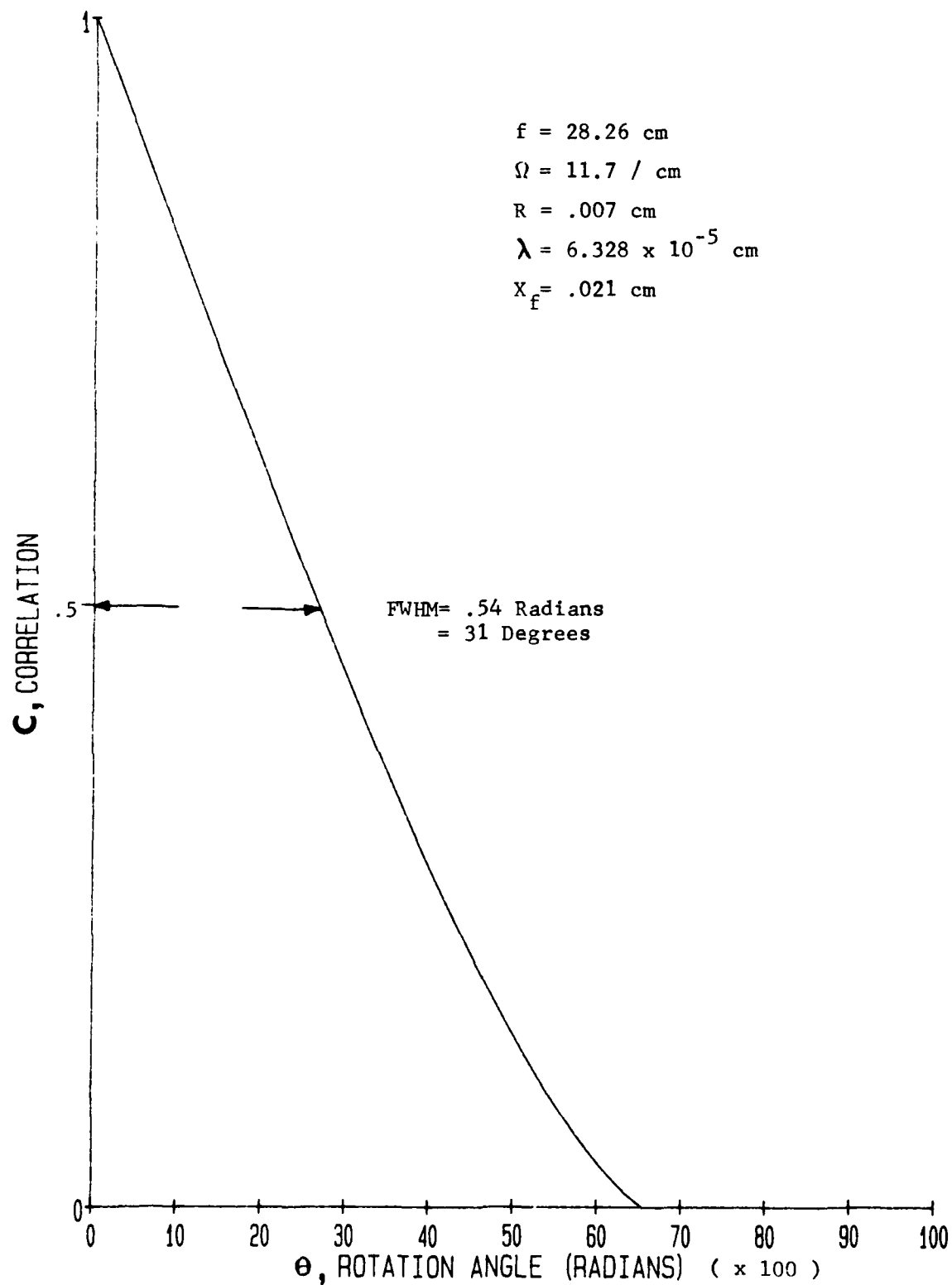
Figure 15. A plot of equation 65 -- predicted correlation versus rotation of input scene.

30

$$C = \frac{2}{\pi R^2} \left[R^2 \cos^{-1} \left(\frac{\Omega \lambda f \theta}{2R} \right) - \frac{\Omega \lambda f \theta}{2} \sqrt{R^2 - \frac{\Omega^2 \lambda^2 f^2 \theta^2}{4}} \right] \quad (67)$$

This is illustrated in Figure 16 for several different values of Ω. As one can see, the width of the correlation curve broadens when the spatial frequency decreases. This will prove useful in understanding some experimental results given later.

E.   Sensitivity to Scale

In the past, one of the problems with using Fourier transform matched filters has been the sensitivity of the correlation to a scale change. This scale change might be brought about by an airplane changing altitude or the target moving in the field of view toward or away from the detector device. Other researchers have observed a 50 percent loss in correlation for a scale change of as little as 0.5 percent [42]. A simple model of this effect is possible. Consider an input scene having a single spatial frequency content Ω, then the location in the Fourier transform plane of the first order exposed spot will be a distance:

$$X_f = \Omega \lambda f \quad (68)$$

from the zeroth order. See also the photograph of Figure 29 and the subsequent calculations. A change in scale of the input scene produces an effective linear change in the spatial frequency content of the scene now addressing the matched filter. This produces a linear shift in the location of the Fourier transform. Let the new distance from the zeroth order be given by:

$$X_f' = \Omega' \lambda f \quad (69)$$

and let

$$\sigma \Omega' = \Omega \quad (70)$$

where σ is the scale change (magnification) factor. If we assume the Fourier transform elements to be roughly circular – see Figure 17, then the area of overlap should be proportional to the correlation, C:

$$A_o = 2 \left[R^2 \cos^{-1} \left(\frac{|X_f - X_f'|}{2R} \right) - \frac{|X_f - X_f'|}{2} \sqrt{R^2 - \frac{|X_f - X_f'|^2}{4}} \right] \quad (71)$$

Thus, the correlation as a function of magnification should be:

$$C = \frac{2}{\pi R^2} \left\{ R^2 \cos^{-1} \left[\frac{\Omega \lambda f}{2R} \left| (1 - \frac{1}{\sigma}) \right| \right] \right.$$
$$\left. - \frac{\Omega \lambda f}{2} \left| (1 - \frac{1}{\sigma}) \right| \cdot \sqrt{R^2 - \frac{\Omega^2 \lambda^2 f^2}{4} \left| (1 - \frac{1}{\sigma}) \right|^2} \right\} \quad , \quad (72)$$

31
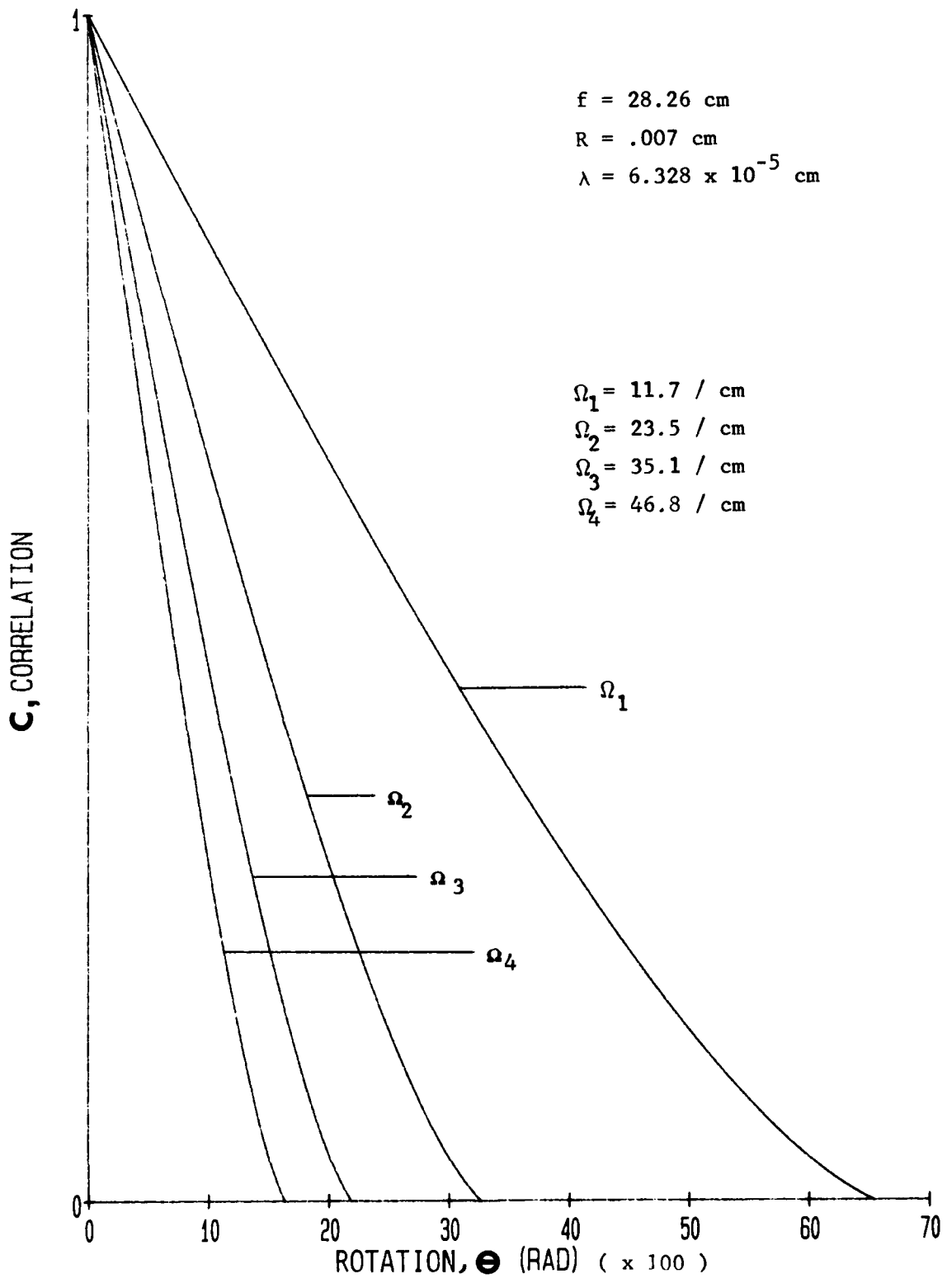
Figure 16. A plot of equation 65 -- predicted correlation versus rotation for various spatial frequency input scenes.
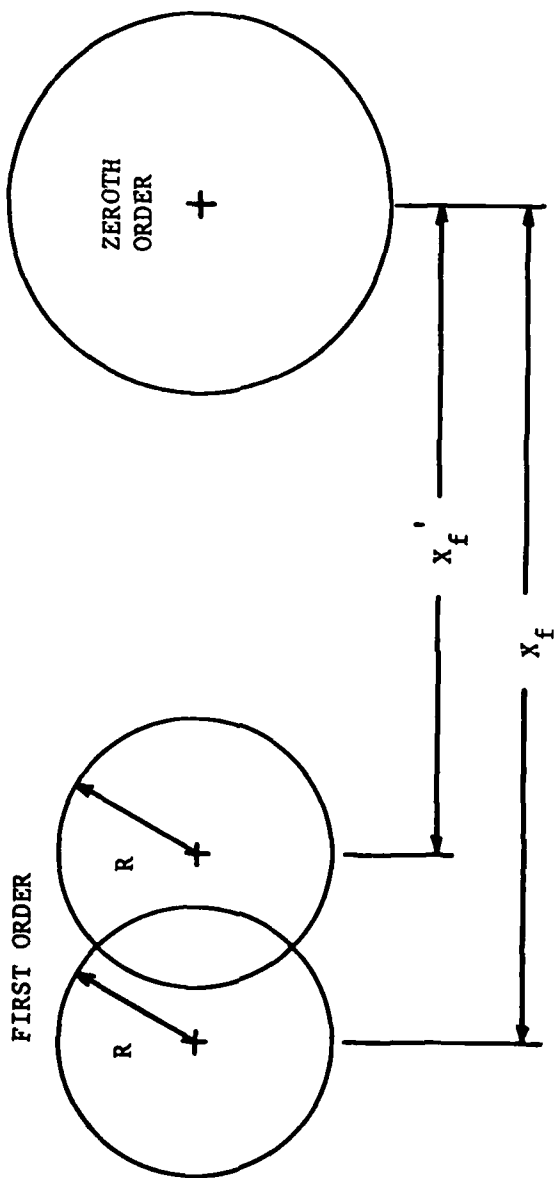
Figure 17. Geometry for scale change and tilt models.

33

where πR^2 is a normalization factor. This is illustrated in Figure 18. Note that a magnification of about 1.37 produces a 50 percent loss in correlation. This, of course, depends on the spatial frequency content much the same as the curves in Figure 16.

F. Sensitivity to Tilt

Using the previous analysis it will be fairly simple to analyze the effect of tilting the input scene. In reality this might occur any time an off-normal approach would be preferred or if the object began to turn on a longitudinal axis. Tilting the input scene (or the correlator) has the effect of changing the spatial frequency content in one direction. Assume the input scene is a Ronchi ruling having a spacing of a . Tilting the ruling with the lines as an axis reduces the effective width by a factor of cos ϕ. The fundamental spatial frequency of the ruling is given by

$$\Omega = \frac{1}{2a} \quad . \tag{73}$$

The effective spatial frequency of the tilted ruling is:

$$\Omega' = \frac{1}{2a \cos \phi} \quad . \tag{74}$$

Thus

$$X_f = \frac{1}{2a} \lambda f \tag{75}$$

and

$$X_f' = \frac{\lambda f}{2a} \sec \phi \quad . \tag{76}$$

Substituting this into Equation (71) gives:

$$C = \frac{2}{\pi R^2} \left\{ R^2 \cos^{-1} \left[\frac{\Omega \lambda f \mid (1 - \sec \phi) \mid}{2R} \right] - \frac{\Omega \lambda f \mid (1 - \sec \phi) \mid}{2} \right.$$
$$\left. \cdot \sqrt{R^2 - \frac{\Omega^2 \lambda^2 f^2}{4} \mid (1 - \sec \phi) \mid^2} \right\} \tag{77}$$

A plot of this is given in Figure 19. Notice that for this simple model, a 38 degree tilt is allowed before the correlation drops by 50 percent. The correlation does not seem to be nearly as sensitive to tilt as it is to rotation and scale change (magnification).

The three previous models of rotation, scale, and tilt are given as illustrations only. In reality an input scene contains many spatial frequencies and usually there is not a single largely-dominate one. A direct comparison between these models and experimental data is not useful except for highly specialized scenes which rarely occur in the real world. These models do, however, illustrate what might be expected in general.

34
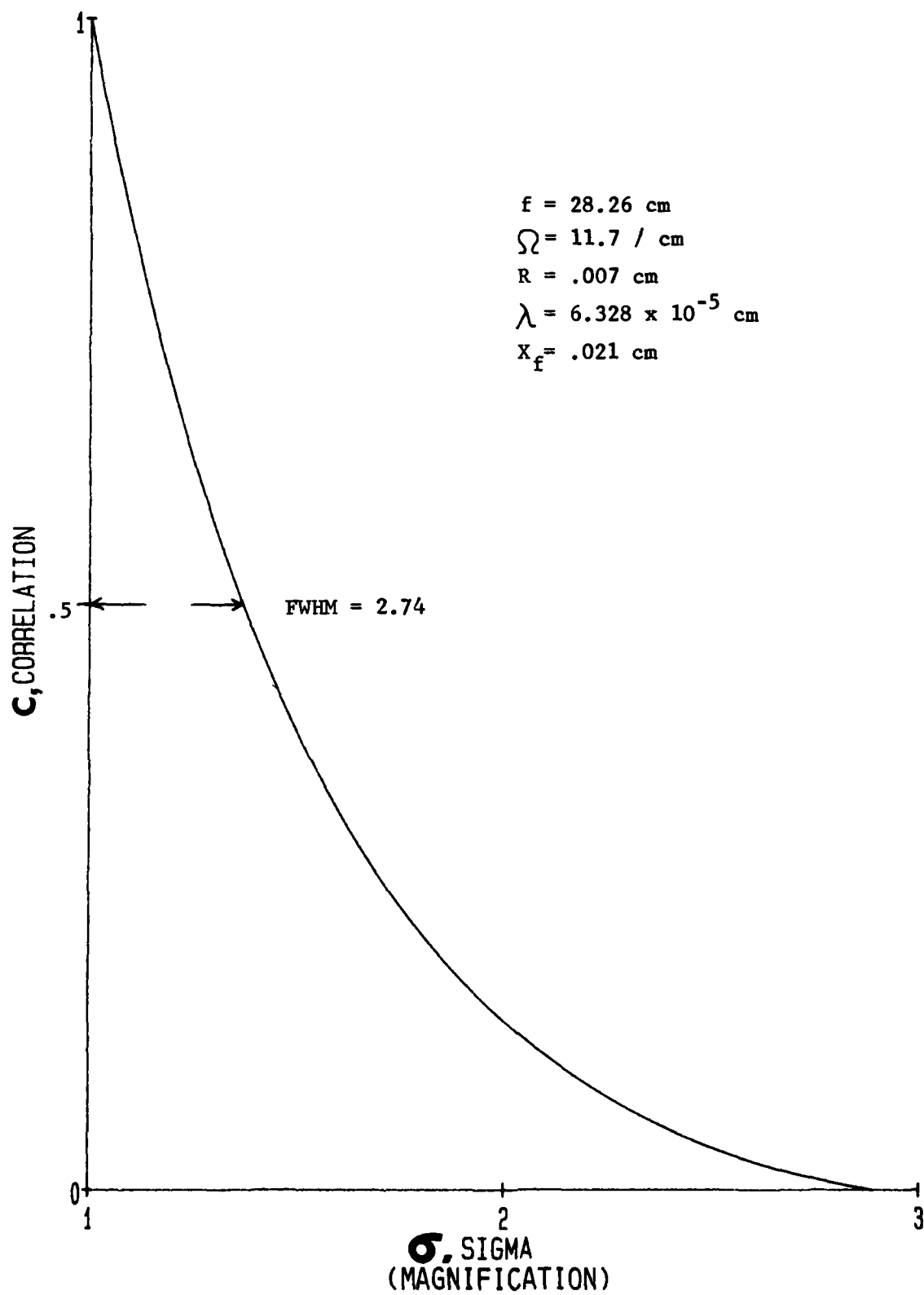
Figure 18. A plot of equation 72 -- predicted correlation versus scale change (magnification).
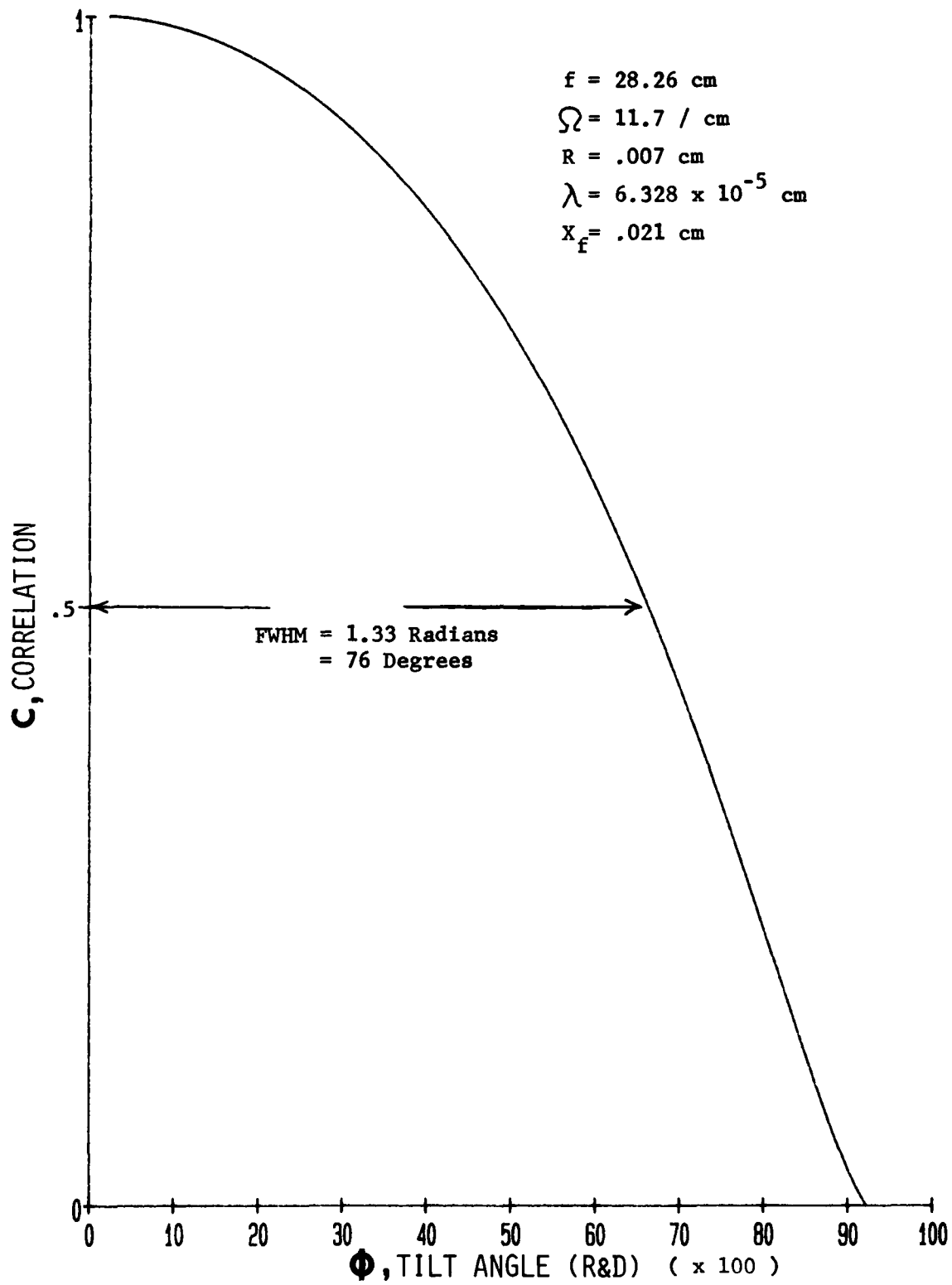
Figure 19.   A plot of equation 77 -- predicted correlation versus tilt.

G. The Multi-Foci Hololens

The details of the production of the multi-foci hololens are given in papers by Liu and Duthie [33] and Gregory and Liu [34] and are not repeated here. A brief description is given which highlights the analysis and experimental procedure. The essential element is a screen, patented by Liu, which will produce a fairly equal intensity 5X5 array of spots each of which contains the information of the incident beam. This screen was developed after much experimentation and many computer simulations. A photomicrograph of a few unit cells of this screen is given in Figure 20. Crudely speaking, the screen consists of an array of crossed broken Ronchi rulings. With the aid of carefully placed neutral density filters, this screen will produce a 5X5 array of spots which serves as the input to the optical system given in Figure 21. The incident beam I (a collimated argon ion laser) impinges upon the contact screen S discussed above; (the neutral density filters are not shown), thus, producing an array of 5X5 bright spots as well as other weaker orders. A lens L_1 is placed a focal length f_1 from the screen S. In the focal plane of this lens a square aperture A is placed to block all but the 5X5 matrix. This is then the input to a standard holographic arrangement. The placement of lens L_2 determines the magnification of the resulting holographic element. At a distance f_2 (the focal length) from the lens, a dichromated gelatin photographic plate is placed. A reference beam, derived from the original argon ion beam, is allowed to interfere with the object beam at the holographic plate F. The exposed plate is then developed and sealed with a thin glass cover plate since dichromated gelatin holograms are known to be humidity-sensitive [43]. The holographic plate, when reilluminated, will thus produce a 5X5 array of Fourier-transform elements off-axis and along the path of the original reference beam; see Figure 22. Figure 23 is an actual photograph of the array – magnified about five times.

The array is produced in focus a distance f_h away from the plate. If the distance d_o in Figure 21 is called the object distance then the image distance is given by:

$$d_i = f_2 + f_h \tag{78}$$

so that the geometrical thin lens equation is:

$$\frac{1}{d_o} + \frac{1}{d_i} = \frac{1}{f_2} \quad . \tag{79}$$

Thus, the focal length of the hololens can be written as:

$$\frac{1}{f_h} = \frac{d_o}{f_2} \left(\frac{1}{f_2} - \frac{1}{d_o} \right) \quad . \tag{80}$$

The magnification is given by:

$$M = -\frac{d_i}{d_o} \tag{81}$$

$$= -\frac{d_i}{f_2 + f_h} \tag{82}$$

37
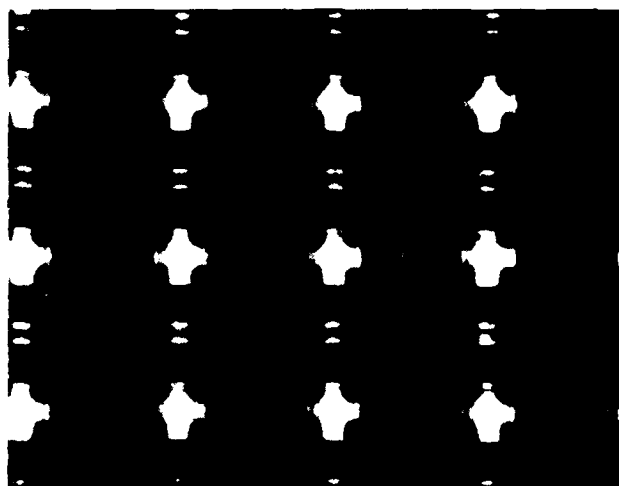
Figure 20. A few unit cells of the diffraction screen used in making the hololens (magnification unknown).

38
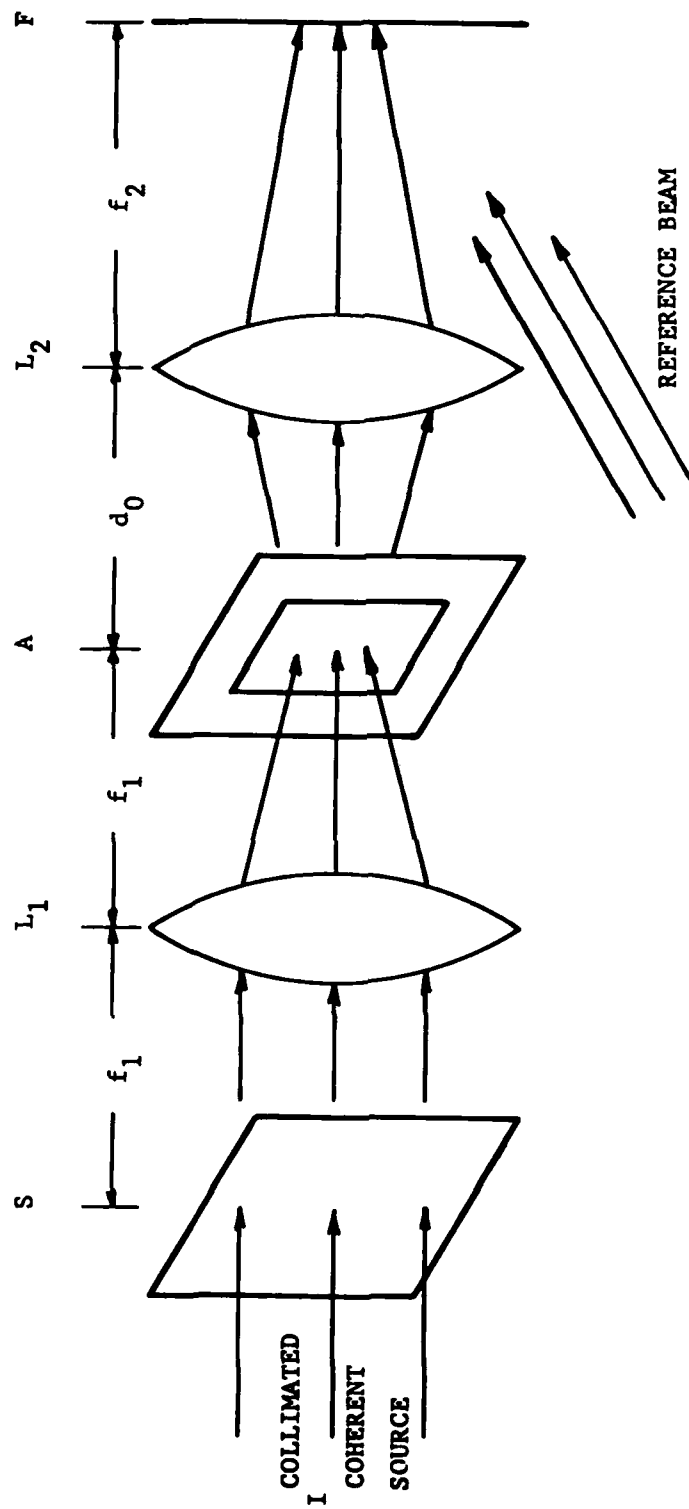
Figure 21. Optical system for making the hololens.

39
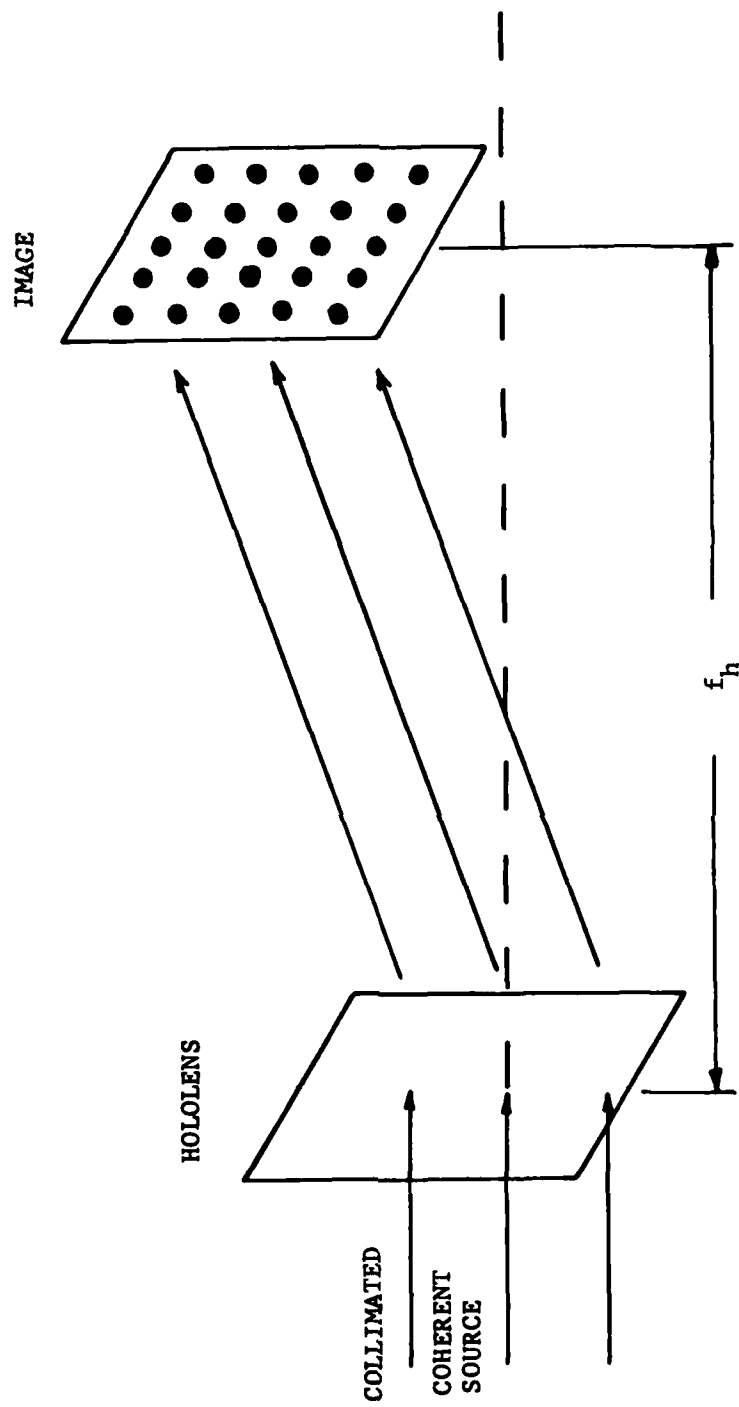
Figure 22. Producing the 5X5 array of Fourier transforms.

40
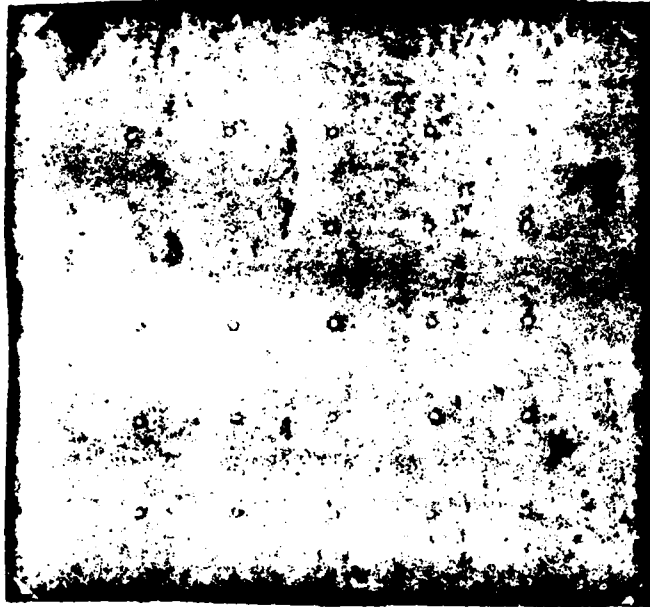
Figure 23. A photograph of the 5X5 array produced
by the hololens (M = 5).

Therefore, it is possible to tailor a hololens to meet the specific require-
ments of the experiment. The hololens used in this investigation had a focal
length of 28.26 centimeters and produced an off-axis array of 5X5 spots with a
separation of 2.7 mm between them. This combination proved to be quite
satisfactory.

III. EXPERIMENTAL PROCEDURES

A. The Experimental Arrangement and Operation

The basic experimental arrangement used to make matched filters has not changed appreciably in 20 years. The Vander Lugt method, as outlined in Section I, is still the most widely used in optical data processing. The fundamental elements are a Fourier-transforming lens (or mirror), a coherent light source and a medium, such as a photographic plate, for recording the filter. The input scene may be a transparency or, in this case, a coherent image produced by a LCLV.

Figure 24 gives the experimental arrangement as set up on a granite table. The image on TV monitor 1 is transmitted from TV camera 1 which views the scene mounted on a table which has rotation and tilt capabilities. The image produced by TV screen 1 is focused onto the "write" side of the Hughes LCLV. The illumination of the "read" side of the LCLV is provided by a 15 MW HeNe laser (Spectraphysics model Stabilite). After going through a beam-expanding and collimating arrangement, the beam is split using a dielectric coated beamsplitter into two reasonably equal intensity beams. One of these beams becomes the reference beam; the other strikes the LCLV causing the polarization of the beam to be spatially modulated according to the intensity modulation provided by the television screen input. The details of the operation of the LCLV are given in a later section.

The beam containing spatial polarization information about the input scene travels back from the LCLV through the beamsplitter and on to polarizer 1. The function of this polarizer is to turn the polarization-modulated beam back into an intensity-modulated beam. The purpose of the apparatus described to this point is to produce a coherent image of the input scene. The hololens performs two functions: the coherent input image is split into 25 identical images and each of these images is Fourier-transformed. The details of this holographic element were discussed in Section II. A photographic plate (Kodak 649F or 120) is placed a focal length (28.26 cm) behind the lens. An exposure is made by removing the beam block from the reference beam and activating the shutter for a specified amount of time. The purpose of polarizer 2 is to insure that the object and reference beam are of the same linear polarization.

The mask shown in Figure 24 allows only one of the elements of the array to pass along with the reference beam. The location of the mask is computer-controlled for accurate positioning. After exposing as many of the elements as desired, the plate is removed and developed using standard techniques [44]. The developing procedure is given in Appendix B. The developed plate is then placed back in the system in its original position. The reference beam is then blocked and the mask removed (for parallel-addressing). The object beams fall on the matched filters just created and if any one of the filters correlates with the input scene now on the TV screen, a reconstructed reference beam will result from the plate. This beam is Fourier-transformed by lens L_2 onto an RCA CCD camera (Model TC 1160) and viewed as a localized bright spot on TV monitor 2. The Colorado video analyzer (Model 321) translates the brightness of the spot into a voltage which is input to a chart recorder
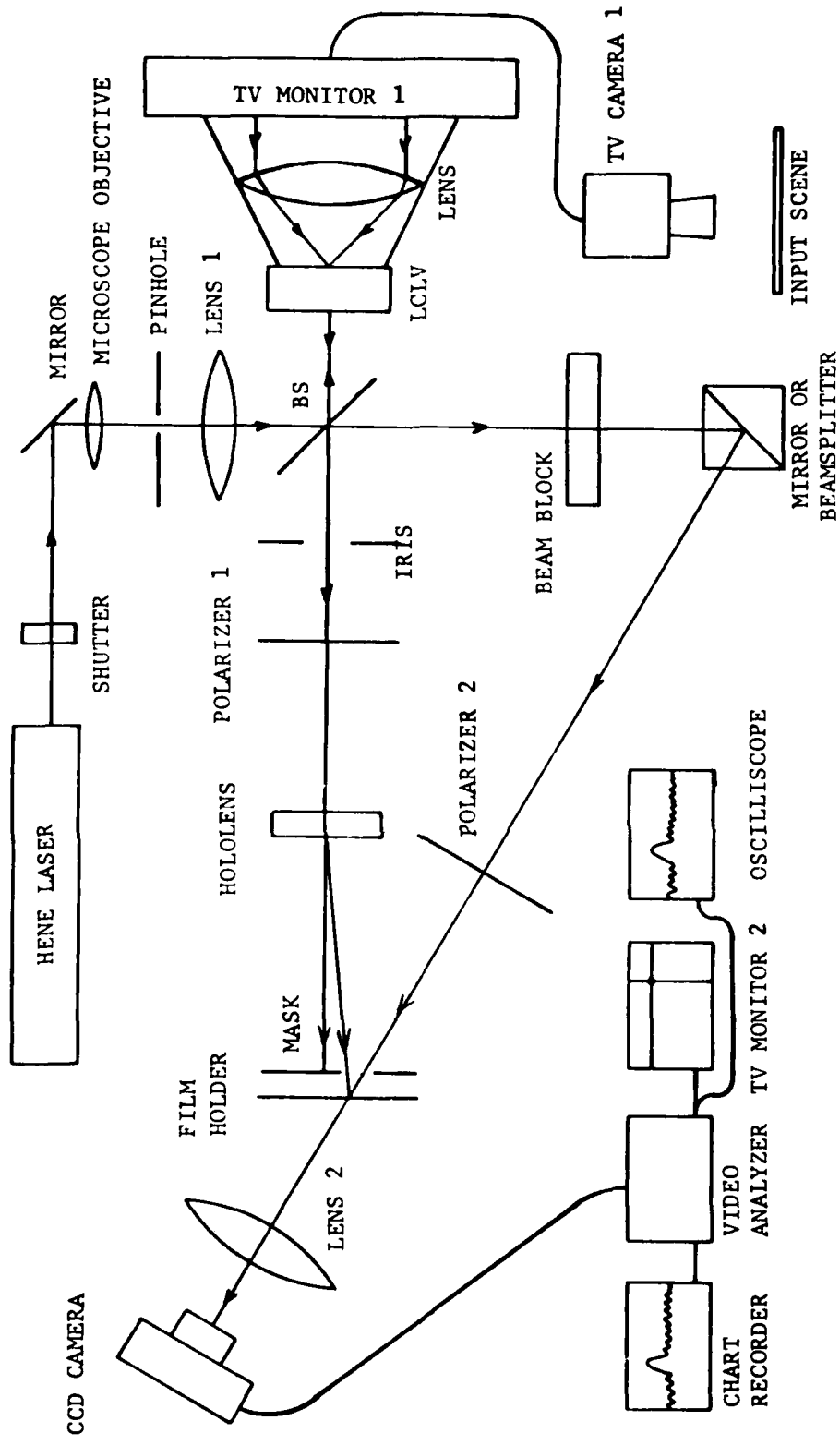
Figure 24. Real time optical correlator -- experimental arrangement.

44

(Hewlett Packard Model 680). The correlation intensity may also be displayed on an oscilloscope directly and photographed if desired. The input scene can then be rotated, tilted, translated, or changed completely as the chart recorder displays the change in intensity of the spot.

B. The Liquid Crystal Light Valve (LCLV)

Figure 25 gives a schematic drawing of the LCLV used in this research. Details of the fabrication and testing of this type device are given in several papers [45] [46]. The LCLV used in this research was made by the Hughes Corporation. In operation [28], incoherent light from a television monitor or other source passes through the transparent glass face plate and through the transparent conductive electrode (a tin oxide indium oxide glass) and strikes the photosensor composed of a layer of cadmium sulfide. This material becomes conductive when the light areas of the image are present. The charges supplied by the power source collect on the surface of the dielectric mirror corresponding to the conductive areas of the photosensor, thus, creating an electric field across the twisted nematic liquid crystal. This liquid crystal has been preoriented using the liquid crystal alignment films which consist of linearly scratched surfaces so that the nematic liquid crystal "needles" go through a 45 degree twist from one surface to the other. The pref- erentially applied electric field causes selected areas of the liquid crystal to untwist proportional to the strength of the localized field and try to align with the applied field. The plane-polarized coherent projection light enters through a transparent glass substrate, passes through the liquid crystal and is reflected back by the dielectric mirror. Selected areas of the beam will undergo a polarizatrion change provided by the preferential twist and the intrinsic birefringence of the liquid crystal: Dark areas of the incoherent "write" image produce areas in the "read" beam that are plane-polarized. Light areas produce (in general) elliptically-polarized areas in the "read" beam. Thus, the reflected beam is polarization-encoded with the original incoherent image. The resulting coherent image may then be decoded using a linear polarizer, producing an image with a continuous intensity variation. Complete details of the operation of this device are given by Grinberg [27].

Since its production, the Hughes LCLV has been tested and analyzed by several authors [47] [48]. Resolution has been one of the main problems along with response time. The resolution of the LCLV used in this investigation was measured using a series of Ronchi rulings consisting of flat black lines on a white background. It was found that slightly less than 20 lines per millimeter (lines/mm) could be distinguished. This was partly due to the resolution of the television monitor used as the input. Assuming 512 lines across a 10-inch television screen focused to a 1-inch image gives a needed resolution of 20 lines/mm. Hughes quotes the LCLV as having a resolution of 60 lines/mm and a modulation transfer function of 50 percent at this frequency. If this is true, it seems the television monitor is the limiting piece of equipment.

The reaction time was not measured in this investigation but is quoted by Hughes as being 25 ms. Other characteristics of the LCLV are given in Table 1 [28]. Even though the LCLV certainly has its limitations, it is still the overall best incoherent-to-coherent converter available today. Research is underway at the Army Missile Laboratory in an attempt to improve its performance.

45

OPTICAL GLASS SUBSTRATE

GLASS FACE PLATE

TRANSPARENT CONDUCTIVE ELECTRODE

COHERENT INCIDENT AND READ LIGHT

INCOHERENT WRITE LIGHT

TRANSPARENT COUNTER ELECTRODE

LIQUID CRYSTAL ALIGNMENT FILMS

NEMATIC LIQUID CRYSTAL

DIELECTRIC MIRROR

PHOTOSENSOR

LIGHT BLOCKING LAYER
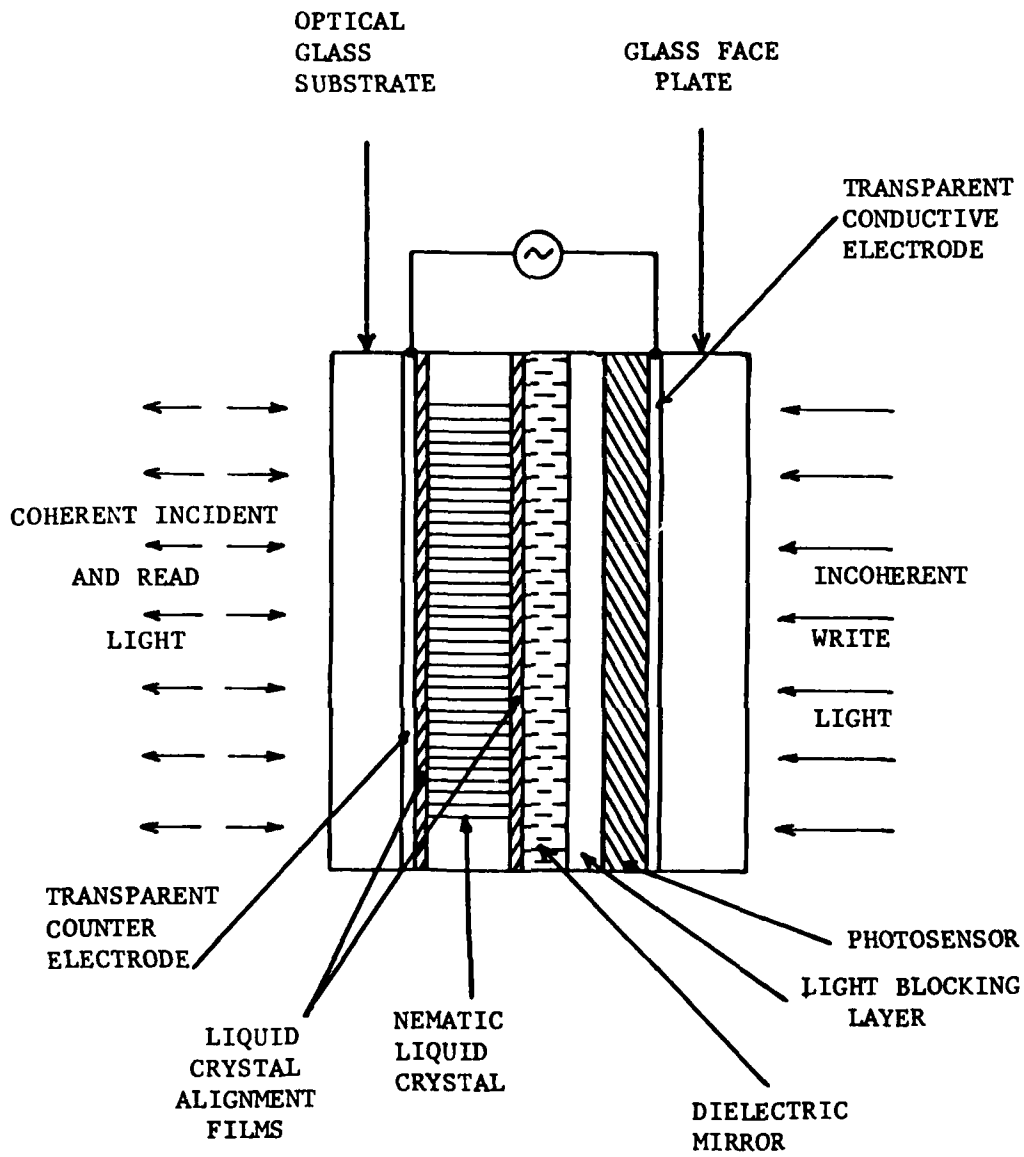
Figure 25.   The Liquid Crystal Light Valve (LCLV).

46

TABLE 1. Characteristics of the Hughes Liquid Crystal Light Valve (LCLV).

Aperture Size	1 in.^{2} (1 in. X 1 in.)
Sensitivity	160 μw/cm^2 AT 5250Å
Resolution	60 lines/mm at 50% MTF
Contrast	> 100:1
Grayscales	9

Speed
  Excitation
  Extinction
	
	10 msec
	15 msec

Reflectivity	> 90%
Optical Quality	< λ/4 at 6328Å
Voltage	6V(rms) @ 10 KHz (variable)

Other light modulators include the Pockel's Read-Out optical Modulator (PROM) and various photoplastic devices. PROM devices are fabricated from several electro-optical crystal materials such as ZnS, ZnSe, and $Bi_{12}SiO_{20}$ and convert an incident intensity pattern to a voltage pattern. The areas of the crystal not experiencing a voltage act like a half-wave retardation plate to the coherent "read" light. Thus, the coherent image is polarization-encoded and an analyzer (polarizer) can convert it back into an intesity-encoded image. This device shows great promise but at the present time is quite expensive and cannot maintain the coherent image for very long when even moderately intense illumination is used. Photoplastics are phase recording materials with the input intensity being recorded as deformations on a pliable surface. At present, these devices are quite slow and not very sensitive [39] (p. 133).

C. Photographic Techniques

Photographic techniques are an integral part of producing holographic matched filters. In this investigation Kodak high resolution holographic plates (649F or 120) were used exclusively. These plates are quoted as having a resolution of better than 2000 lines/mm [49]. The high resolution film allows separation between spatial frequencies that are very similar.

Figure 26 is a photograph of a magnified matched filter. The input scene was an aerial photograph of Huntsville, AL discussed later in Section IV. The magnification in this photograph is about 100; thus, the actual diameter of the filter is roughly .035 cm. The minimum sensitivity of Kodak 649F is about 8 X 10^{-5} Joules per square centimeter (J/cm^2) and about 4 X 10^{-5} J/cm^2 for type 120 [49]. The exposed area is roughly 1 X 10^{-3} cm^2 (assuming a circle of diameter .035 cm). The average power of each of the elements was typically .15 μW.

Figure 26. <u>A photograph of a matched filter of an</u>
<u>aerial map of Huntsville, AL (M = 100)</u>.

Thus, the exposure time needed to reach minimum sensitivity is given by:

$$t_{min} = \frac{P}{\rho A} \quad , \tag{83}$$

where t_{min} is the minimum exposure time, P is the power, ρ the minimum sensitivity, and A is the area being exposed. Using the previously given rough values, t_{min} is found to be about 2 seconds for 649F film and about 4 seconds for type 120. In practice, exposure times of 10 to 12 seconds were used to obtain the best matched filters. The calculated times served as a good starting point to begin the investigation. The emulsion thickness of each of the films was about 17 μm for 649F and about 6 μm for type 120 [50]. Six μm, is considered an average thickness for photographic emulsions. The film was developed using well established procedures: 6 minutes in slightly agitated D-19 developer, 3 minutes in Kodak stop bath, and 1 minute in Hunts Aerofix fixer. The plate was then placed in a water bath for at least 5 minutes, rinsed with absolute ethanol and allowed to air-dry. Complete details are given in Appendix B.

D. Multiply Exposed Filters

Previously it was mentioned that Christensen was able to obtain good correlation of eight targets addressed in series by multiply exposing the photographic plate [31]. This was also used in this investigation; results are given in Section IV. A phenomena called the intermittency effect should be mentioned at this point: several exposures are not, in general, equal to a single exposure of the same total duration [51]. A paper by Johnson [52], dealing with multiply exposed holograms gave data that indicated that the exposure times used should be roughly a function of the square of the number of exposures made:

$$\varepsilon_N = AN^2 + B \tag{84}$$

where A and B are constants and N is the order of the exposure. ε_N is the exposure time for the Nth exposure. Biedermann [53] suggests the exposure time be increased about 12 percent over the previous one for each successive exposure using Scientia 10E70 plates which are similar to Kodak 649F. In the present investigation, multiple exposures were made by rotating the input scene by computer control between exposures. The exposure times required were also programmed into the computer as necessary.

E. Equipment

The following is a list of the equipment used throughout this investigation along with appropriate identification and serial numbers where applicable. The USA designation indicates a local property control number:

1. Helium-Neon laser, Spectraphysics Model, Stabilite, S/N CJ-111 (USA).

2. Liquid crystal light valve, Hughes Research, 45° biphenyl nematic, S/N 10962, CJ 137 (USA).

3. Television camera, CCD, RCA Electronics, Model TC-1160, S/N B001669.

4. Television camera, vidicon, RCA Electronics, Model TC-1005, S/N CJ 043 (USA).

5. Image digitizer, Colorado Video Model 321, S/N 231.

6. Hololens, Lumin Electro-Optics (H. K. Liu), Model LUMIN025.

7. Television monitor, Videotek, Model VM12PR, S/N 1282118B.

8. Television monitor, Sony Model CVM-194, S/N 015612.

9. Computer, Hazeltine, Model 1500, S/N CJ266 (USA).

10. Translation stages, Ealing (2 each), Model 352427 and 352419, S/N CJ 273 (USA) and CJ 103 (USA).

11. Ealing rotation stage, Model 344614, S/N CJ 141 (USA).

12. Isolation table, Granite Do-All, S/N 2486-3.

13. Power meter, NRC, Model 880, S/N 1010178.

14. Photographic plate, Kodak 649F and type 120.

15. Various lenses, polarizers and beamsplitters supplied by several vendors.

16. Power supply, Hewlett-Packard, Model 8116A, S/N CJ 089 (USA).

17. Rotation and tilt stage, Scientific Atlanta, Model 4116-10, S/N CJ 051 (USA).

18. Oscilloscope, Tektronix, Model 7603, S/N CJ 162 (USA).

19. Chart recorder, Hewlett-Packard Model 680

20. Digital voltmeter, Keithley, Model 179.

IV. EXPERIMENTAL RESULTS

A. Testing of Hololens

The hololens used in this investigation was made by H. K. Liu of the University of Alabama, Tuscaloosa. A lens of this type had never been used or tested before so two basic experiments were devised to measure its performance. The screen used by Liu and Duthie had several problems associated with it, the major one being the lack of uniformity in intensity of the array produced by the element [33]. The first test was to photograph the array using a long exposure and look for extraneous diffraction orders. The photograph is shown in Figure 27. One can see that the extra orders are visible but are down in intensity several orders of magnitude when compared with the 25 primary elements of the array; thus, the "cross-talk" was not expected to be a problem. The separation between the elements was found to be a regular 2.7 mm. The focal length of the hololens was measured to be 28.26 cm. In order to have "cross talk" between elements it would be necessary to have a scene with a spatial frequency component which would extend half the distance between elements, thus, giving overlapping exposures. Equations (66) predicts this spatial frequency to about 75/cm which is almost four times the highest fundamental spatial frequency that can be obtained using a 10-inch, 512 line standard television.

As previously mentioned, the intensity distribution in earlier diffracting holographic elements was quite nonuniform. The power contained in each element of the present array was carefully measured using a detector (NRC Model 880) tuned to the HeNe wavelength. The results of this measurement are given in Table 2. As one can see, there is still a variation in intensity over the field, but the uniformity is greatly improved over that measured by Liu and Duthie.

TABLE 2. Power Distribution in the Image Plane of the Hololens.

y-order	x-order				
	-2	-1	0	1	2
2	.40	.54	.34	.48	.33
1	.52	.68	.43	.62	.41
0	.77	1.00	.61	.94	.60
-1	.52	.70	.44	.66	.44
-2	.40	.53	.34	.52	.33

Note: Power distribution (in μw) of each of the 25 focuses of the holographic element with a uniform LCLV input. LCLV is driven at f = 1400 Hz and V = 6.5 volts.
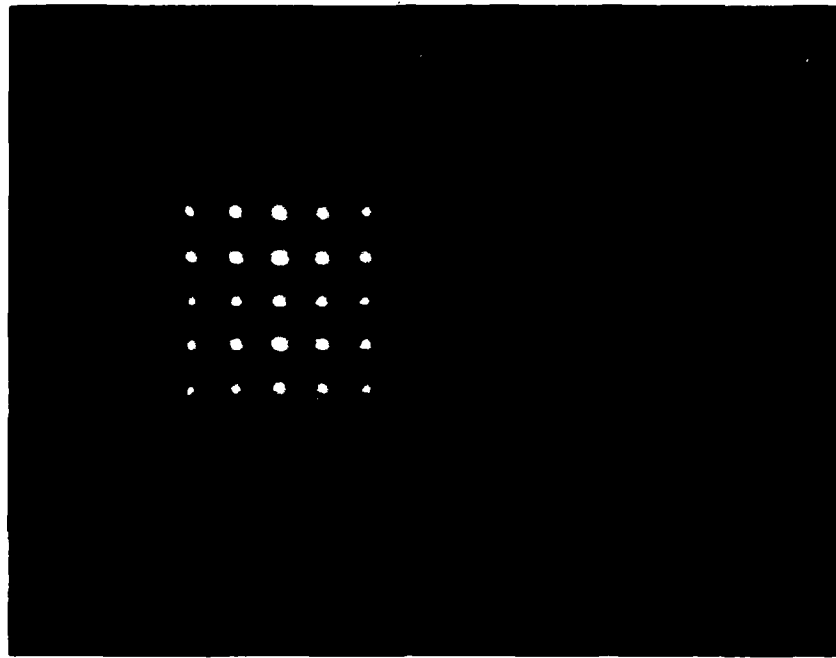
Figure 27. A long exposure photograph of the 5X5
array showing higher orders (M = 2.3).

The voltage and current used to drive the LCLV is typical of that used throughout this investigation. It is interesting to observe that the average power over all 25 elements is .54 µW which is the value of the power measured at location (-1,2). This experiment was repeated several times with different adjustments of the LCLV with the same result; position (-1,2) was the average power of the array. The standard deviation σ was calculated to be .18 µW for the 25 data elements of Table 2. The variation in intensity of the elements generally caused no major problems until the last phase of the research when many filters were stored at each of the elements. The exposure times and beam ratios became critical at this point and a very uniform array would have made for better correlations.

The efficiency of the hololens was next investigated. It is known that holograms stored using dichromated gelatin plates can have efficiencies of 70 percent or better [54]. The hololens made by Liu and used in this investigation was quite disappointing in this respect. An incident power of 104 µW in a well-collimated HeNe beam resulted in a total power of 5 µW in the 5X5 array. This is an efficiency of about 5 percent. The remaining power went mostly into the zeroth (undiffracted) order. The laser used for this entire work was a 15 mW Spectraphysics (Stabilite Model). Thus, even with a low efficiency hololens it was possible to obtain enough power to produce the exposures needed. Because of the low efficiency, however, some exposure time were inordinately long (15 seconds) which can certainly cause problems if vibrations of the system are present. This problem was not observed, however.

The next test was to see if the screen actually performed that task of a lens under the same circumstances. That is, does each spot represent the Fourier transform of the coherent input? According to Goodman [38] (p. 86), the distribution of the field in the back focal plane for a transparency (aperture, etc.) located in the front focal plane illuminated with a coherent plane wave is:

$$U(x_f, y_f) = \frac{A}{j \lambda f} \iint\limits_{-\infty}^{\infty} t_o(x_o, y_o) \exp\left[\frac{-j 2\pi}{\lambda f}(x_o x_f + y_o y_f)\right] dx_o dy_o \qquad (85)$$

where A is the amplitude of the incident plane wave, f is the focal length of the lens and λ is the wavelength of the light. (x_o, y_o) represents the front focal plane while (x_f, y_f) denotes the Fourier transform plane and $t_o(x_o, y_o)$ is the transmission function.

For a circularly symmetric aperture a transformation of coordinates is possible, resulting in [38] (p. 16)

$$U(\rho) = \frac{A \pi R^2}{\lambda j f} \left[\frac{2 J_1(2\pi\rho R)}{2\pi\rho R}\right] \qquad (86)$$

where

$$\rho = \frac{1}{\lambda f} \sqrt{x_f^2 + y_f^2} \tag{87}$$

is the radial spatial frequency, J_1 is a Bessel function of the first kind, order one and R is the radius of the circular aperture. The intensity is then proportional to $U(\rho)$ times its complex conjugate.

$$I(\rho) = \frac{A^2 \pi^2 R^4}{\lambda^2 f^2} \left[\frac{2J_1(2\pi\rho R)}{2\pi\rho R} \right]^2 . \tag{88}$$

The first zero in J_1 occurs when

$$2\rho R = 1.22 \tag{89}$$

or

$$\frac{2R}{\lambda f} \sqrt{x_f^2 + y_f^2} = 1.22 . \tag{90}$$

Looking only at the x_f dependence because of circular symmetry:

$$\frac{2R}{\lambda f} x_f = 1.22 \tag{91}$$

or, solving for x_f

$$x_f = \frac{1.22 \lambda f}{D} \tag{92}$$

where D = 2R is the diameter of the aperture.

If the hololens actually behaves as well as a lens, then this equation should be valid when a circular aperture is placed a focal length before the element (28.26 cm). Using an aperture of about 2.5 mm (an adjustable iris) and a wavelength of .6328 μm, the pattern of Figure 28 results. This is a photograph of the exposed and developed Kodak 649F plate used to record the intensity pattern. The distance to the center of the first dark ring is predicted to be

$$x_f = \frac{1.22 \ (.6328 \times 10^{-6} M) \ (.2826 \ M)}{.0025 \ M} \tag{93}$$

$$x_f = .0089 \ cm. \tag{94}$$

A measurement yielded .0080 cm which is reasonable agreement (10 percent error).
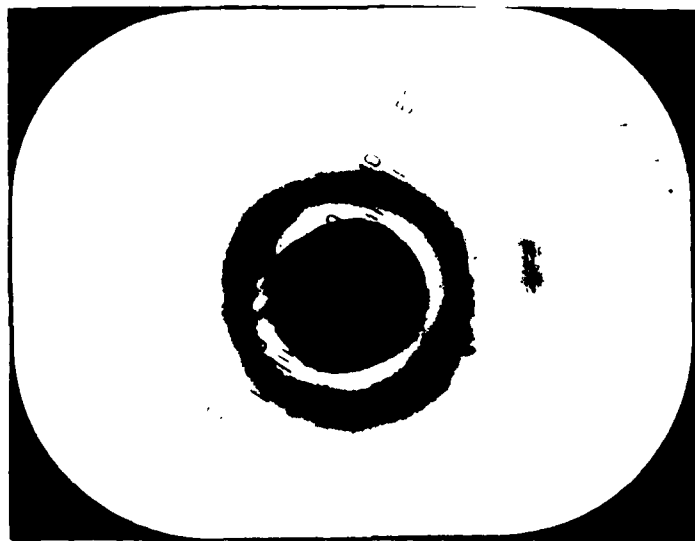
.008 cm

Figure 28. A photograph of the pattern produced using a 2.5 mm circular aperture as the input to the hololens (M = 200).

Figure 29. <u>A photograph of the pattern produced using a Ronchi</u>
<u>ruling as the input scene to the hololens (M = 80)</u>.

A Ronchi ruling type input scene was then used as the input to the television camera of Figure 24. The ruling consisted of equally spaced flat black lines on a white background. The lines were 1/4-inches wide and 1/4-inches apart. A photograph of the Fourier transform produced is given in Figure 29. The Fourier transform, in this case, was viewed via a television camera, with associated optics, placed in the focal plane. The image was then viewed on a television monitor and photographed. The separation between spots should be (from Section II):

$$\Omega = \frac{x_f}{\lambda f} \qquad (95)$$

or

$$x_f = \Omega \lambda f \qquad (96)$$

where Ω is the spatial frequency, λ is the wavelength (HeNe) and f is the focal length of the hololens (28.26 cm). The fundamental spatial frequency of the input scene is 2 per inch or .79 per cm. In this case a magnification factor of 1/8 is involved in transferring the image from the TV camera to the output of the LCLV so that the actual spatial frequency is about 6.3 per cm. The above equation thus predicts the separation between the zeroth and first order to be:

$$x_f = (6.3 \text{ cm}^{-1})(6.328 \times 10^{-5} \text{ cm}) (28.26 \text{ cm}). \qquad (97)$$

Thus, x_f should be about .011 cm. The magnification of the photo in Figure 29 was found to be about 80. This gives an average measured separation of about .012 cm, which is within 10 percent of the calculated value.

The pattern of Figure 29 is not very distinct due to the low spatial frequency of the input scene. It might be compared to results obained when looking at the diffraction pattern produced by a few slits. The greater the number of slits, the more distinct the pattern. The tests thus completed showed that the hololens does, with reasonable accuracy, perform at least some of the tasks of an ordinary lens. Difficulties did show up later and will be discussed in this Section.

B. The K Ratio

In Section III the experimental procedure outlining the making of a matched filter was given. A detail not mentioned was that of determining the optimum K ratio. The K ratio is defined as the ratio of the reference beam intensity to the object beam intensity [25]. It might seem obvious that this ratio should be one – the reference beam intensity being equal to the object beam intensity. It seems that this ratio should optimize the interference between the two beams at the photographic plate. However, the intensity at the photographic plate corresponding to one of the spatial frequency components of the input scene will not, in general, be equal to the intensity contribution due to a different spatial frequency component of the input scene. Thus, it is

57

impossible to determine a single K value that will be valid for all input scenes. This value must be determined experimentally. This knowledge will allow a matched filter to be tailored to a specific frequency component of the scene if desired. As an example, if only the outline of an object is of importance, such as an airplane, then the filter can be made using a K ratio tuned to maximize the interference in the low spatial frequency range. If, however, the problem is to distinguish between a plane with windows and a plane with no windows, the higher spatial frequencies must be emphasized. In this investigation a scene comtaining both high and low spatial frequency components was used to obtain a K value to start from initially. The scene was an aerial photograph of Huntsville, AL, shown in Figure 30. As one can see there are both fine and coarse details present. This also afforded an opportunity to study the exposure times that would be needed. Table 3 gives the results for a series of matched filters made of the Huntsville scene. The intensity of the reference beam was changed with a pair of polarizers.

TABLE 3. K-Ratio Values.

$\dfrac{P_R}{P_o}$	t (sec) Intensity (Arbitrary Units)				
1.1	9 sec	12 s	15 s	18 s	21 s
	1.34	1.62	1.47	1.27	0.98
2/1	6 s	9 s	12 s	15 s	18 s
	1.49	1.56	1.10	0.60	0.34
3/1	3 s	6 s	9 s	12 s	15 s
	1.12	1.52	0.83	0.43	0.20
5/1	3 s	6 s	9 s	12 s	15 s
	1.48	0.40	0.14	0.00	0.00
10/1	3 s	6 s	9 s	12 s	15 s
	0.62	0.00	0.00	0.00	0.00

P_o = .15 μW

NOTE: The intensities of the correlation output vs the reference to object beam ration $\dfrac{P_R}{P_o}$ and the exposure time (seconds) of a single matched filter of the photograph of the city of Huntsville.

Figure 30. A photograph of the aerial map of Huntsville (M = .36).
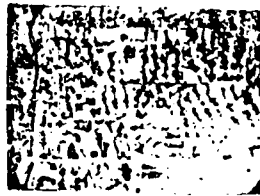
Figure 31. A photograph of the image produced by the LCLV (M = 1.4).

With available equipment, it was only possible to measure power; so in order to get an estimate of the intensity of the beams, a mask with a small (~ 1 mm) hole was placed over the detector and used consistently for all measurements. Thus, the value of K in this work may not be compared with that given by other researchers. In many cases authors will call K the ratio of the total power in the reference beam to the total power in the Fourier-transformed object beam. This K will be very large on occasions when the reference beam is much larger than the object beam as is often the case. This method of determining K did not seem reasonable for this investigation; and equipment was not readily available to determine K as Casasent did using specialized detectors and micropositioning techniques [55], thus, a compromise was sought. Placing a mask over the detector with a hole in it large enough to ensure that all the spatial frequency components would pass and using this same mask/detector arrangement to measure the power in the reference beam seemed to be a reasonable way of determining a "working value" of K. The same mask and detector were used throughout this investigation.

The intensity of the object beam, P_o, remained constant, as it was not easily changed without changing the quality of the resulting image. The best image resulted in an average power in the array of .15 μW per element. The best correlations were obtained using a K between 1 and 3 and an exposure time of about 12 seconds.

C. A Single Matched Filter

The previous tests and calculations set the foundation for making the first matched filters themselves using the hololens. It was desired to test the ability of the hololens against a glass lens in making matched filters. The hololens was replaced by a high quality glass lens of approximately the same focal length and a matched filter made of the aerial Huntsville scene. Figure 32 gives the comparison between the correlation obtained using a glass lens and that obtained with one element of the hololens. The input scene was rotated to produce the curve shown. As one can see, the hololens performed well. The full width at half maximum (FWHM) is about 2.8 degrees for the hololens and slightly less for the glass lens. The background observed using the hololens is discussed in Paragraph E of this Section. The correlation appeared as a very bright spot on the television monitor and was easily detected. These particular filters were made using a K value near one and an exposure time of 12 seconds and 649F film. The correlation curve is quite symmetric about zero degrees rotation – the position of the scene where the matched filter was made. This was found to be true to a high degree in all cases studied. It is obvious that the signal-to-noise ratio is enormous for this single matched filter. This is not the case however, when many filters are stored. This is demonstrated in the following sections. The matched filters themselves were very similar to the photograph of Figure 26. It is interesting to try to calculate the highest spatial frequency recorded. In Figure 26 the most distant dark spot is at a distance of about .055 cm. Equation (66) predicts this to correspond to a spatial frequency of about 30 per cm. This is somewhat in agreement with Upatnieks for a similar input scene and experimental arrangement [56].
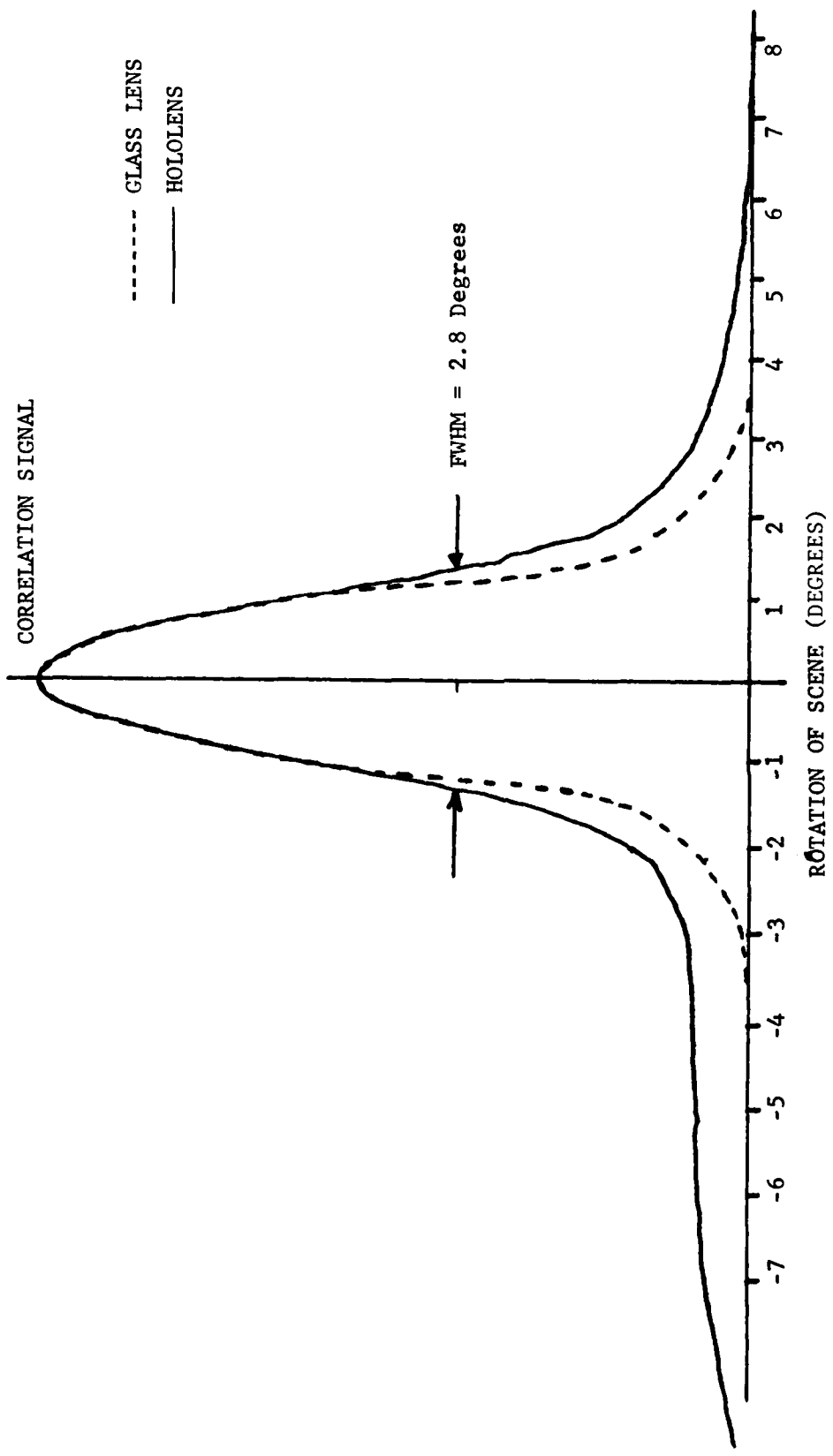
Figure 32. A comparison of correlations obtained using the hololens and using a conventional glass lens -- the input scene was an aerial map of Huntsville, AL.

D. Multiple Exposures - Eight Filters

Other researchers have shown that it is possible, using a conventional glass Fourier-transforming lens, to store several matched filters at a single location and address the filter in series [57]. A test was thus devised in this investigation to examine the possibility of doing the same thing with the hololens. A mask was used to block all but one element of the 5X5 array and this element was exposed eight times. The input scene was again the aerial view of Huntsville. In this instance, 2.5 seconds was used for each exposure with a K value of 1. The resulting correlations are given in Figure 33. The intensities are weak but clearly visible. The signal-to-noise is greater than 2 for all filters. All eight of the filters have about the same FWHM - about 3 degrees of rotation. Very little hololens background noise was observed, as was the usual case when correlations were read out in series. Some of the higher frequency noise superimposed on the curves was electrical in nature. The sensitivity of the equipment had to be increased in order to detect the weaker signals. Some of the noise could, no doubt, be filtered out with additional equipment. This was not attempted in this investigation. This part of the research did show up to eight filters can be stored using one element of the hololens. This is about the best that has been done using a conventional lens.

E. Twenty-Five Filters of One Scene - Hololens Noise

Early in the investigation all 25 elements were exposed at the same time with a single input scene. This afforded the first observation of a problem with the hololens. Figure 34 shows a typical correlation curve for the rotated aerial view of Huntsville. Notice the nonzero baseline even after a large rotation of the scene. This is a hololens contribution - not due to the scene itself. This had not been observed before and required some investigation. It was observed that this background was always much larger when all 25 elements were exposed simultaneously with the same input scene and the filters thus made addressed in parallel. This is quite likely a coherence effect. The 25 separate beams from the filters may add somewhat coherently at the detector thus producing a larger background intensity than would be expected. It was known that the correlation spot observed on the television monitor was translation-insensitive to a large degree, that is, the input scene could be linearly translated without losing the correlation spot. The bright spot would move along with the scene. The first test was to observe whether the spot would still track the scene. When the scene was translated, an interesting result took place, which perhaps should have been expected: the correlations separated. The bright spot contribution due to the scene moved as always, but another portion of the spot did not. This is illustrated in Figure 35. The scene correlation still possessed the normal rotational variance; but the "noise" correlation did not. It remained fairly constant through a 360 degree rotation of the scene. It was concluded that the noise correlation was due to the hololens itself. Thus, the correlation intensity observed on the television monitor consists of two separable parts - that due to the scene itself and that due to the hololens. It was believed that any imperfections (dirt, smudges or artifacts from the production) would show up in the correlation plane as a background. This contribution may be very small when only one element of the 5X5 array is used but it becomes quite large when all 25 elements are employed. In order to test the hololens noise contribution idea, it was
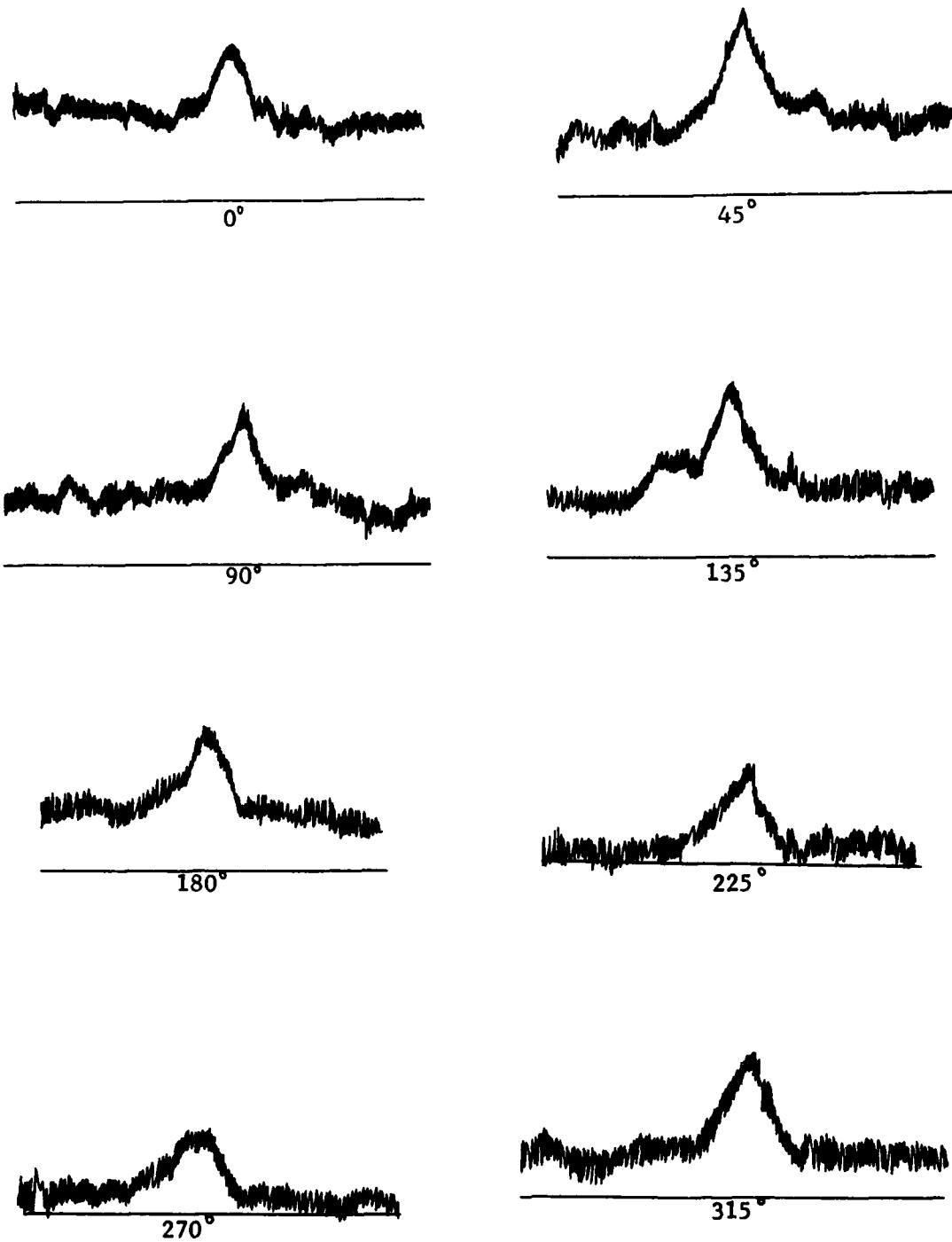
Figure 33. Correlations of eight filters stored at one element of the 5X5 array. The input scene was an aerial photograph of Huntsville, AL.
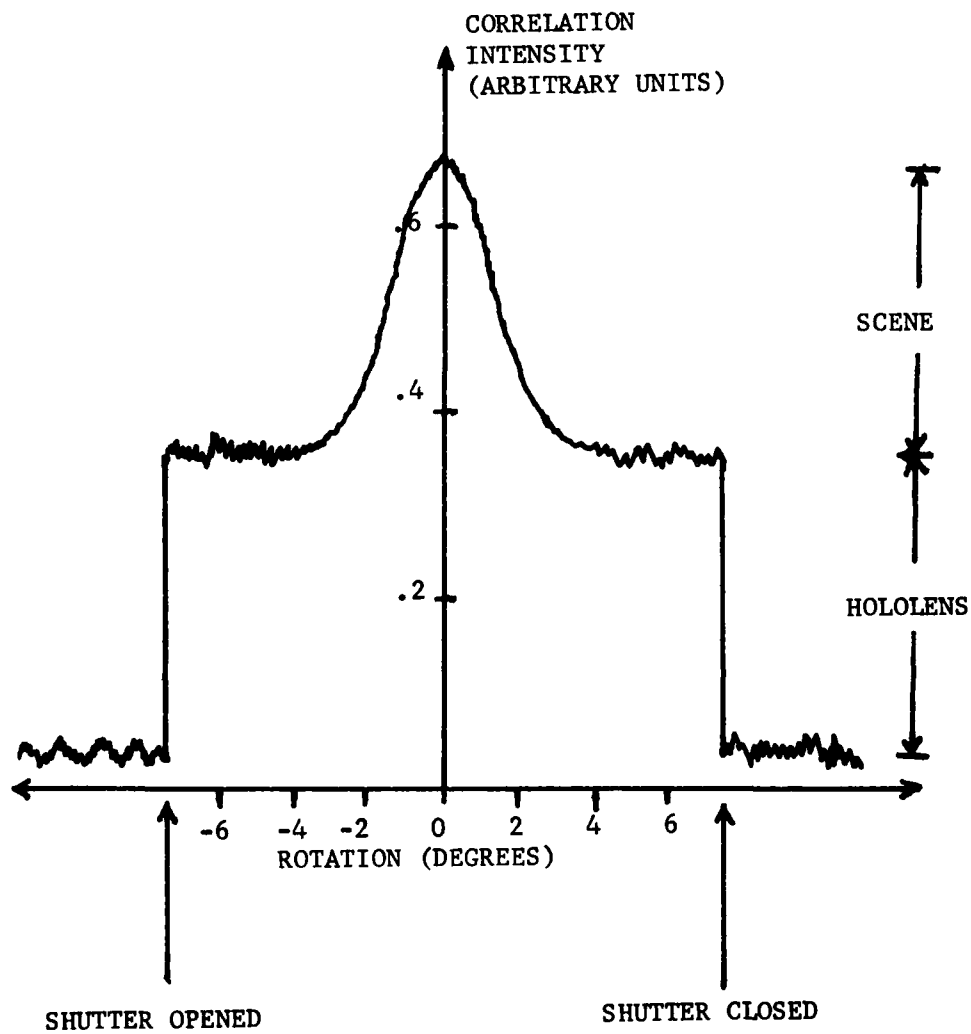
Figure 34. The correlation intensity from all 25 elements versus the angular rotation of the input scene. The scene correlation and background correlation due to the hololens are superimposed.
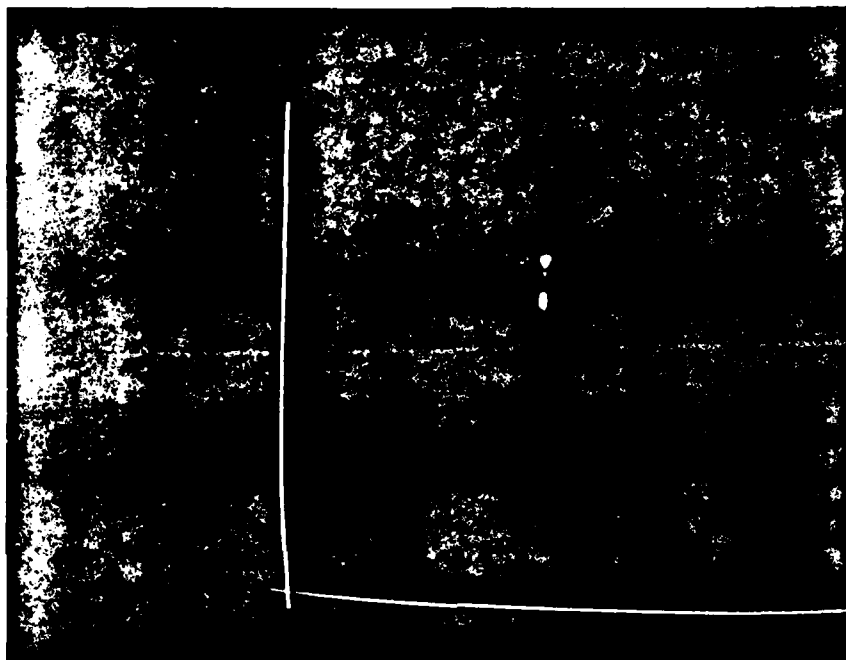
Figure 35. A photograph of the television screen displaying
            the separation of scene and hololens correlations.

65

necessary to try to duplicate the phenomenon using a "noiseless" lens. This was done by replacing the hololens with a high quality glass lens of approximately the same focal length and adding "noise" to the clean lens. The added noise consisted of three regular array mesh screens placed directly in contact with the front surface of the lens – one at a time. Each of the screens contained a different fundamental spatial frequency. It was observed that all three screens produced background correlations very similar to those observed using the hololens. The highest spatial frequency screen seemed to produce the largest, most localized background. Perhaps this indicates that the noise contained in the hololens was also of a high spatial frequency content.

An interesting pictorial result of using the 25 element array is given in Figure 36. The input scene was a military tank (side view). The photograph was made by placing a Polariod (type 52) film a few inches after (for magnification) the next image plane past the Fourier transform plane of the hololens and exposing for about .2 seconds. This graphically illustrates the hololens's ability to produce 25 images from a single input scene.

F. Twenty-Five Different Filters

The obvious next step was to attempt to store 25 different filters and address all of them simultaneously. This was accomplished after experimentation with the computer-controlled rotation stage and exposure times. The input scene in this instance was the aerial view of Huntsville. Exposures were made for every 14 degrees of rotation of the scene. The K ratio was again about 1 and the exposure time a constant 12 seconds. Only one element of the 5X5 array was used per exposure. This was controlled by the mask/translation stage combination described earlier. The first experiment was to access all 25 filters simultaneously, but a problem arose. Many of the correlations were excessively weak and completely masked by electrical and hololens noise. A translation of the input scene might have alleviated some of the problem (hololens), but was not done. It was decided, rather, to access the filters one at a time (series access) and try to obtain better correlations. The results are given in Figure 37. As one can see, the peaks are clearly visible. The hololens noise is minimal when the filters are accessed in series. It was believed at this stage of the investigation that the filters might be too closely spaced (in rotation of the scene) for one filter to be distinguished from another. This proved not to be the case, as will be discussed in a later section. It was observed that the correlation curves of Figure 37 had a smaller FWHM than previously measured. This is probably due to a small change in scale of the input scene due to refocusing and adjustment to the zoom lens of the input camera. The correlation as a function of scale change was discussed in Section II and will be further discussed later in this Section. The important aspect is that 25 filters were stored on the glass plate in an area of about 1.2 cm^2 – less than the area of a thumbnail. A high speed method of accessing these filters in series would make even this early result useful for a variety of applications.

The goal, of course, was to access these filters in parallel – not series. This was attempted using the same scene under identical circumstances except that the amount of scene rotation between exposures was increased from 14 to 20 degrees and the exposure time was shortened to 10 seconds instead of 12. This produced the parallel-addressed correlations of Figure 38. The zero

Figure 36. A photograph of the 25 images of a tank produced by the hololens and LCLV.
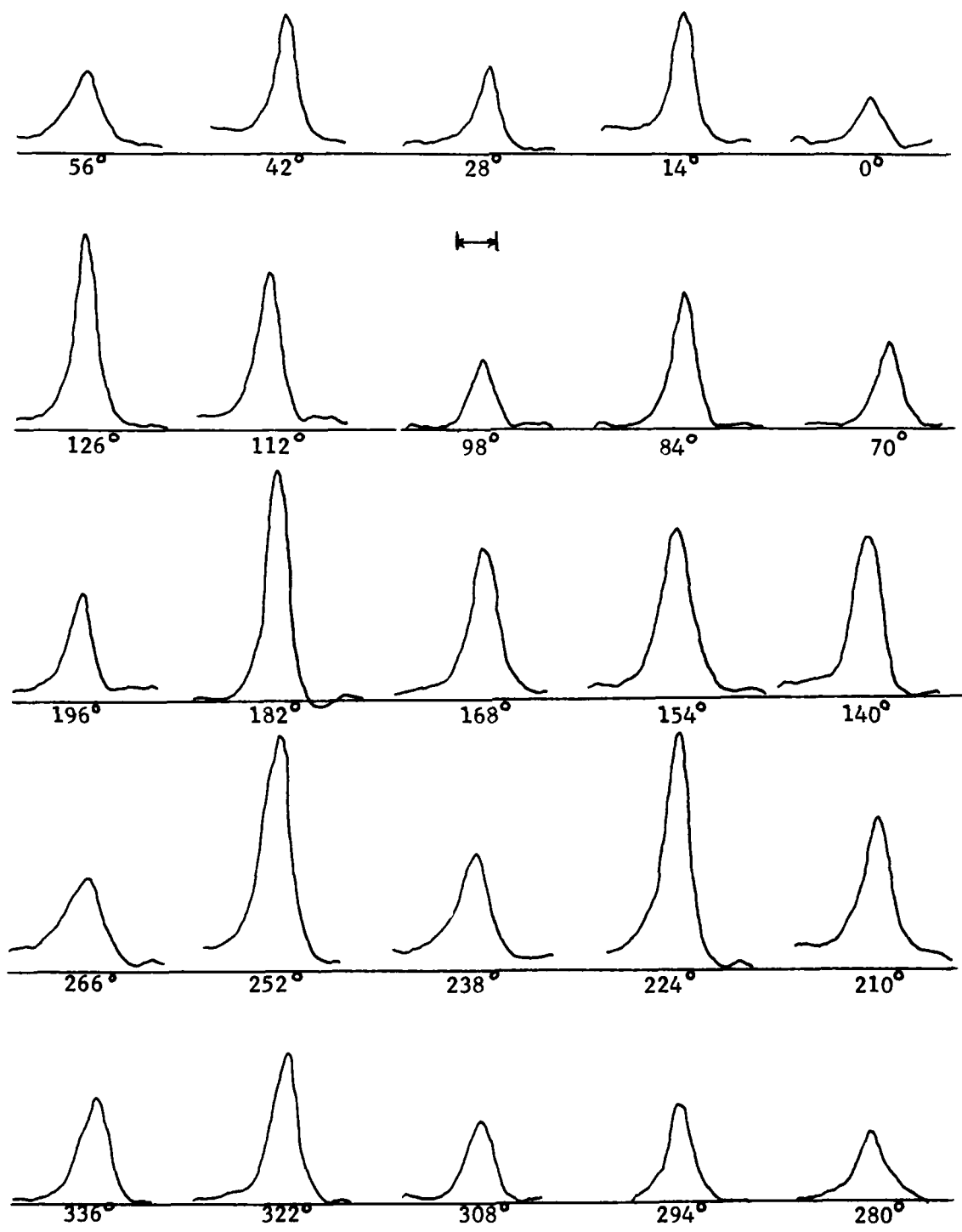
Figure 37. Correlation of 25 different filters of an aerial photograph of Huntsville -- filters addressed in series.
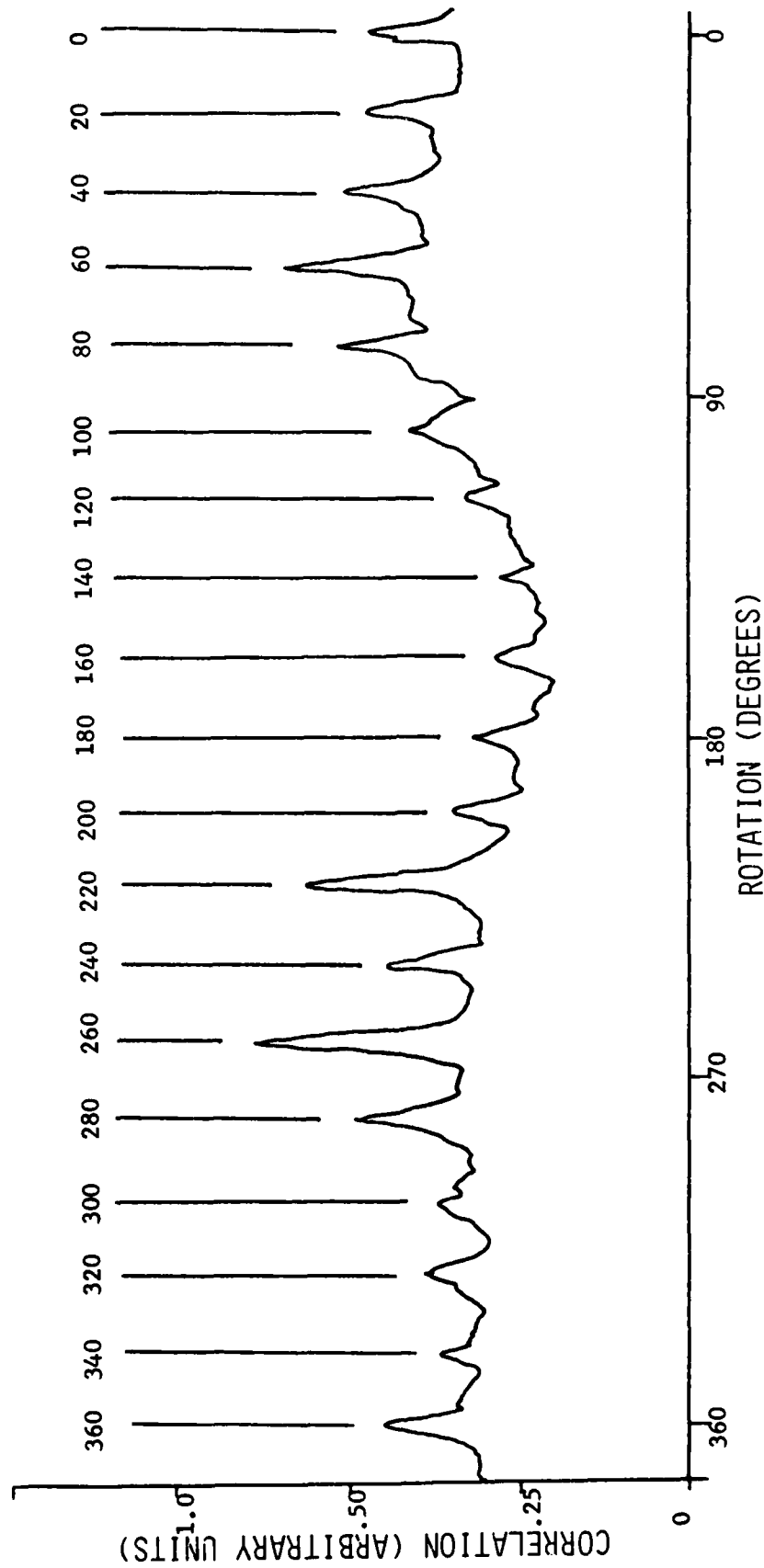
Figure 38. Correlation of 18 different matched filters, addressed in parallel, through the hololens. The input scene was an aerial photograph of Huntsville, AL.
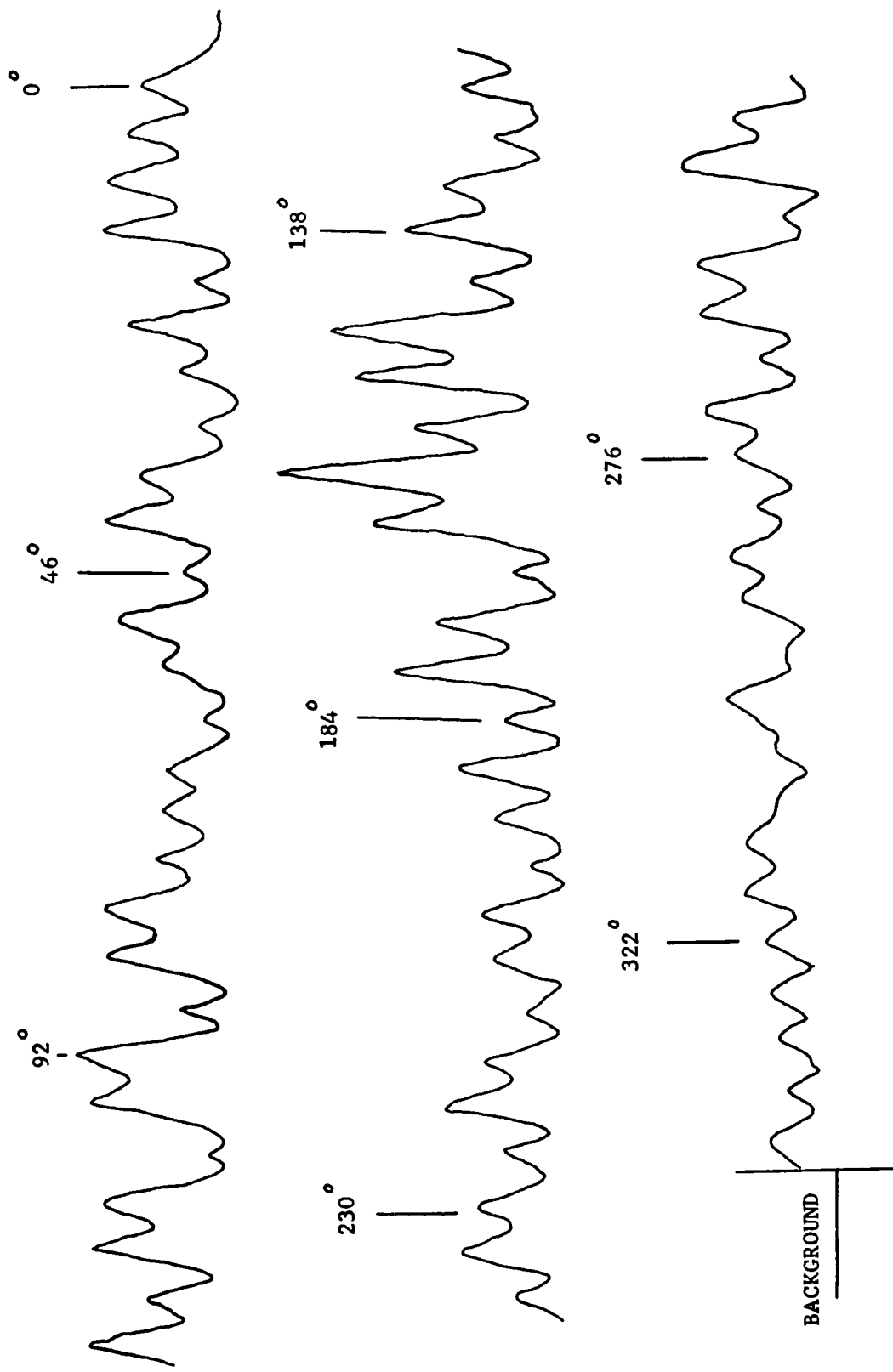
Figure 39. Correlation of 75 filters addressed in parallel -- tank input scene.

70

correlation intensity axis represents the background due to the hololens. A possible explanation for this result is that perhaps the shorter exposure time allowed less of the high spatial frequency components (associated with the hololens) to be recorded in the filter. Even though, as stated earlier, this background is fairly constant, even small variations are enough to destroy an already weak correlation signal.

G. Seventy-Three Different Filters

The success of the 25 filter correlation experiment prompted investigation into storing even more information. The attempt to store 75 filters required exposing each element of the array three times. Preliminary investigation of this procedure, and use of Equation (84), determined that the exposure times should be 3 seconds for the first exposure, 4 seconds for the second and 5 seconds for the third. The subject was a scale model of a T62A military tank. The average power in each of the 25 elements was .12 W. The LCLV was set at $f = 1400$ Hz @ 6.5 volts, as usual. The optimum K value was experimentally determined to be about 1.0. Exposures were made for every 4.6 degrees of rotation of the tank. The exposures, rotation, and movement of the photographic plate were computer-controlled so that after making all the preliminary adjustments, the entire 75 exposures took only about 15 minutes. Results of the experiment after developing and placing the filter back in the correlator are given in Figure 39. All 25 elements were addressed in parallel. Seventy-three of the correlations are quite distinct. The very weak correlations occurring on the graph are those corresponding to weak elements in the array. A higher quality hololens would no doubt allow all 75 filters to correlate. It was also observed that the background did not overwhelm the correlations as had been the case before when all 25 elements were addressed in parallel. Perhaps the lower spatial frequency input scene caused this effect. The correlation of more than 70 matched filters on a single plate represents a vast (fivefold) increase over any similar object recognition system reported to date.

H. Sensitivity to Scale

A model was given in Section II for the effect that a scale change should have upon the correlation intensity. The model was for a highly specialized input scene (Ronchi ruling). In order to test this model using experimental techniques, a Ronchi ruling type input scene was used in the correlator and matched filters made as before. The ruling was composed of flat black strips of tape on a white paper background. The black strips were one-quarter inch wide with a one-quarter inch wide separation between them. The image produced by the LCLV had a fundamental spatial frequency of .73 per mm -that is, the dark areas were about 0.68 mm wide and separated by the same distance. All 25 elements were exposed simultaneously as in Paragraph E of this section. The matched filters made looked very much like the photograph of Figure 29. The separation between the zeroth and the first order was measured to be about .013 cm. An exposure time of 12 seconds with K = 1 was found to produce good correlations. The scale (magnification) of the input scene was then changed using a motorized zoom lens made by COHU Corporation. The correlation intensity was measured using a Keithley (Model 179) digital voltmeter connected to the Colorado Video image digitizer. The magnification was determined by direct measurement of the input scene on a television monitor. Figure

71

40 gives the experimental data and the prediction of the model given in Section II. The agreement is better than expected given the crudeness of the model, which neglects all but the fundamental spatial frequency. Scale changes for a more "real world" type scene were done later and those results are given in Figure 41. The general trands are similar. Of course, the widths of the curves are different, the Huntsville scene having a higher spatial frequency content than the Ronchi ruling. The downward pointing arrows on the x axis indicate that the true zero is somewhat below the axis in Figure 34. This is due to the hololens noise previously discussed. Notice that a scale change of only 2 percent is necessary to decrease the correlation by half for the Huntsville scene.

I. Sensitivity to Tilt

The previous experiment was repeated with tilt as the variable. The same Ronchi ruling input was used as before. The tilt model of Section II proved again to be reasonably valid for this specialized input scene. Tilting the input scene was attempted using the Scientific Atlanta stage descibed in Section III, but a problem arose. Tilting the scene with this stage is accomplished via a pivot below the stage. Thus, when the stage is tilted, it is also translated and this should not be allowed for the simple model to be valid. This was corrected by using another stage which had its pivot in the same plane as the stage. Unfortunately, this stage was not automated so data had to be taken manually by reading the voltage, normally going to the chart recorder, on a digital voltmeter. This proved to be adequate even though continuous curves were not possible. Figure 42 gives the results for the Ronchi ruling input scene; again the fit is marginally good. Figure 43 gives the results for the Huntsville scene discussed previously. The FWHM for the Huntsville correlation is about 16 degrees – slightly less than that for the Ronchi ruling scene, as should be expected.

J. Sensitivity to Rotation

Throughout this investigation, most of the data has been taken with rotation of the input scene being the variable. The simple model of Section II can be used to predict the change in correlation intensity with rotation of the scene when the scene is fairly specialized as in the preceding sections of this section. Figure 44 compares the theory to experimental results for a Ronchi ruling type input scene. The results are similar to those obtained in the preceding two sections except for the widths of the curves. In this experiment it was possible to use the motorized rotation stage, although experimental data is plotted as points to be consistent with the previous two sections. Figure 45 gives the results for the experiment performed using the Huntsville scene. The FWHM is observed to be about 2.9 degrees which is consistent with that of Figure 32 – a correlation produced by a different filter of the same scene. It is interesting to compare results from this section to those of the previous. The two experiments were done as closely alike as possible in K ratio, exposure times, etc. This shows that the correlation is much less sensitive to tilt angle than to rotation. This is an important result, because it means that fewer matched filters are needed to keep an objective "in sight" when only the angle of approach is important. On the other hand, it also means the angle of approach cannot be known with a very great accuracy in actual circumstances.

72
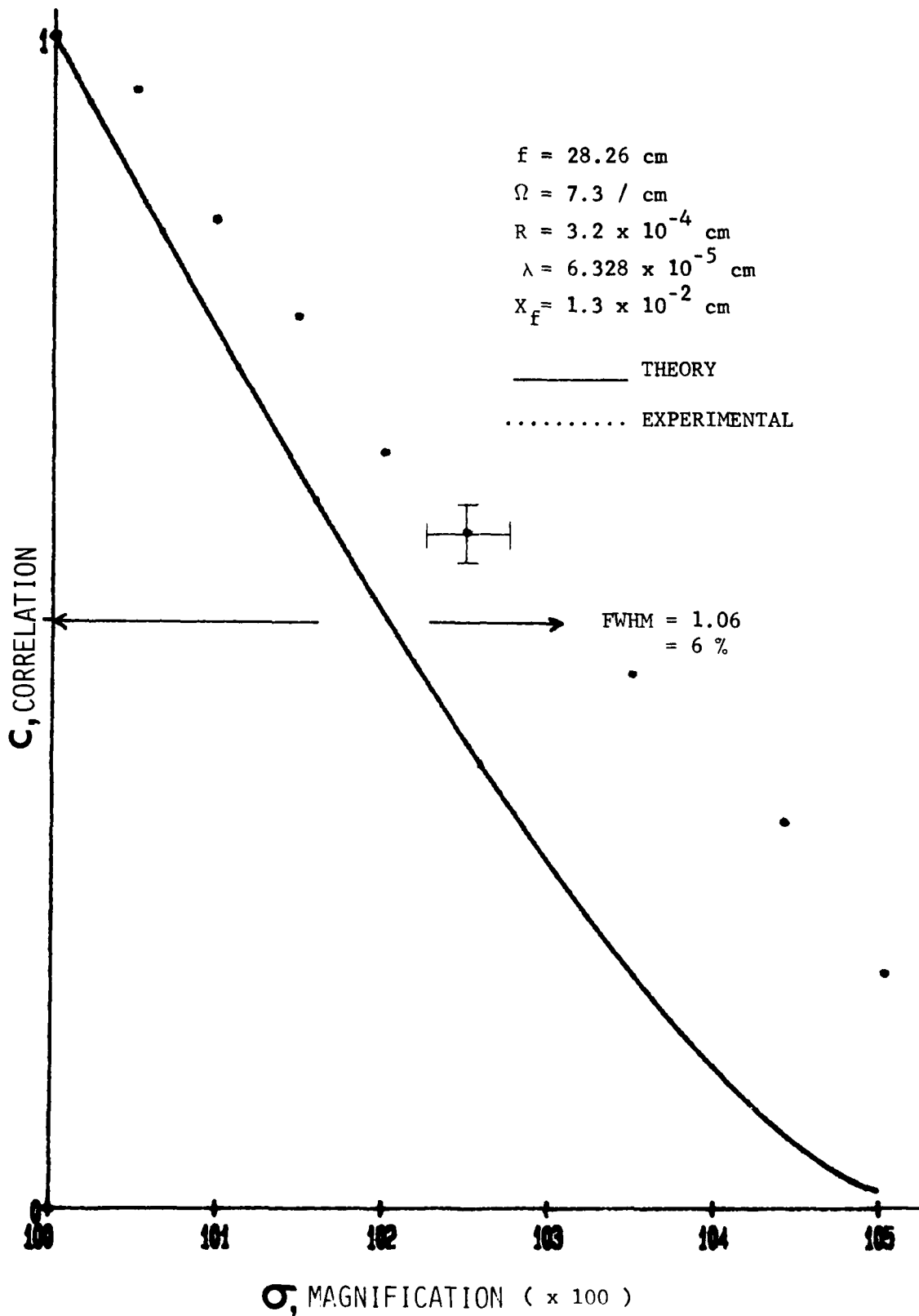
Figure 40. Theoretical prediction and experimental results -- correlation versus magnification for a Ronchi ruling input scene.
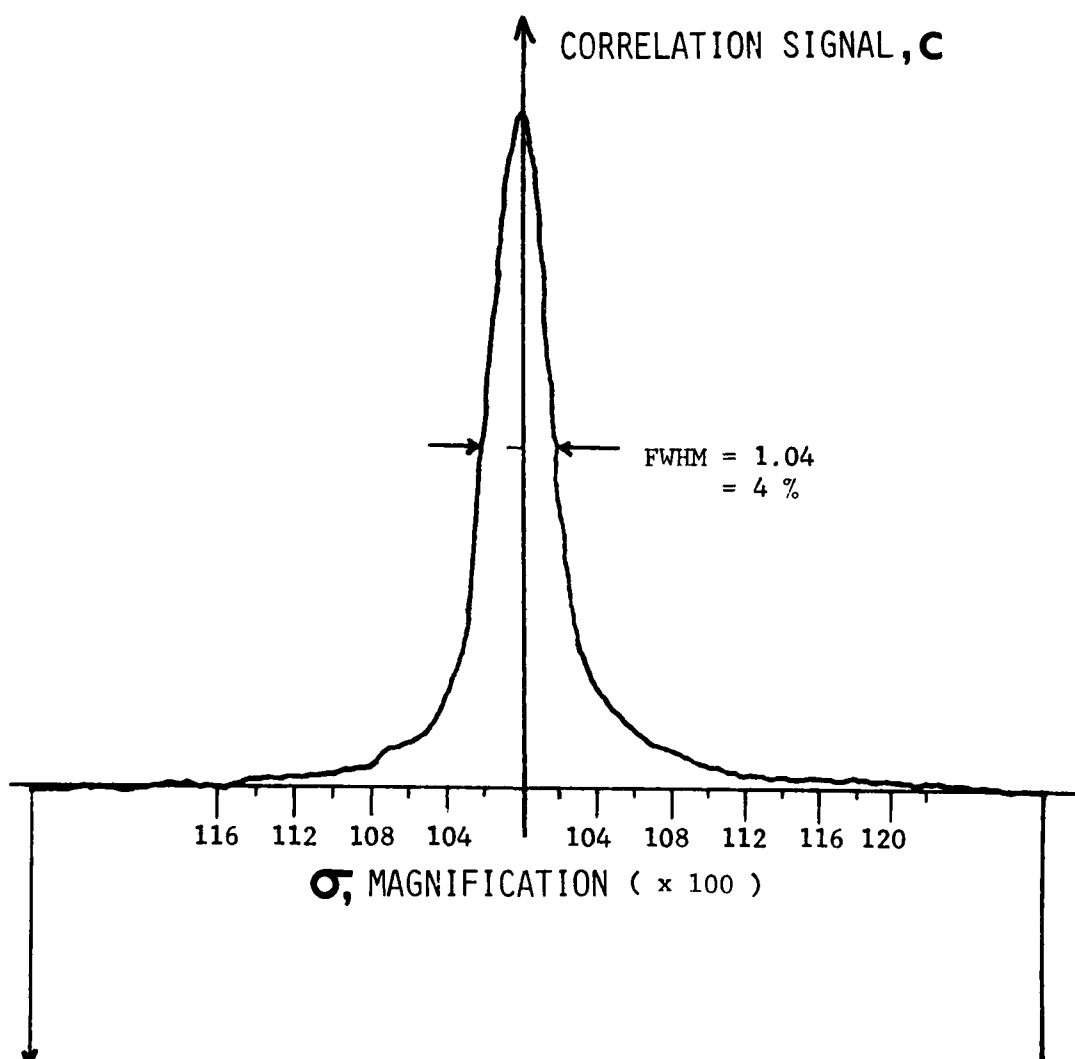
Figure 41. Correlation versus scale change (magnification) for a filter of the aerial map of Huntsville.
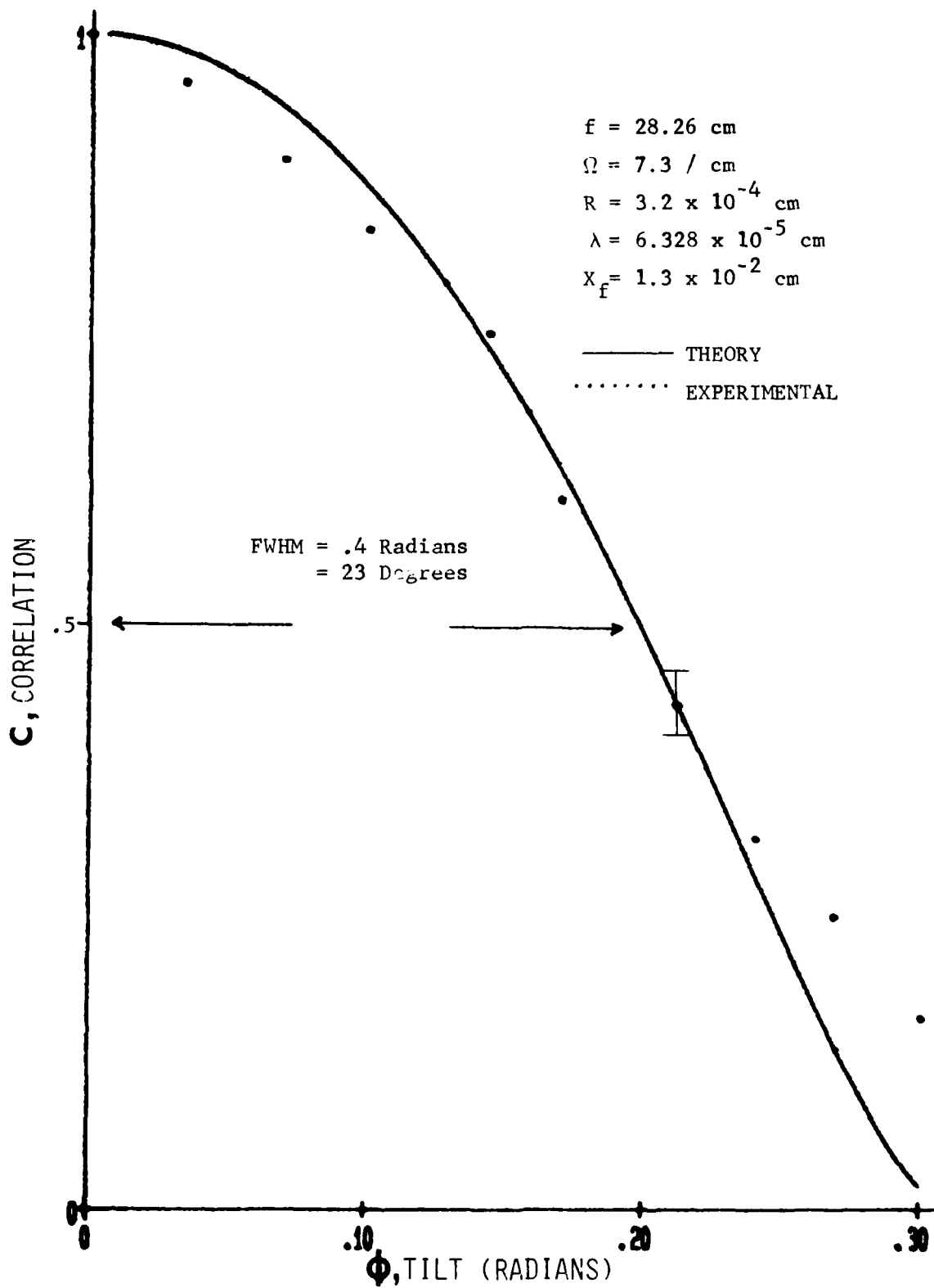
Figure 42. Theoretical prediction and experimental results --
correlation versus tilt for a Ronchi ruling input scene.

75
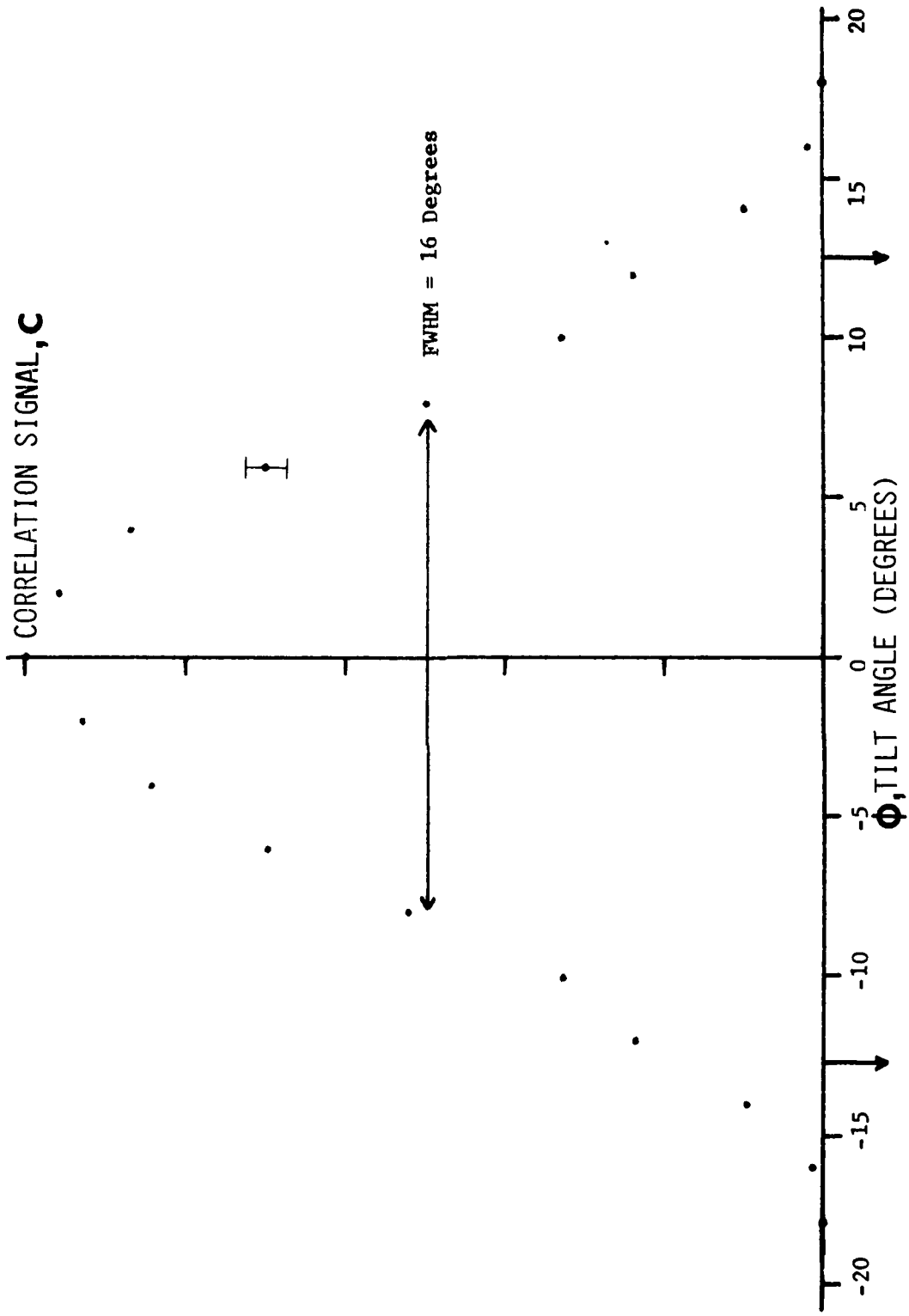
Figure 43. Correlation versus tilt for a filter of the aerial map of Huntsville, AL.
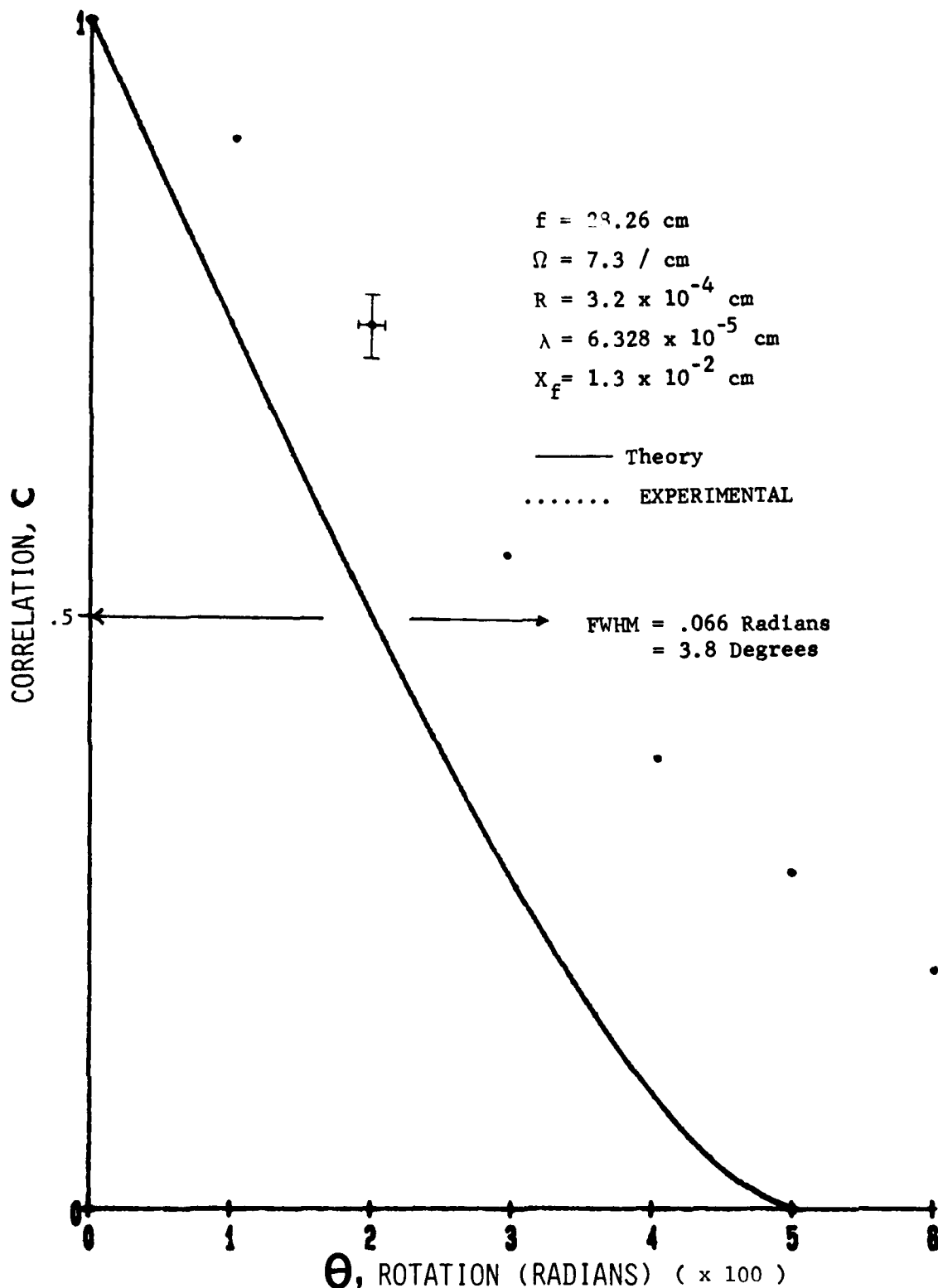
Figure 44. Theoretical prediction and experimental results -- correlation versus rotation for a Ronchi ruling input scene.
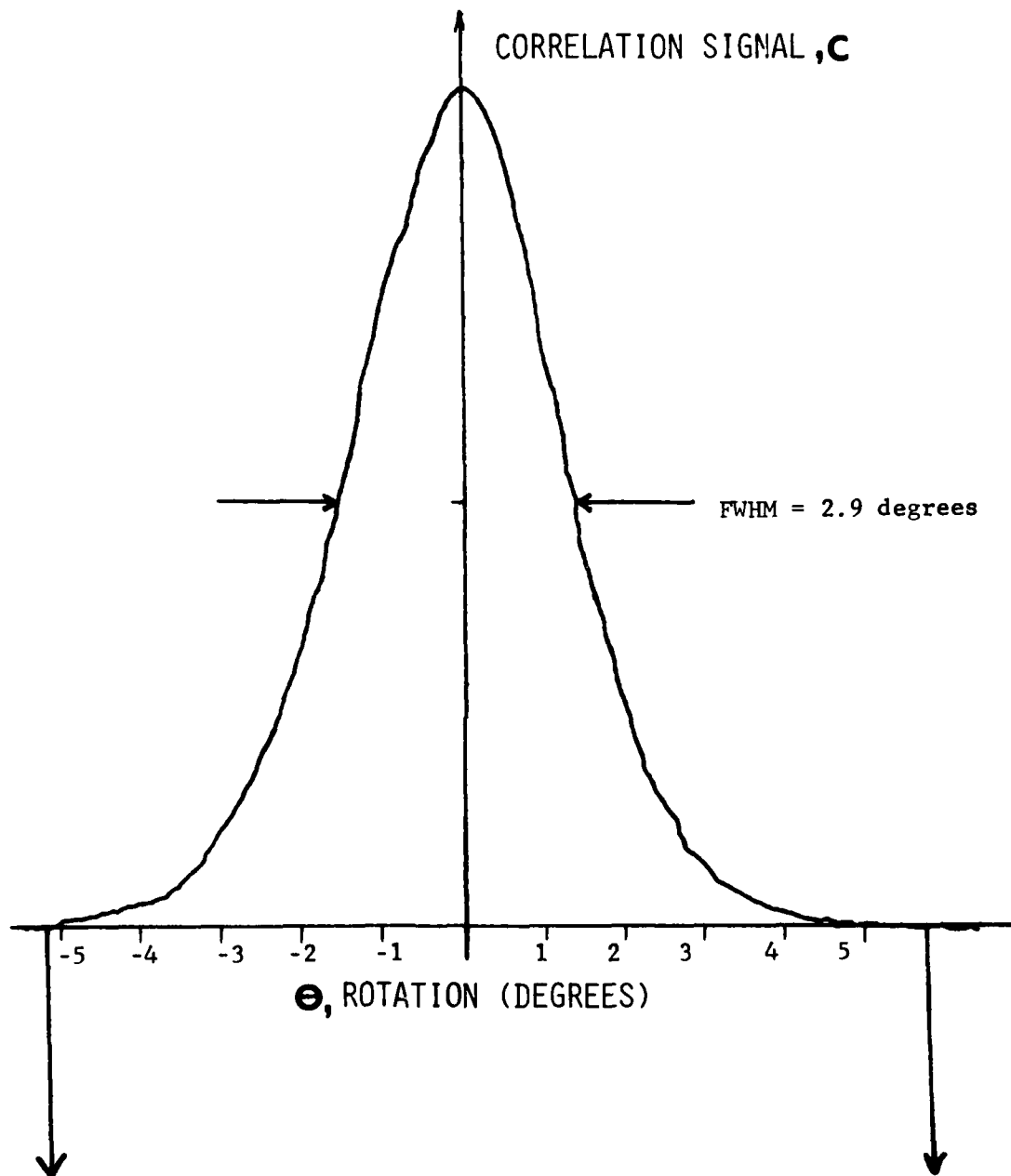
Figure 45. Correlation versus rotation for a matched filter made of the aerial Huntsville, AL, map.

K. Resolving Closely Spaced Optical Correlations

The ability to store a large number of matched filters and obtain correlations of them presented a problem which had not been encountered previously. If many matched filters are made of a scene only slightly rotated after each exposure - how are the correlations to be resolved from each other? Often the orientation of the scene is of primary interest. Many filters must often be used so that the recognition device never completely "loses sight" of the target for any long period of time. The experiment consisted of doubly-exposing a photographic plate (overlapping matched filters) to an input scene at two slightly different rotations positions. Classic lineshapes were used to model examples of experimental results and some conclusions are drawn using the Rayleigh criterion as a guideline.

A Gaussian intensity distribution has the form [58]

$$I_1 = I_o \, e^{-2r^2/w^2} \quad , \tag{98}$$

where r is the radius from the center of the distribution and 2w is the full linewidth at $I = 1/e^2 \, I_o$. If another distribution of the same form is located a small distance δ_1 away

$$I_2 = I_o \, e^{-2(r-\delta_1)^2/w^2} \tag{99}$$

then the sum of these distributions is

$$I = I_1 = I_2 = I_o \left[e^{-2r^2/w^2} + e^{-2(r-\delta_1)^2/w^2} \right]. \tag{100}$$

Let

$$\rho_1 = \frac{I(r=0)}{I(r=\delta_1/2)} \quad . \tag{101}$$

Substituting from above gives

$$\rho_1 = \frac{1}{2} \left(e^{\delta_1^2/2w^2} + e^{-3\delta_1^2/2w^2} \right). \tag{102}$$

ρ_1 is thus the ratio of the peak at $r = 0$ to the height of the valley between the two distributions. Solving for δ_1, using the fact that the second term is much smaller than the first, gives

$$\delta_1 = w \, [2 \, \text{Ln} \, (2\rho)]^{1/2} \quad . \tag{103}$$

Using the Rayleigh criterion as a rough guideline, $\rho_1 = 1.23$, [59] and substituting this into Equation (6) yields

79

$$\delta_1 = 1.34 \ w \ . \tag{104}$$

The same sort of analysis may be applied to a Lorentzian distribution having the form [58] (p. 154)

$$I = \frac{A}{r^2 + (\sigma/2)^2} + \frac{A}{(r - \delta_2)^2 + (\sigma/2)^2} \tag{105}$$

where A is a constant equal to $I_0(\sigma/2)^2$, r is the radius and σ is the full linewidth at half the maximum intensity. This produces a δ_2:

$$\delta_2 = \frac{\sigma}{2} \left[4\rho_2 - 3 + \sqrt{16\rho_2(\rho_2-1) + 1} \right]^{1/2} \ . \tag{106}$$

Then for $\rho_2 = 1.23$ as a value of the intensity ratio

$$\delta_2 = 1.03 \ \sigma \ . \tag{107}$$

For a sinc^2 distribution [60]

$$I = I_0 \left(\frac{\sin \alpha r}{\alpha r} \right)^2 + I_0 \left[\frac{\sin \alpha(r-\delta_3)}{\alpha(r-\delta_3)} \right]^2 \tag{108}$$

where, again, r is the radius from the center of the distribution and

$$a = \pi/r(o) \tag{109}$$

where r(o) is the value of r at the first zero of intensity. This distribution yields

$$\rho_3 = \frac{\alpha^2 \delta_3^2 + \sin^2 \delta_3}{8 \sin^2 (\alpha \delta_3/2)} \tag{110}$$

which must be solved graphically or by iteration using $\rho_3 = 1.23$. For small values of δ_3, note that $\alpha^2 \ \delta_3^2 \gg \sin^2 \delta_3$

Figure 46 shows these three distributions compared with experimental data taken as before. All three distributions have been arbitrarily fit to experimental data at r = 0 and r = 2.95° using w = 2.80°, σ = 2.07°, and α = .775 deg^{-1}. This gives δ_1 = 3.8°, δ_2 = 2.13°, and δ_3 = 4.0°. Note that these widths should depend upon the spatial frequency of the input scene as well as other factors and, thus, serve only as examples here. In this particular experiment the input scene was a low resolution black and white aerial photograph of Huntsville, AL. The photograph was placed on a rotatable stage
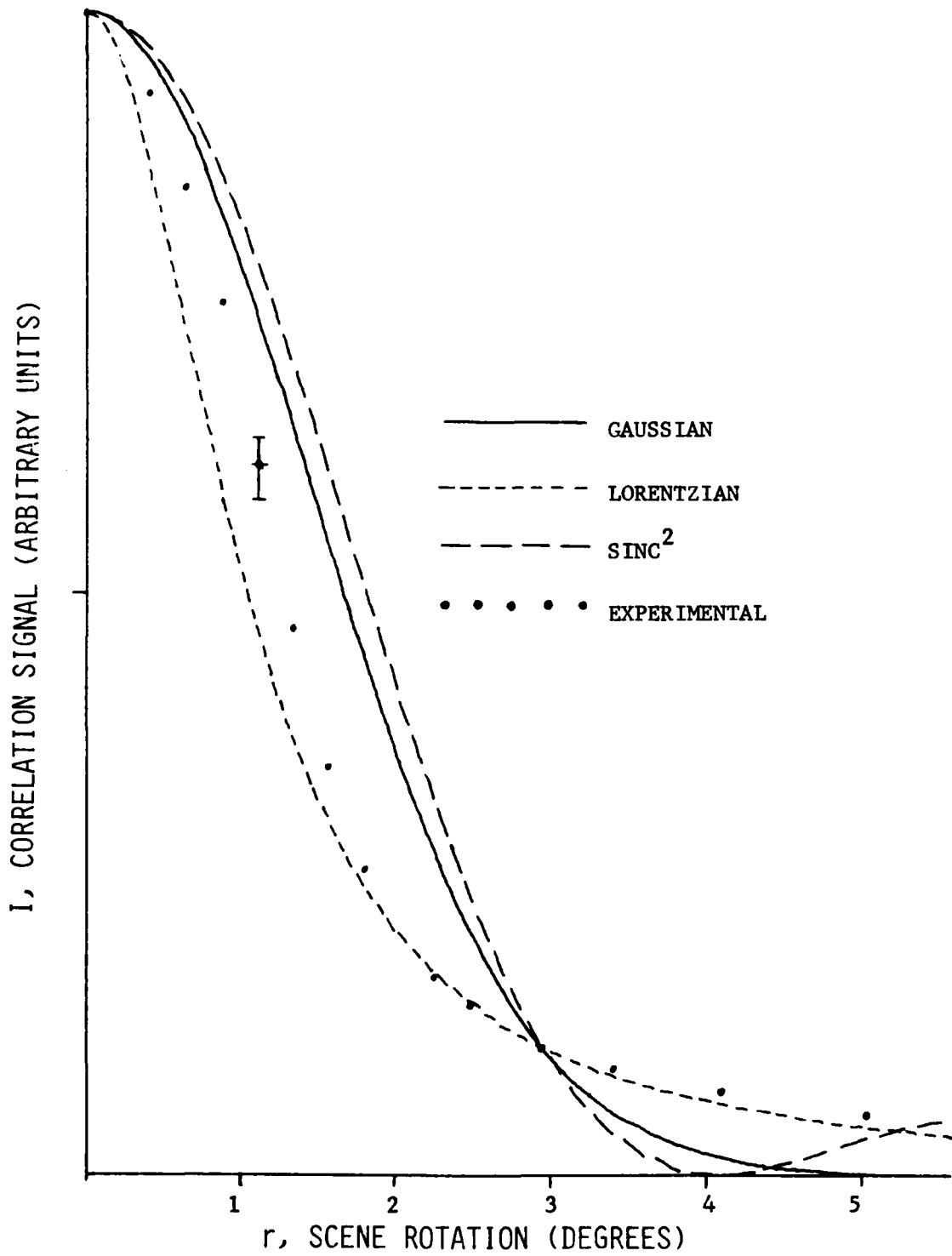
Figure 46.   Correlation versus rotation for Huntsville aerial map
input scene compared to three classical lineshapes.

and matched filters made at the desired rotation angles. Experimental data in Figure 46 is the correlation intensity for a filter made at 0 degree rotation of the input scene. After development of the film plate (Kodak 649F) it was replaced in the correlator and the input scene rotated slowly as the corresponding correlation intensity was measured.

In order to investigate multiply-stored filters, a single plate was exposed twice with different rotation angles of the input scene. After development, the filter was reinserted into the correlator and data taken as before. Figure 47 shows the actual data and a plot of Equation (105) using the Rayleigh criterion. The exposures were made using the same criteria for δ_2 of 2.13 degrees of scene rotation. The agreement is reasonably good. Some variation is expected due to the difficulty in obtaining equally intense correlations for the two filters. This depends upon the exposure times used, film response, and several other variables. In the theoretical analysis the calculations could easily have been done using distributions having different peak heights but then the value of δ would depend upon these heights which cannot be known with any certainty in advance of doing the experiment. In the calculation presented, it was also assumed that individual correlation intensities should be added directly rather that adding the corresponsing fields then squaring for the intensity. This has been justified experimentally by storing one filter made at 0 degree scene rotation and another filter at a 90 degree scene rotation, then adding the resulting correlation intensities algebraically. This distribution was then compared with data similar to Figure 47. The results were found to be essentially equal. This indicates that there is little, if any, phase addition contribution to the sum of the two correlation intensities from multiply exposed filters.

In this section, results have been presented from several experiments dealing with the production and analysis of optical matched filters made using a holographic lens. The hololens itself was tested to determine if it could reproduce well-known Fourier transforms and the efficiency of the lens was measured. The matched filters produced by the hololens were then compared with those made using a conventional glass lens. Finally, the hololens was used in a variety of experiments that until now could not have been done. Large numbers of matched filters were stored on photographic plates and addressed in parallel and series. These filters produced correlations that were tested for sensitivity to rotation, scale, and tilt of the input scene. Matched filters were made of a simple Ronchi ruling and compared to the theoretical predictions of Section II. Lastly, an investigation was made into resolving correlations produced by scenes separated only a few degrees in rotaion. It was found that 2.13 degrees of rotation of the Huntsville scene was necessary to satisfy the Rayleigh criterion and thus produce easily separable correlations.

82
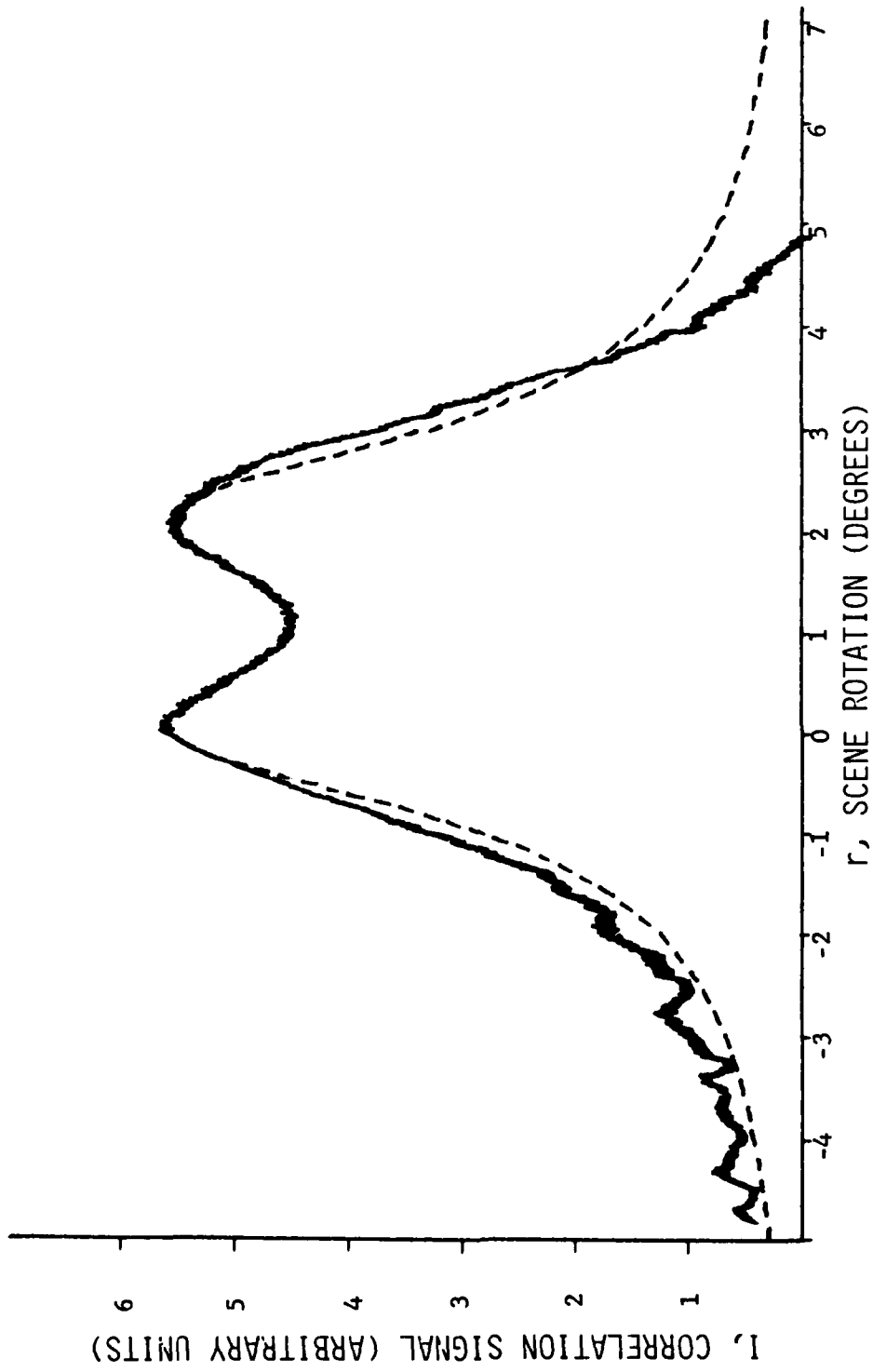
Figure 47. Correlations from two matched filters of an aerial photograph of Huntsville -- stored 2.13 degrees of rotation apart. The dashed line is a Lorentzian curve fit to the data.

83

V.   DISCUSSION

A.   Theory

A discussion of the work presented here should begin with the theoretical analysis used to model some of the results. The idea for the overlapping circles came from a paper by Casasent [42]. In that paper the model was used to predict the correlation intensity decrease as the input scene was rotated. Unfortunately, the model was fit to the correlation of a complex, real world scene – the situation where the model should be least applicable. Imagining that the Fourier transform of a simple Ronchi ruling consists of circular spots might not be so unreasonable but the Fourier transform of a complicated scene such as the aerial view of Huntsville does not resemble a series of circular spots by any means. It is for this reason that none of the correlations of complicated scenes were modeled in this investigation. A model which has the capability of handling hundreds of spatial frequencies is probably achievable but beyond the scope of this work. The simple model of Casasent was quite adequate in predicting general trends, however. In this work, the rotational model of Casasent's was expanded so as to predict scale and tilt variance in correlation and gave some insight into the results obtained when complex scenes were used.

There are several reasons for performing the correlation calculations in the Fourier transform plane instead of the image plane. The correlation actually occurred in the Fourier transform plane, that is, matched filters were made of the Fourier transform of the scene, not the scene itself. The calculations were also much easier to do in the Fourier transform plane. The scale change and tilt calculations would be especially cumbersome to do in the image plane, while in the Fourier transform plane these effects are viewed as a change in location of the spatial frequency components characteristics of the image. The results should be the same whether the calculations are done for the image plane or the Fourier transform plane. This was found to be true for the rotation model when the calculations were done both ways.

B.   Holographic Lens and LCLV

This work represents the first attempt to study a multiple focus holographic lens in a real time optical correlator. The results of tests performed on the hololens showed that it could perform almost as well as a conventional glass lens in a similar situation. The hololens faithfully produced the Fourier transform of well-known input scenes such as a circular aperture and a Ronchi ruling. It was encouraging to find that measurements taken from the photograph of the Fourier transform agreed with the calculations to within about 10 percent. This 10 percent could easily have come from errors associated with determining the magnification of the input scene before it addressed the hololens or in the direct measurement of the separation of the rings in the Airy disk (or lobes produced by the Ronchi ruling).

The modulation transfer function (MTF) of the hololens was not measured directly. In order to do this type of measurement, an input scene with a higher resolution than that of the television monitor and LCLV would be needed. In routine observations of the image produced by the LCLV it seemed

84

that the contrast versus spatial frequency (the MTF) [49] (p. 118), was limited by the television monitor, not the LCLV. Consider a typical television monitor measuring about 10-inches across and containing 512 lines alternating black and white. The maximum fundamental spatial frequency produced is about 2 per mm. When focused onto a 1-inch LCLV this produces a fundamental spatial frequency of about 20 per mm which is well within the capability of the quoted resolution of the LCLV. The contrast at this spatial frequency is not known precisely for the LCLV, but it is better than 50 percent [28]. Bleha quotes the liquid crystal light valve he tested (very similar to the one used in this work) as having 60 lines/mm resolution at 50 percent MTF so at about 20 lines/mm the MTF is prob-ably much higher than 50 percent.

Experiments reported in Section IV of the present investigation using a Ronchi ruling input scene did demonstrate some of the capabilities of the LCLV. The LCLV could faithfully produce an image having a fundamental spatial frequency of about 6.3 per cm (0.63 per mm) and maintain a very sharp contrast. This spatial frequency was then increased by zooming the camera lens away from the Ronchi ruling scene until the fundamental spatial frequency addressing the LCLV was slightly less than 20 per mm (about 2 per mm on the TV monitor). A Ronchi ruling having a fundamental spatial frequency of 2 per mm was barely distinguishable on the television monitor and the image was of poor contrast. The image produced by the LCLV was also barely distinguishable. This investigation indicated that the MTF of the LCLV is at least as good as the television monitor, if not better.

The MTF of the hololens was examined in a similar manner. It was found that by observing the image two focal lengths away from the lens (an image plane) the hololens could reproduce anything the television monitor/LCLV combination was capable of sending it. All 25 images were good (see Figure 36) with the overall intensities of some being less than others as would be expected from the testing reported in Section IV. While the MTF of the optical system was not measured in a very systematic manner it can be said that the MTF of the hololens and LCLV was probably at least as good as the television camera and monitor used as the input.

The efficiency and intensity distribution produced by the hololens proved to be adequate but considerable improvement should be expected in the next generation of hololens. Discussions with the manufacturer have led to placing an order for a hololens which produces a 7X7 array with an overall efficiency better than 15 percent and a more uniform intensity distribution [61]. This should lead to about 150 stored matched filters. This is enough matched filters to ensure no more than a 50 percent decrease in correlation intensity regardless of the rotational position of the scene with the present optical correlator and a scene similar to the aerial view of Huntsville. The FWHM of the correlation intensity versus rotation curve for the Huntsville scene was about 2.9 degrees (Figure 45) so that 126 filters would be needed for no more than 50 percent decrease in correlation intensity. For a tilt of ± 60 degrees, about 57 filters would be needed and about 25 filters would be required for a 100 percent change in scale. This, unfortunately, does not tell the whole story. Suppose that at each rotational position it is desired that the correlation intensity be tilt-invariant. A total of more than 7000 filters

would be needed. When scale change is included, the problem is magnified even more. For very specialized applications, the 147 filters may be enough, however. In fact, for a stationary aerial observation the 75 filters investigated here would produce about a 10 to 15 percent correlation, which, for some applications might be sufficient.

The background correlation signal observed using the hololens did not prove to be a major problem in this investigation. Fortunately, this background was fairly constant throughout a full 360 degree rotation and the scene correlations were usually distinguishable above the background. However, if this were not present, perhaps more than three filters could be stored at each location. This, of course, would increase the overall recognition capabilities of the system. More than three filters at each location were attempted, but fewer than half the correlations were of significant intensity.

C. Matched Filters

The experimental results obtained in this research covered several aspects of matched filtering. The results, however, are much more graphic than perhaps has been indicated in this report. In actual practice the observation of the correlation spot on the television monitor is quite dramatic. The correlation intensity's sensitivity to rotation, tilt and scale is extremely pronounced. For this reason, many of the experimental results were videotaped.

The making of the initial matched filters in this investigation required a great deal of trial and error with exposure times and developing techniques. Fortunately, many of the procedures were known from earlier work done by laboratory personnel with conventional photography.

Early in the research it was obvious that the correlations obtained using the present arrangement were different in some respects from those obtained by the Harris group [24]. A major difference was the correlation widths. The Harris group, using a similar input scene, obtained widths much narrower than those presented here (fractions of a degree) for rotating the input scene. The major difference, it turns out, was the fact that that group used high resolution 35 mm slides as the input scene. This enabled them to record much higher spatial frequencies than the commercial television monitor used in this work. Section II discussed how this should affect the correlations obtained; the higher the spatial frequency, the narrower the width. The use of a television monitor, however, has its advantages. The input scene can be instantly changed. The input scene can be a moving object and, of course, using the television monitor is much more convenient than having to produce a 35 mm slide. The television monitor in conjuction with the LCLV is what makes this a "real time" recognition system.

D. Optical Memory

In the course of this investigation, it was possible to significantly increase the optical memory of the correlator over anything attempted in the past. Until the advent of the hololens the only way to achieve more than one memory was through multiply-exposing the photographic plate. This was limited to about eight images being stored, which in itself is quite an accomplishment. These filters, however, could only be correlated with an input scene one at a

time; and it was not possible to determine which filter was being correlated. The hololens arrangement, as described in this work, allowed 25 filters to be addressed simultaneously and allowed the observer to determine, visually or electronically, which filter was producing the correlation. For the first time a target could be identified by observing the location of the bright correlation spot alone. This was accomplished by a slight defocusing of the final lens in front of the CCD detector. This produced a spatial distribution of the correlations as they occurred (see Figure 48). In many applications, however, it is not necessary to know which target is being observed - only that one of the preselected targets is being observed by the correlator. Adjusting the position of the final lens in front of the CCD detector can bring all 25 possible correlation spots to the same location; thus, only one detector need be used in this application.

Expanding the memory further by using multiple exposure techniques in conjunction with the hololens allows the total number of recognizable scenes to be increased at the expense of not being able to tell exactly which scene produced the correlation. In this investigation, 75 scenes were attempted by storing three at each of the 25 locations produced by the hololens; 73 of the filters produced distinguishable correlations. The correlations were detected with the CCD lens adjusted so that all correlation spots would occur at the same coordinates on the TV monitor. If this lens had been repositioned, it would have been possible to obtain results similar to those when only 25 filters were stored - however, the exact scene being observed would not have been identifiable. It would have been possible, however, to narrow the possibilities to three scenes. The 7X7 hololens, which is being produced, should allow 49 targets to be distinguished and up to 147 or more total scenes to be stored, without absolute distinguishability.

E. Rotation, Scale, and Tilt

The experiments using a Ronchi ruling input scene were suggested as a test of the simple theory given in Section II [62]. Results were actually better than expected given the simple nature of the model. A Ronchi ruling had been used very early in the investigation to test the hololens. It is realized that the three variables (rotation, scale, and tilt) do not form a complete picture. In the rotation experiment, the other two variables were kept constant - similarly for the scale and tilt experiments. Using the experimental results obtained, it may be possible to infer the effects of a simultaneous rotation and scale change or other combinations of the three variables. It was shown in Section IV (Paragraph K) that the correlation intensities could be added directly. Using this as a guideline, it should be possible to predict the effect of rotation, scale, and tilt performed simultaneously. As an example, consider the Huntsville scene correlation results of Section IV. A rotation of 1 degree might produce a 20 percent loss in correlation intensity; a scale change of 1 percent might cause another 30 percent loss; while a tilt of 4 degrees might cause a 15 percent loss. Combining all three losses one would expect to achieve a 48 percent correlation on the scene. This result is somewhat conjecture but seems reasonable. Experiments of this type were not performed but should be simple enough to do in the future.
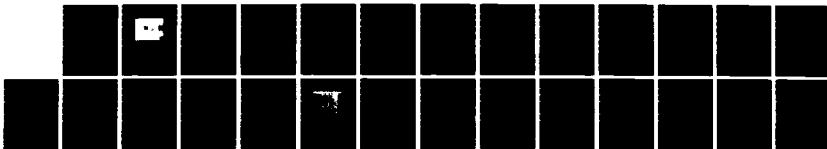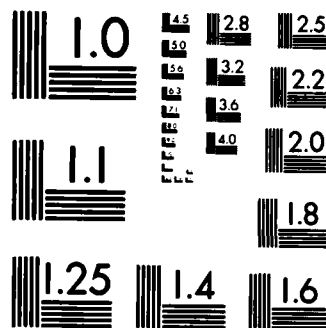
MICROCOPY RESOLUTION TEST CHART

NATIONAL BUREAU OF STANDARDS-1963-A
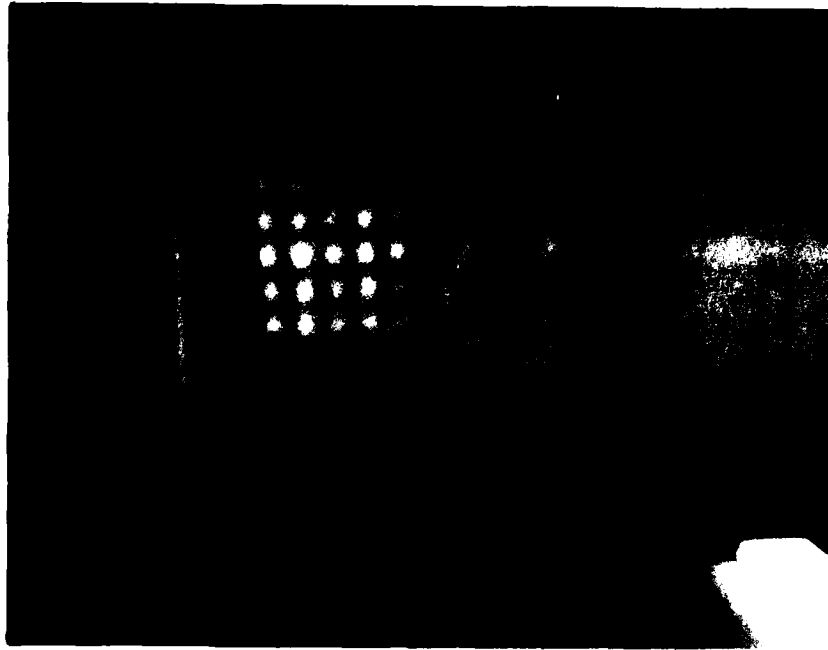
Figure 48. Slightly defocused correlation signals as they appear on the television monitor (M = .14).

F. Resolution Between Correlations

Later in the investigation when multiple exposure and arrays of filters were being made, it was observed that a limit existed for being able to separate the correlation profiles of scenes separated by only a few degrees of rotation. An experiment was, thus, devised and performed to determine what this limit was for a specific scene. Results of this experiment were given in Section IV and in a paper [57]. The experiment was done using rotation as the only variable, but the analysis technique should carry over into scale and tilt experiments. The idea to use the Rayleigh criterion seemed to be quite natural after observing the correlation curves produced as in Figure 47. It was necessary, in order to model the results, to assume some type distribution of intensity versus rotation. Three well-known distributions were fit to the experimental data. The best fitting distribution (Lorentzian) was then used to predict the sum of two correlation curves. It should be mentioned, however, that the shape may not be the best fit for other input scenes. This experiment was done mostly to point out the need for resolution criteria; none exists at this time. The Rayleigh criterion is well known and accepted and should serve as an adequate beginning for resolving matched filters.

VI. CONCLUSIONS AND SUGGESTIONS FOR FUTURE INVESTIGATIONS

This investigation represents the initial research into large optical memories consisting of arrays of photographically stored matched filters. A number of specific conclusions can be drawn from the work given in this report.

A prototype holographic element which produced a 5X5 array of Fourier transforms of a scene was tested and found to be acceptable for simple optical correlation applications. Limits of the holographic element were found, however, in that the element itself contained imperfections, which, at times, made the correlation signal difficult or impossible to detect.

A definite source of the background noise observed was not discovered but several possibilities exist. The general cleanliness of the optical arrangement used to produce the hololens is certainly important. Any fingerprints, dust or contaminated chemicals used could leave artifacts on the hololens which would appear in the correlation signal. The neutral density filters used in the aperture of Figure 21 to equalize the intensities of the individual elements could possibly add an unwanted background if they contained scratches, fingerprints, etc.

Cross talk between adjacent filters was not observed. Initially it was feared that the higher order diffraction elements, which were charcteristic of the diffraction screen used to make the hololens, might overlap, thus, allowing adjacent filters to interfere. The hololens used in this investigation did contain higher order diffraction elements but they were lower in intensity, by at least an order of magnitude, than the 25 primary elements. The normal exposure times used did not allow these higher orders to even be detected on the photographic plate. A new holographic element, also produced by H. K. Liu, will be tested in the near future. This new element produces a 7X7 array of Fourier transform elements which will allow up to 49 scenes to be stored with discrimination between them and more than 147 scenes may be recognized without absolute discrimination. If the background noise is lower on this new holographic element, it may be possible to expose each element more than three times, thus, allowing an even greater number of scenes to be recognized.

The use of the LCLV allowed the filters to be addressed in real time and the correlations to be measured directly while varying the input scene. Experiments of this type included changing the angular and linear location of the input scene as well as the magnification while observing the change in intensity of the correlation. It was found that the correlation intensity was much more sensitive to rotational motion of the input scene than to tilt. The simple models developed in Section II proved adequate in predicting the trends observed experimentally.

The LCLV proved to be adequate in producing coherent images from an incoherent input scene, at least to the limitation of the television screen input. A higher resolution input scene might show the limitations of the LCLV. The television screen, however, probably represents the type of input one might expect to be used in an actual application such as automatic target

acquisition. Higher resolution television screens are available and might approach the LCLV's limits, but none were used in this investigation. Research is underway at this time to improve the resolution as well as the reaction time of the LCLV. If the potential users (and current funders) agree that the LCLV is the best approach, then it is very likely that advances will be made rapidly. At this time, the LCLV is in competition with other devices and techniques, such as erasable photoplastics and white light processing, where a coherent monochromatic source is not necessary [63].

The resolution between correlations produced by very similar scenes was investigated out of necessity, giving some insights that might have otherwise gone unnoticed. Matched filters of very similar scenes were recorded and the correlations observed took the shape of the Rayleigh double star curve. This observation, thus, led to the development of a simple model which fit experimental data reasonably well. This model can probably be modified to predict the resolution needed as a function of the spatial frequency of the input scene. It seems that this would be quite useful in the future.

The hololens approach combined with the LCLV has proven itself to be quite worthy of consideration, even in its present state, for use by various agencies of the government for target acquisition, discrimination, and tracking. The present investigation has shown that more than 70 matched filters can be stored in a very small area and addressed in parallel. This investigation has also shown that by storing only one filter per array location, parallel discrimination can be achieved. This was accomplished by a slight defocusing of the lens just in front of the small CCD camera. A visual discription is given by the photograph of Figure 48. If a detector were placed at each location of a bright spot, automatic discrimination could be achieved without the presence of an observer. If the array of Figure 48 were focused to a point by the CCD camera lens, then only one detector would be necessary; but the discrimination would be lost.

Other investigators, notably at Grumman [64], are at this time, experimenting with a hololens of their own design. Thus far, they have used a 2X2 array with multiple exposures to achieve better than 16 matched filter correlations. The 5X5 array investigated here represents a better than fourfold increase over this number.

The field of optical computing has received a much needed boost in the past year, largely due to the promising future of holographic elements and coherent light converters such as those investigated in this research. Optical recognition, as presented in this report is but one area in the larger field of optical computing; but it is the first area that has been advanced to the point of implementation in government and industrial projects.

In summation, the specific accomplishments of this investigation were:

1. The first testing of a holographic element that could produce a 5X5 array of Fourier transformed images.

2. The first real time addressing of 73 matched filters.

3. The first true discrimination in real time by an optical correlator - an individual scene was identified by the spatial location of the correlation signal.

4. The first investigation of the effects of rotation, scale, and tilt on the correlation of a scene in real time using a liquid crystal light valve.

5. The first investigation of how two correlation signals may be distinguished from each other when their respective scenes are very similar.

6. The first investigation of using multiple exposure techniques to produce matched filters of a scene Fourier transformed by a holographic element.

7. The first investigation of noise associated with a Fourier transforming holographic element.

A few, somewhat surprising, results were obtained in this investigation. The separation of the correlation signal from the hololens noise was observed when the input scene was translated slightly. The correlation signal displayed the expected translation invariance while the noise signal did not. This background was found to be quite constant throughout a 360 degree rotation of the input scene.

Defocusing the camera used to detect the correlations also provided an unexpected result. This allowed a spatial distribution of the correlation signals so that the correlation produced by an individual filter could be distinguished, thus, making absolute discrimination possible.

Some uncertainties involved in this investigation might also be worthy of more consideration:

1. The Videotek image digitizer used was not calibrated for absolute measure of the correlation intensities; only relative measurements were possible. A systematic method for measuring these intensities should provide a more quantitative measure of the recognition abilities of an optical correlator.

2. The display produced by the LCLV was not consistent on a day-to-day basis and often had to be adjusted before an experiment could be done. A method of monitoring the image produced by the LCLV could possibly be employed as the exposures are made. This could be done by using a beamsplitter to remove a percentage of the image intensity which could be monitored visually as the experiment progresses.

3. The output power from the HeNe laser used to produce the coherent image was periodically checked but not monitored continuously. A slight decrease in power could give erroneous decrease in the correlation intensities observed. A beamsplitter and detector placed in the output beam of the laser would alleviate this problem. The detector output voltage could be continuously displayed by a chart recorder as the experiment progresses.

Suggestions for further work on the topics discussed in this report might include:

1. Repeating the experiments dealing with rotation, scale and tilt using a higher resolution input scene which would take full advantage of the LCLV's quoted resolution of 60 lines/mm. A significant narrowing of curves such as Figure 45 might be expected; thus, making for a more accurate measurement of the position of the scene.

2. The correlation intensity separation from the hololens noise as given in Figure 35 should possibly be investigated more closely as a method for reducing the background signal. This background signal might possibly be used advantageously in that it provides a general location where detectors should be placed for the detection of the expected correlation signal.

3. A 5X5 array of individual detectors placed in the correlation plane to detect, independently, the intensities displayed in Figure 48 would provide the opportunity to measure directly the detection crosstalk that might be experienced in an actual application of this technology. Excessive crosstalk could possibly produce recognition errors.

4. Matched filters using dichromated gelatin photographic techniques should be investigated for use with the hololens. The efficiency of dichromated gelatin is much greater than the 649F plates used in this investigation. More efficient matched filters would produce larger, more easily detectable correlation signals.

5. A method for electronically subtracting the hololens background signal should be investigated. A device such as a Quantex image digitizer might be employed for this purpose as it has the capability of subtracting a stored scene from a displayed scene. An electronic subtraction of background might allow a larger number of multiple exposures to be made than was done in this investigation.

REFERENCES

1. Abbe, E., _Archiv. Mikroskopische Anat._ 9: 413, (1873).

2. Czapski, S., _Grundzuge der Theorie der Optischen Instruments nach Abbe_, 2nd ed., Barth, Leipzig, p. 27, (1904).

3. Porter, A., _Phil. Mag._ 6, 11: 154, (1906).

4. Zernike, F., _Z. Tech. Phys._ 16: 454, (1935).

5. Gabor, D., _Nature_ 161: 777, (1948).

6. North, D., _RCA Lab. Rpt._ PTR-6C, (1943).

7. Peterson, W., Birdsall, T., and Fox, W., _Trans. IRE_ PGIT-4: 171, (1954).

8. Marechal, A. and Croce, P., _C. R. Acad. Sci. Paris_ 237: 607, (1953).

9. Elias, P., _J. Opt. Soc. Am._ 43: 229, (1953).

10. O'Neill, E., _IRE Trans. Inform. Theory_ IT-1: 56, (1956).

11. O'Neill, E., ed., _Communication and Information Theory Aspects of Modern Optics_, General Electric Co., Electronics Laboratory, Syracuse, NY, (1962).

12. Maiman, T., _Nature_ 187: 493, (1960).

13. Cutrona, L., _IRE Trans. Inform. Theory_, IT-6: 386, (1960).

14. Cutrona, L., _Proc. IEEE_ 54: 1026, (1966).

15. Leith, E. and Upatnieks, J., _J. Opt Soc. Am._, 52: 1123, (1962).

16. Leith, E. and Upatnieks, J., _J. Opt. Soc. Am._ 53: 1377, (1963).

17. VanderLugt, A., _Radar Lab Rpt._, No. 4594-22-T, Institute of Science and Technology, The University of Michigan, Ann Arbor, MI, (1963).

18. LaMachia, J., and White, D., _Appl. Opt._ 7: 91, (1968).

19. VanderLugt, A., _Appl. Opt._ 5: 1760, (1966).

20. Leith, E., Kozma, A., Upatnieks, J., Marks, J., and Massey, N., _Appl. Opt._ 5: 1303, (1966).

21. Groh, G., _Opt. Commun._ 1: 454, (1970).

22. Shi, N., _Opt. Lett._ 3: 85, (1978).

REFERENCES (Continued)

23. Grumet, A., "Automatic Target Recognition System," US Patent 3,337,492, (1972).

24. Kozma, A., and VanderLugt, A., "Optical Data Processing for Terminal Guidance," Final Technical Report, Contract No. DAAH01-72-C-0297, prepared for US Army Missile Command, Redstone Arsenal, AL, by Harris Electro-Optics Center of Radiation, Ann Arbor, MI, (1972).

25. Casasent, D., and Furman, A., Appl. Opt. 16: 1662, (1977).

26. Leib, K., Bondurant, R., Hsiao, S., Wohlers, R., and Herold, R., Appl. Opt. 17: 2829, (1978).

27. Grinberg, J., Jacobson, A., Bleha, W., Miller, L., Fraas, L., Boswell, D., and Myer, G., Opt. Eng. 14: 217, (1975).

28. Bleha, W., Lipton, L., Wiener-Avnear, E., Grinberg, J., Reif, P., Casasent, D., Brown, H., and Markevitch, B., Opt. Eng. 17: 371, (1978).

29. Guenther, B., Christensen, C., and Upatnieks, J., IEEE J. Quant. Elect. QE-15: 1348, (1979).

30. Farr, K., "Real-Time Vehicle Tracking," Research Directorate, US Army Missile Command, Redstone Arsenal, AL, (unpublished video tape).

31. Christensen, C., Upatnieks, J., and Guenther, B., Technical Report T-79-18, US Army Missile Command, Redstone Arsenal, AL, (January 1979).

32. Leib, K., and Mendelsohn, J., SPIE 317: 148, (1981).

33. Liu, H., and Duthie, J., Appl. Opt. 21: 3278, (1982).

34. Gregory, D., and Liu, H., Submitted, Appl. Opt., (1984).

35. Yu, F., Proc. SPIE 232: 9, (1980).

36. Sklansky, J., and Wassel, G., Pattern Classifiers and Trainable Machines, Springer-Verlag, New York, (1981).

37. Jackson, J., Classical Electrodynamics, Wiley and Sons, New York, (1975), p. 65.

38. Goodman, J., Introduction to Fourier Optics, McGraw Hill, New York, (1968).

39. Yu, F., Optical Information Processing, Wiley and Sons, New York, (1983).

40. Arfken, G., Mathematical Methods for Physicists, Academic Press, New York, (1978), p. 682.

41. Selby, S., ed., CRS Standard Mathematical Tables, Chemical Rubber Co., Cleveland, OH, (1968).

REFERENCES (Continued)

42. Eg.: Casasent, D., and Furman, A., _Appl. Opt._ 16: 1652, (1977).

43. Zech, R., _Data Storage in Volume Holograms_, PhD Dissertation, University of Michigan, Ann Arbor, MI, (1974).

44. Caufield, H., _Handbook of Optical Holography_, Academic Press, New York, (1979), p. 281.

45. Beard, T., Bleha, W., and Wong, S., _Appl. Phys, Lett._ 22: 90, (1973).

46. Gara, A., _Appl. Opt._ 18: 172, (1979).

47. Guenther, B., Upatnieks, J., and Christensen, C., in "Proc. Intl. Conf. on Lasers," 11 (December 1978), p. 587.

48. Montgomery, P., _J. Opt. Soc. Am._ 70: 287, (1980).

49. Pennington, K., in _CRC Handbook of Lasers with Selected Data on Optical Technology_, R. Pressley, ed., The Themical Rubber Co., Cleveland, OH, (1971), p. 549.

50. Newport Research Corporation, 1977-78 Catalog, Fountain Valley, CA, p. 92.

51. Mees, K., _The Theory of the Photographic Process_, 3rd ed., McMillian and Co., New York, (1966), p. 143.

52. Johnson, K., Hesselink, L., and Goodman, J., _SPIE_ 367: 20, (1980).

53. Biedermann, K., _Appl. Opt._ 10: 584, (1971).

54. Chang, B., and Winick, K., _Proc. SPIE, 215_, 1980.

55. Casasent, D., and Furman, A., _Appl. Opt._ 15: 1690, (1976).

56. Upatnieks, J., Guenther, B., and Christensen, C., "Real Time Correlation for Missile Terminal Guidance," Technical Report. H-78-5, US Army Missile Command, Redstone Arsenal, AL, (January 1978).

57. Guenther, B., Upatnieks, J., and Christensen, C., "Real Time Optical Vehicle Identification and Tracking," Proc. International Conference on Lasers, 11-15 (December 1978), p. 587.

58. Yariv, A., _Quantum Electronics_, 2nd ed., Wiley and Sons, New York, (1975), p. 123.

59. Hecht, E., and Zajac, A., _Optics_, Addison-Wesley, Reading, MA, (1974), p. 310.

60. Yu, F., _Introduction to Diffraction, Information Processing, and Holography_, MIT Press, Cambridge, MA, (1973), p. 55.

REFERENCES (Concluded)

61. Liu, H. K., private communication.

62. Davis, J. H., private communication.

63. George, N., and Morris, G., SPIE 338, "Advances in Optical Information Processing," (1983).

64. Leib, K., "Investigation and Implementation of Optical Memory for a Correlation Seeker," Final Report, Contract No. DAAH01-C-A143, prepared for the US Army Missile Command, Redstone Arsenal, AL, by Grumman Aerospace, Bethpage, NY, (1983).

65. Shulman, A., Optical Data Processing, Wiley and Sons, New York, (1980).

66. Pittaro, E., ed., Photo Lab Index, Morgan and Morgan Publishers, Dobbs Ferry, NY, (1979).

APPENDIX A

THE FOURIER TRANSFORM OF A RONCHI RULING

The Fourier Transform of a Ronchi Ruling

In Section II a simple correlation theory was developed which was based upon the overlap of two circles. Later, in Section IV, this simple model was used to predict the correlation versus several variables for a Ronchi ruling input scene. The rationale was that the Fourier transform of a Ronchi ruling produced a roughly circular series of exposures on a photographic plate. In this appendix, the Fourier transform of a finite Ronchi ruling is calculated exactly. Many standard textbooks give solutions to this problem for a ruling extending an infinite distance but the solution to a finite ruling is worth examining because of the application to some of the experiments presented in Section IV.

Figure A-1 gives the transmission versus ξ for a Ronchi ruling. For a ruling extending over an infinite distance, this transmission may be written:

$$t(\xi) = \sum_{n=-\infty}^{\infty} \text{rect} \left(\frac{\xi - 2na}{a} \right) \tag{111}$$

where, in general, the rect function is written:

$$\text{rect}(Z) = \begin{cases} 1 & |z| \leq \frac{1}{2} \\ 0 & \text{otherwise} \end{cases} . \tag{112}$$

A finite ruling is best represented as a convolution of a rect function with a comb function bounded by a rect function window — illustrated by the dashed line in Figure A-2.

$$t(\xi) = \left[\text{rect} \left(\frac{\xi}{a} \right) \ * \ \text{comb} \left(\frac{\xi}{2a} \right) \right] \cdot \text{rect} \left(\frac{\xi}{Na} \right) \tag{113}$$

where, in general, the comb function is written:

$$\text{comb}(z) = \sum_{n=-\infty}^{\infty} \delta(z-n) . \tag{114}$$

It is desired to illuminate this Ronchi ruling with plane wave unit amplitude light, then Fourier-transform the transmitted field using a lens. If the ruling is placed in the front focal plane of the lens then the field in the back focal plane will be proportional to the Fourier transform of Equation (113):
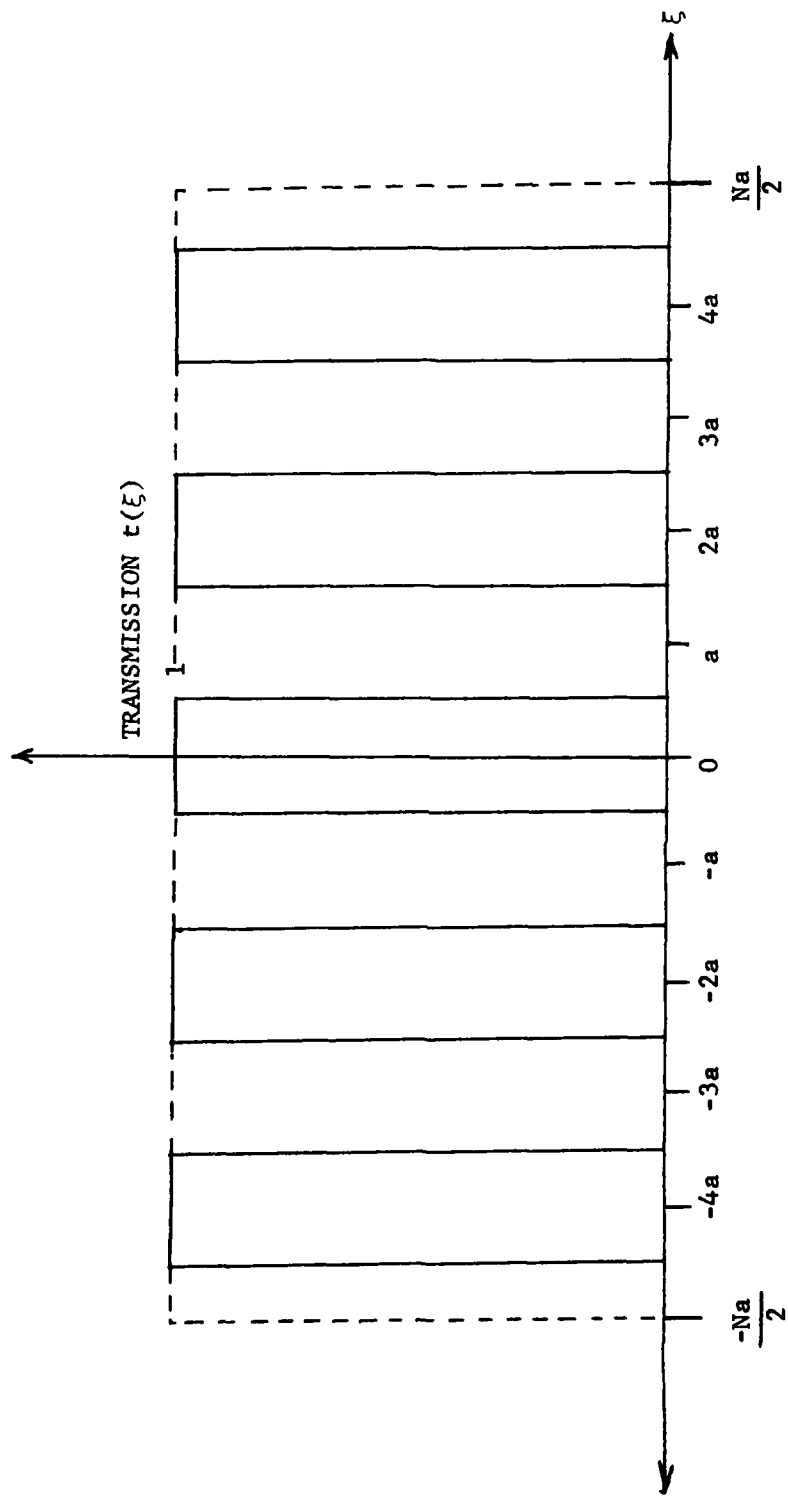
Figure A-1. Transmission versus displacement, ξ, for a Ronchi ruling.

$$F\{t(\xi)\} = F\left\{\left[\text{rect}\left(\frac{\xi}{a}\right) * \text{comb}\left(\frac{\xi}{2a}\right)\right] \text{rect}\left(\frac{\xi}{Na}\right)\right\} . \qquad (115)$$

Note that, in general: [38] (p. 26)

$$F\{g(y)h(y)\} = F\{g(x)\} * F\{h(y)\} . \qquad (116)$$

Thus:

$$F\{t(\xi)\} = F\left\{\text{rect}\left(\frac{\xi}{a}\right) * \text{comb}\left(\frac{\xi}{2a}\right)\right\} * F\left\{\text{rect}\left(\frac{\xi}{Na}\right)\right\} . \qquad (117)$$

Also, in general: [38] (p. 10)

$$F\{h(y) * g(y)\} = F\{h(y)\} \cdot F\{g(y)\} . \qquad (118)$$

Thus:

$$F\{t(\xi)\} = \left[F\left\{\text{rect}\left(\frac{\xi}{a}\right)\right\} \cdot F\left\{\text{comb}\left(\frac{\xi}{2a}\right)\right\}\right] * F\left\{\text{rect}\left(\frac{\xi}{Na}\right)\right\} . \qquad (119)$$

Now:

$$F\left\{\text{rect}\left(\frac{\xi}{a}\right)\right\} = a \; \text{sinc}\,(\Omega a) \qquad (120)$$

where, according to Goodman [38] (p. 14):

$$\text{sin}\,(\Omega a) = \frac{\sin\,(\Omega \pi a)}{\Omega \pi a} \qquad (121)$$

and:

$$F\left\{\text{comb}\left(\frac{\xi}{2a}\right)\right\} = 2a \; \text{comb}\,(2a\Omega) . \qquad (122)$$

Therefore:

$$F\{t(\xi)\} = \left[a \; \text{sinc}\,(\Omega a) \cdot 2a \; \text{comb}\,(2a\Omega)\right] * F \; \text{rect}\left(\frac{\xi}{Na}\right) \qquad (123)$$

and

$$F\left\{\text{rect}\left(\frac{\xi}{Na}\right)\right\} = Na \; \text{sinc}\,(Na\Omega) \qquad (124)$$

Thus:

$$F\{t(\xi)\} = \left[2a^2 \; \text{sinc}\,(\Omega a) \; \text{comb}\,(2\Omega a)\right] * Na \; \text{sinc}\,(Na\Omega). \qquad (125)$$

A-5

The term in brackets is

$$2a^2 \text{ sinc } (\Omega a) \sum_{n=-\infty}^{\infty} \delta(2\Omega a - n) \quad . \tag{126}$$

The delta function determines the allowed values of Ω in the sinc term

$$\Omega = \frac{n}{2a} \quad , \tag{127}$$

therefore, the term in brackets may be rewritten as [38] (p. 24)

$$2a^2 \sum_{n=-\infty}^{\infty} \text{ sinc } \left(\frac{n}{2}\right) \delta(2\Omega a - n) \quad . \tag{128}$$

Therefore:

$$F\{t(\xi)\} = 2a^2 (Na) \left[\sum_{n=-\infty}^{\infty} \text{ sinc } \left(\frac{n}{2}\right) \delta(2a\Omega - n) \right] * \text{ sinc } (Na\Omega) \quad . \tag{129}$$

Performing the convolution is simple due to the presence of the delta function [38] (p. 24):

$$= 2Na^3 \sum_{n=-\infty}^{\infty} \text{ sinc } \left(\frac{n}{2}\right) \text{ sinc } \left[Na \left(\Omega - \frac{n}{2a}\right) \right] . \tag{130}$$

The intensity in the focal plane is proportional to the square of this field; therefore:

$$I \propto 4N^2 a^6 \left\{ \sum_{n=-\infty}^{\infty} \text{ sinc } \left(\frac{n}{2}\right) \text{ sinc } \left[Na \left(\Omega - \frac{n}{2a}\right) \right] \right\}^2 \quad . \tag{131}$$

Noting that $\Omega = x_f/\lambda f$ as in Section II, the intensity distribution in the focal plane is found to be:

$$I \propto 4N^2 a^6 \left\{ \sum_{n=-\infty}^{\infty} \text{sinc}\left(\frac{n}{2}\right) \text{sinc}\left[Na \left(\frac{x_f}{\lambda f} - \frac{n}{2a} \right)\right] \right\}^2 \qquad . \qquad (132)$$

This is plotted in Figure A-2. No "adjustable parameters" were used but rather experimental values of the ruling were substituted for f, a, and N. Results are quite good for the separation between peaks. In Section IV, the separation was found to be about 1.3×10^{-2} cm between the first order and the zeroth. This agrees very well with the prediction of Figure 42. Only the odd orders are present - as should be expected. A square wave may be written as a sum of sines or cosines [65] (p. 244):

$$f(\xi) = \frac{1}{2} \left(1 + \frac{4}{\pi} \cos \Omega\xi - \frac{4}{3\pi} \cos 3\Omega\xi + \frac{4}{5\pi} \cos 5\Omega\xi \right) , \qquad (133)$$

or

$$f(\xi) = \frac{1}{2} \left(1 + \frac{4}{\pi} \sin \Omega\xi + \frac{4}{3\pi} \sin 3\Omega\xi + \frac{4}{5\pi} \sin 5\Omega\xi \right) . \qquad (134)$$

In either representation, only the odd orders of Ω are present.

The width of the first order is also important. In the model presented in Section II and used in Section IV the value of R, the radius of the exposed first order was taken directly from photographs. In the analysis presented in this appendix, a computed value can be taken directly from Figure A-2. The FWHM of the first order is about 7.4×10^{-6} M. Therefore R is equal to 3.7×10^{-4} cm. This represents an error of about 14 percent when compared to experimental values taken in Section IV.

It was possible to experimentally verify the calculated Fourier transform given in Figure A-2. The Ronchi ruling described in Section IV was again used as the input to the optical system of Figure 24, with the reference beam blocked. A small telescope was placed at the location usually reserved for the film holder. The overall intensity of the laser light was decreased, using neutral density filters, to the point where the optical Fourier transform could be viewed by the naked eye. The resulting image was then projected into a small television camera and displayed on a television set. The image was quite similar to the photograph of Figure 29. In order to obtain an intensity profile of the image, the signal from the television camera was input to a Tektronix oscilloscope which could display scans of single television lines. The oscilloscope trace was then photographed. This is shown in Figure A-3. The zeroth order and successive odd orders are present. This compares well with the calculation done earlier in this appendix and plotted in Figure A-2.
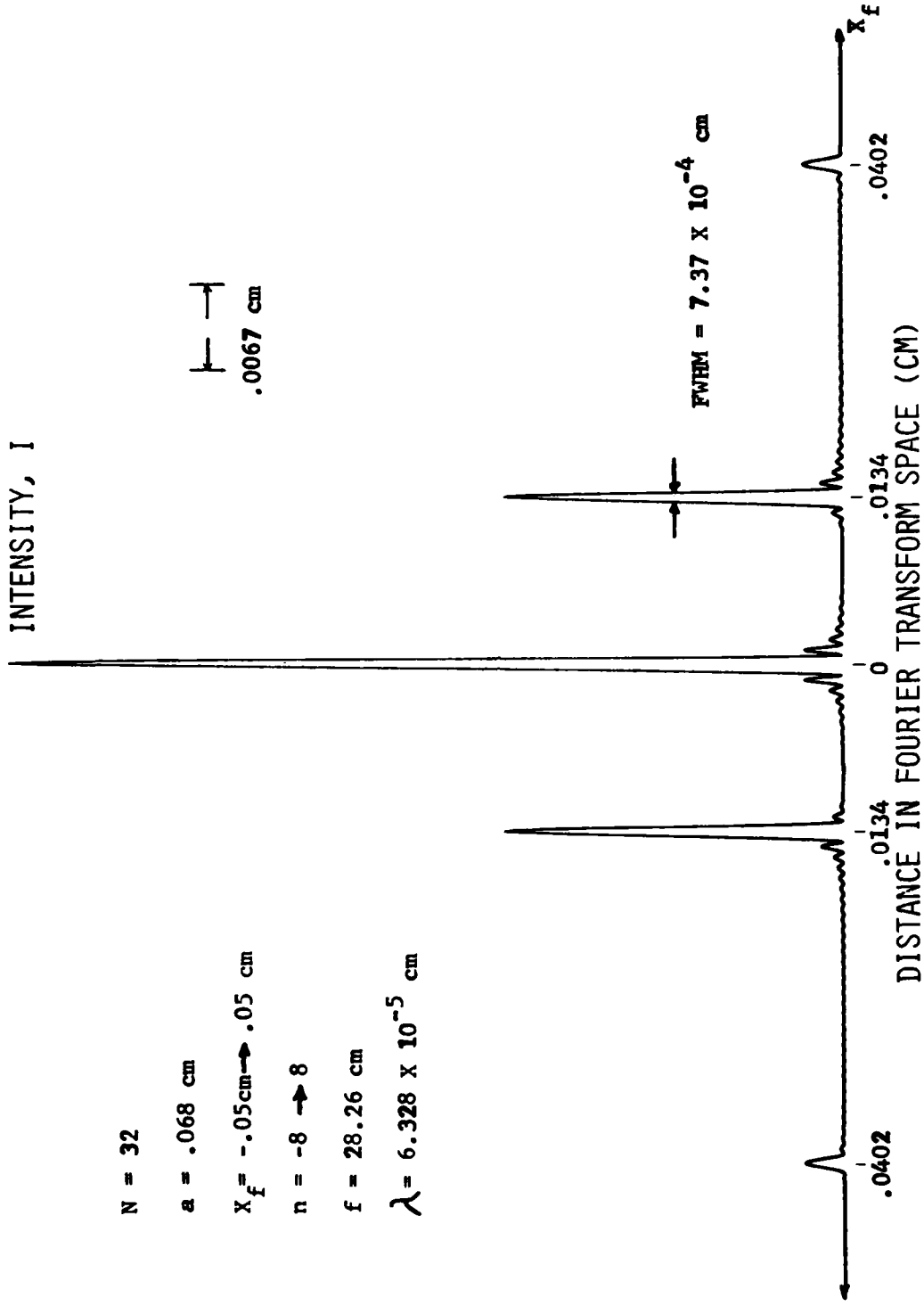
Figure A-2. The Fourier transform of a finite Ronchi ruling.

INTENSITY, I

.0067 cm

N = 32

a = .068 cm

x_f = -.05cm ⟶ .05 cm

n = -8 ⟶ 8

f = 28.26 cm

λ = 6.328 x 10^{-5} cm

.0402

FWHM = 7.37 x 10^{-4} cm

.0402

.0134

0

.0134

x_f

DISTANCE IN FOURIER TRANSFORM SPACE (CM)

A-8
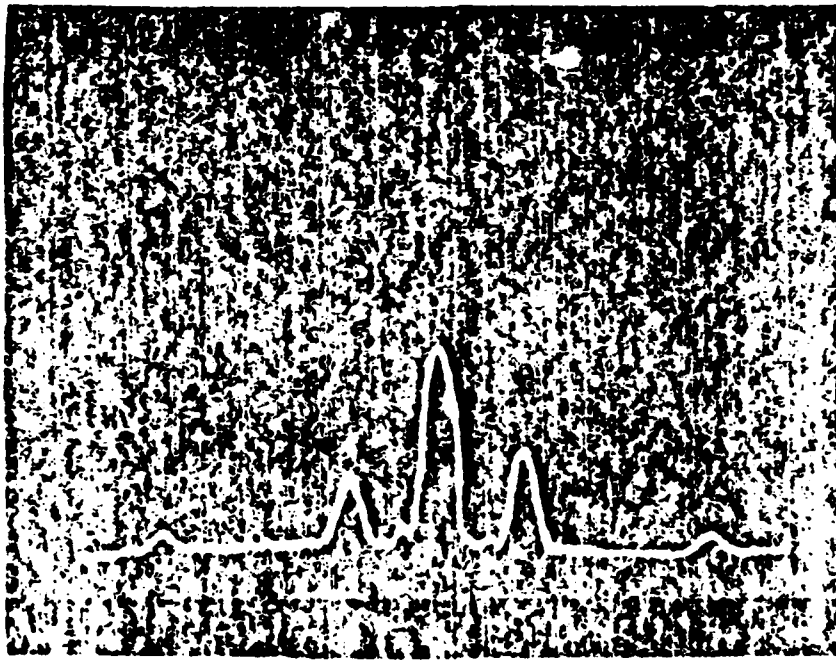
Figure A-3. Oscilloscope display of the Fourier transform of a Ronchi ruling.

A-9

The previous analysis seems to somewhat justify the simple overlapping circles model presented in Section II. The higher orders present in the frequency spectrum have been ignored. The intensity of the third order is quite weak compared to the first; therefore, the neglection of higher orders is probably justifiable.

The analysis presented in this appendix was satisfying in that the separation between peaks as well as the width of the first order peaks was calculated and proved to be comparable to experimental values.

APPENDIX B

FILM CHARACTERISTICS AND DEVELOPING TECHNIQUES

Film Characteristics and Developing Techniques

Almost all the experimental work done in the investigation involved photographic plates. It is for this reason that this appendix is included. Some of the techniques given here are well established; others were developed and tested as the need arose.

A. Kodak 694F Film [66]

Kodak 649F spectroscopic plates used in this investigation are some of the highest resolution plates available - 3000 lines/mm. It is a fairly thick (17 μm) emulsion on a .040-inch thick glass plate. The granularity is given as less than 5 where 30 is considered coarse. It is the lowest in granularity of any Kodak film. It is used for a wide variety of spectroscopic applications. The spectral response is fairly flat from 425 nm to 675 nm. The MTF of 649F film is greater than .70 as far out as 2000/mm spatial frequency [49] (p. 572). The sensitivity is given as 8×10^{-5} J/cm^2 in the spectral response region.

B. Developing [65]

The developer used throughout this investigation was Kodak D-19. The receipt for this developer is:

Water (50°C)	500 cc
Kodak Elon	2 g
Sodium Sulfide	90 g
Hydroquinone	8 g
Sodium Carbonate	52.5 g
Potassium Bromide	5 g
Cold water to make	1 liter

The principle ingredient in Kodak Elon developing agent is p-methylaminophenol sulfate. The proportions of Elon and hydroquinone in a developer will vary according to the film being developed. Elon alone produces a low contrast image with some fog. Hydroquinone alone produces a high contrast image with a high fog level. The stop bath used was Kodak indicator stop bath. The receipt for this is:

Water	1 liter
Acetic acid (29%)	48 ml

The function of the acidic stop bath is to stop the developing procedure caused by the alkaline components of the developer. The fixer used was Hunt's Aerofix. The receipt for this is:

Water (50 °C)	600 ml
Sodium thiosulfate	360 g
Ammonium chloride	50 g
Sodium sulfide	15 g
Acetic acid (28%)	48 ml
Boric acid crystals	7.5 g
Potassium alum	15 g
Cold water to make	1 liter

The developing procedure was as follows: All chemicals were kept at 20 °C by using a temperature-controlled water bath. The first four steps were carried out in complete darkness.

1. Immersion with agitation in D-19 developer for 6 minutes.

2. Immersion with agitation in stop bath for 3 minutes.

3. Immersion with agitation in fixer for 1 minute.

4. Flowing water rinse for at least 10 minutes.

5. Final rinse in absolute ethanol for at least 5 minutes.

6. Air dry for at least 20 minutes.

The previous procedure seemed to give consistently good matched filters. Slight variations of this procedure are possible without causing problems.

DISTRIBUTION

No. of
Copies

Commander   5
US Army Research Office
ATTN: AMXRO-PH, Dr. R. Lontz
P. O. Box 12211
Research Triangle Park, NC 27709

US Army Research and Standardization Group (Europe)   1
ATTN: AMXSN-E-RX, LTC D. R. Reinhard
Box 65
FPO New York 09510

Commander
US Army Materiel Development and Readiness Command
ATTN: Dr. James Bender   1
       Dr. Gordon Bushey   1
5001 Eisenhower Avenue
Alexandria, VA 22333

Headquarters   1
Department of the Army
Office of the DCS for Research, Devleopment & Acquisition
ATTN: DAMA-ARZ
Room 3A474, The Pentagon
Washington, DC 20301

OUSDR&E   1
Room 3D1079, The Pentagon
Washington, DC 20301

Director   1
Defense Advanced Research Projects Agency
1400 Wilson Boulevard
Arlington, VA 22209

OUSDR&E   1
ATTN: Dr. G. Gamota
Deputy Assistant for Research (Research in Advanced Technology)
Room 3D1067, The Pentagon
Washington, DC 20301

Director of Defense Research and Engineering   1
Engineering Technology
Washington, DC 20301

DISTRIBUTION (Continued)

No. of
Copies

Director
Defense Advanced Research Projects Agency/STO
ATTN: Commander T. F. Wiener   1
       D. W. Walsh   1
1400 Wilson Boulevard
Arlington, VA 22209

Commander   1
US Army Aviation Systems Command
12th and Spruce Streets
St. Louis, MO 63166

Director
US Army Air Mobility Research & Development Laboratory   1
Ames Research Center
Moffett Field, CA 94035

Commander
US Army Electronics Research & Development Command
ATTN: AMSEL-TL-T, Dr. Jacobs   1
       AMLEW-R, Henry E. Sonntag   1
Fort Monmouth, NJ 07703

Director
US Army Night Vision Laboratory
ATTN: John Johnson   1
       John Deline   1
       Peter VanAtta   1
Fort Belvoir, VA 22060

Commander   1
US Army Picatinny Arsenal
Dover, NJ 07801

Commander   1
US Army Harry Diamond Laboratories
2800 Powder Mill Road
Adelphi, MD 20783

Commander
US Army Foreign Science and Technology Center
ATTN: W. S. Alcott   1
Federal Office Building
220 7th Street, NE
Charlottesville, VA 22901

Commander   1
US Army Training and Doctrine Command
Fort Monroe, VA 22351

DISTRIBUTION (Continued)

No. of
Copies

Director
Ballistic Missile Defense Advanced Technology Center
ATTN: ATC-D   1
       ATC-O   1
       ATC-R   1
       ATC-T   1
P. O. Box 1500
Huntsville, Al 35808

Commander   1
US Naval Air Systems Command
Missile Guidance and Control Branch
Washington, DC 20360

Commander   1
US Naval Air Development Center
Warminster, PA 18974

Chief of Naval Research   1
Department of the Navy
Washington, DC 20301

Commander
US Naval Ocean Systems Center
Code 6003, Dr. Harper Whitehouse   1
San Diego, CA 92152

Director
Naval Research Laboratory
ATTN: Dave Ringwolt   1
       Code 5570, T. Gialborinzi   1
Washington, DC 20390

Commander
Rome Air Development Center
US Air Force
ATTN: James Wasielewski, IRRC   1
Griffiss Air Force Base, NY 13440

Commander
US Air Force
AFOSR/NE
ATTN: Dr. J. A. Neff   1
Building 410, Bolling Air Force Base
Washington, DC 20332

DISTRIBUTION (Continued)

Commander
US Air Force Avionics Laboratory
ATTN: D. Rees   1
        W. Schoonover   1
        Dr. E. Champaign   1
        Dr. J. Ryles   1
        Gale Urban   1
        David L. Flannery   1
Wright Patterson Air Force Base, OH 45433

Commander   1
AFATL/LMT
ATTN: Charles Warren
Eglin Air Force Base, FL 32544

Environmental Research Institute of Michigan
Radar and Optics Division
ATTN: Dr. A. Kozma   1
        Dr. C. C. Aleksoff   1
        Juris Upatnieks
P.O. Box 8618
Ann Arbor, MI 41807

IIT Research Institute   1
ATTN: GACIAC
10 West 35th Street
Chicago, IL 60616

Dr. J. G. Castle   1
9801 San Gabriel, NE
Albuquerque, NM 87111

Commander
Center for Naval Analyses
ATTN: Document Control   1
1401 Wilson Boulevard
Arlington, Va 22209

Dr. J. W. Goodman   1
Information Systems Laboratory
Department of Electrical Engineering
Stanford University
Stanford, CA 04305

Eric G. Johnson, Jr.   1
National Bureau of Standards
325 S. Broadway
Boulder, CO 80302

DISTRIBUTION (Continued)

Dr. Nicholas George   1
The Institute of Optics
University of Rochester
Rochester, NY 14627

Naval Avionics Facility   1
Indianapolis, IN 46218

Dr. David Casasent   1
Carnegie Mellon University
Hamerschage Hall, Room 106
Pittsburg, PA 15213

Professor Anil K. Jain   1
Department of Electrical Engineering
University of California, Davis
Davis, CA 95616

Terry Turpin   1
Department of Defense
9800 Savage Road
Fort George G. Meade, MD 20775

Dr. Stuart A. Collins   1
Electrical Engineering Department
Ohio State Univeristy
1320 Kennear Road
Columbus, OH 43212

US Army Materiel System Analysis Activity   1
ATTN: AMXSY-MP
Aberdeen Proving Ground, MD 21005

US Army Night Vision Laboratory   1
ATTN: DELNV-L, Dr. R. Buser
Ft. Belvoir, VA 22060

Dr. F. T. S. Yu   1
Penn State University
Department of Electrical Engineering
University Park, PA 16802

Dr. William P. Bleha   1
Liquid Crystal Light Valve Devices
Hughes Aircraft Company
6155 El Camino
Carlsbad, CA 92008

	No. of Copies
US Army Missile Command	
AMCPM-PE-E, Mr. John Pettitt	1
-PE	1
AMSMI-LP, Mr. Voigt	1
-O	1
-Y	1
-R, Dr. M. McCorkle	1
-RN, Mr. J. Hagood	1
-RE, Mr. W. Pittman	1
-RD	3
-RG	1
-RG, Mr. J. A. McLean	1
-RR, Dr. R. L. Hartman	1
-RR, Dr. J. S. Bennett	1
-RR, Dr. J. G. Duthie	1
-RR, Dr. D. A. Gregory	40
-RPR	15
-RPT, Record Copy	1

END

FILMED

10-85

DTIC